Patching a Blade

Investigation into the Application of Straight-Fibre Variable Stiffness Laminates in Wind Turbine Blade Design

M.A.V. Caruso

TUDelft   DTU

Patching a Blade

Investigation into the Application of Straight-Fibre Variable Stiffness Laminates in Wind Turbine Blade Design

by

M.A.V. Caruso

to obtain the degrees of
Master of Science in Aerospace Engineering at Delft University of Technology, and
Master of Science in Wind Energy Engineering at the Technical University of Denmark.

Organisations	Delft University of Technology (TU Delft) & Technical University of Denmark (DTU)
Student Number	4796268 (TU Delft) & s213778 (DTU)
Master Programme	European Wind Energy Master (EWEM)
Master Track	Structures and Composite Materials
Project Duration	November, 2022 - August, 2023
Supervisors	Dr. ir. J.M.J.F. van Campen, TU Delft
	Dr. ir. F. Zahle, DTU

Abstract

Over the last decades, wind turbine blades have continuously grown in size to harvest further power from the wind. Longer blades have an increased structural mass and thus suffer from increased gravitational and inertial loads. Current developments in the field of wind turbine blade design strive for lightweight, high-bending stiffness, yet cost-effective structures. An approach to drive down mass is through the combined optimisation of aerodynamic and structural properties of a blade, which is commonly referred to as aeroelastic tailoring. Current structural optimisation strategies of wind turbine blades could benefit from existing aerospace structural tailoring approaches, such as straight-fibre variable stiffness design. Straight-fibre variable stiffness, also referred to as multi-patch laminate blending, consists in partitioning a structure into constant laminate regions that are locally optimised. Those regions are then blended to bring back continuity, thus ensuring structural integrity and manufacturability. Locally optimising regions allows the stiffness to be tailored to the specific needs of each region and allows the definition of load paths within the laminate. Laminate blending enables further structural tailoring through variable stiffness composite design while preferring the use of conventional laminate patches over more costly continuous fibre angle variation.

The present research aims to investigate the structural performance potential for straight-fibre variable stiffness laminates in wind turbine blade design. This research objective was tackled in two phases. First, a design methodology is proposed to couple a wind turbine aeroelastic optimisation framework with a laminate blending design algorithm. Second, the proposed design framework was applied to a blade section to evaluate the achievable structural performance when straight-fibre variable stiffness laminates are introduced in large-scale structures. The design framework for straight-fibre variable stiffness design of a blade section first optimises the lamination parameter distribution for each laminate region of the design. Then a conversion of the lamination parameters design to a stacking sequence is performed, followed by the enforcement of laminate blending constraints.

To quantify the performance of the blending approach, the DTU 10MW reference turbine blade was selected as the baseline structure. Specifically, a section of this blade was assessed, taken at the maximum chord location. At this site, the largest trailing-edge panels are present, and structural requirements such as buckling are critical. The objective of the laminate blending optimisation was extended to maximise the buckling performance of the considered section while matching a tip deflection requirement. When refining the number of laminate regions present on the trailing-edge panels, improvements in buckling performance up to 68% are achieved, with a limited increase in tip deflection of 4.8%. Overall, the methodology presented in this research highlights the potential improvements achieved with straight-fibre variable stiffness laminates when applied to a blade section. Further research is recommended in refining the modelling of a blade structure, namely to define sandwich materials and shear webs. Even though a methodology to evaluate the aeroelastic response of a full blade with variable stiffness structures is presented, this methodology was not assessed. The application of this approach to a full blade design could highlight the tailoring potential of stiffness variation and load redistribution enabled through laminate blending for aeroelastic applications.

Preface

Even though this page stands at the beginning of this thesis, it marks the end of a meaningful chapter for me. Even though this page is limited to a few lines, I would like to acknowledge those involved over the last five years.

I would like to thank my supervisors for their patience and guidance throughout this project. Thank you Frederik for our fruitful discussions, and your support in using the AESOpt framework. Thank you Julien for always pushing my curiosity a step further. Thank you also to Professor Kassapoglou for accepting to be the chair of my assessment committee. I enjoyed every experience you shared during your lectures. Thank you also to Christian Frier Hvejsel for taking the time to review my research, and be part of my graduation committee. Thank you to my predecessor Thore for providing me with such a powerful design tool. Thank you also to my fellow students from the ASCM master room, especially to Rakshith. I valued working next to you, I hope I could help you at least as much as you did for me when I was confused by these lamination parameters and optimisation formulations. Thank you also to the research team at DTU Wind Energy, especially to Rasmus, Sergei, and Riccardo, for providing me access to and support with the AESOpt framework.

To my family: Thank you for your everlasting support and guidance. To Margaux: Thank you for the wonderful years together. To Giorgio, Noah, Jaimy, Luca, and Loek: Thank you guys for the amazing memories we created right from when we started in Delft. I am grateful for the long hours spent together on campus, for our memorable ski trips, and lately for our much-appreciated coffee breaks. Thank you to many more friends in Delft: Thibaut, Marnix, and Nicolas; EWEM fellows: Sebastiaan, Carlos, Sowmya, and Fien; and fellows from Denmark, Jean, David, Josh, Esther, and Sofus. Thank you all for sharing these wonderful years.

Mateo
Delft, August 2023

Contents

Acronyms

Notation	Description
AEP	Annual Energy Production
AESOpt	Aero-Structural Optimization Framework
BECAS	BEam Cross-Section Analysis Software
BRM	Blade Root Moment
BTC	Bend-Twist Coupling
CA	Cellular Automaton
CC	Cap Centre
COE	Cost of Energy
DMO	Discrete Material Optimisation
GA	Geometrical Adaptive
GA	Genetic Algorithm
HAWT	Horizontal Axis Wind Turbine
ICC	Initial Capital Cost
LE	Leading Edge
MA	Material Adaptive
MDO	Multidisciplinary Design Optimisation
NREL	National Renewable Energy Laboratory
PA	Pitch Axis
PS	Pressure Side
SFVS	Straight-Fibre Variable Stiffness
SLSQP	Sequential Least Squares Programming
SS	Suction Side
TE	Trailing Edge
TER	Trailing Edge Reinforcement
UD	Unidirectional
VS	Variable Stiffness

Nomenclature

Symbol	Definition
β	Penalty term in an augmented objective function
$\boldsymbol{\Gamma_i}$	Material invariant matrices
δ	Structural deflection
ε	Bonus term in an augmented objective function
ε	In-plane strain
$\boldsymbol{\theta_i}$	Stacking sequence of a region i
λ	Critical buckling load factor
ν_{12}	Major Poisson's ratio
ρ	Density
Φ	Augmented objective function
$\boldsymbol{A}$	Laminate extension stiffness matrix
$\boldsymbol{B}$	Laminate coupling stiffness matrix
B	Buckling load
C_P	Power coefficient
c	Chord length
$\boldsymbol{D}$	Laminate flexural stiffness matrix
E_1, E_2, E_3	Longitudinal and transverse Young's moduli
f	Optimisation objective function
G_{12}, G_{23}, G_{13}	Longitudinal and transverse shear moduli
g	Buckling constraint
h	Laminate thickness
$\boldsymbol{K^{geo}}$	Geometric stiffness matrix
$\boldsymbol{K^{mat}}$	Material stiffness matrix
M_x	Flapwise bending moment
m	Structural mass
P	Aerodynamic power
R	Rotor radius
t/c	Airfoil relative thickness
V	Free-stream wind speed
$\boldsymbol{V_i^A}$	In-plane lamination parameters
$\boldsymbol{V_i^B}$	Coupling lamination parameters
$\boldsymbol{V_i^D}$	Flexural lamination parameters
$\boldsymbol{x}$	Design vector of an optimisation

Flowchart Convention

In the present report, several flowcharts are presented. The following convention was used for those diagrams, unless stated otherwise.

| Input / Output | Description of input or output data. |

| Process Description | Description of a process (e.g. manipulation of variables or iterative process). |

| Optimisation | Description of an optimiser. |

| Condition | Decision node distinguishing paths depending on the condition specified. |

| Data/ Decision → | Indication of the process flow, possibly together with a description of the data or condition transfered between two blocks. |

1

Introduction

The present research takes context into the challenges that arise when harvesting power from the wind. Increasingly large rotors allow to extract further energy from the wind. Yet larger rotors have heavier blades, that suffer from gravitational and inertial loads. The need for high stiffness-to-weight ratio and cost-effective blade structures makes the use of composite materials relevant. To further exploit the properties of such materials, variable stiffness laminate designs can be applied to extend the design space for wind turbine blades through tailoring and load redistribution. An approach to achieving such variable stiffness structures is with straight-fibre variable stiffness laminates. The objective of this research is therefore to evaluate the performance of this design approach in the field of wind turbine blade design.

To achieve this objective, two research design tools are extended, one focused on conceptual aero-structural blade design, and the other on variable stiffness laminate design. Furthermore, a coupling approach between them is proposed to investigate the use of straight-fibre variable stiffness laminates in the design of wind turbine blades. The application of straight-fibre variable stiffness laminates was demonstrated in the work by Gomaa (2019) to improve the buckling performance of a plate under compression. The design framework for those variable stiffness structures was further extended and applied to more complex structures in the work of Roepman (2021), which considered the design of an aircraft fuselage. The present research, therefore, follows in line with the performance assessment of those laminates in complex aerospace structures.

Four main parts organise this report. In Part I, the reader will be provided with some context on current challenges and context in which wind turbine blades are designed, followed by a review of the design approaches for blades, and a review of design approaches for variable stiffness composite materials. To conclude this part, the scope of the research will be defined with a set of research questions. Part II will then introduce the methodology developed to answer the research question specified. An overview of this methodology will be provided in Chapter 8, with a focus on the aeroelastic optimisation framework covered in Chapter 6, and on the design tool for straight-fibre variable stiffness laminates in Chapter 7. These two frameworks will then be applied to a benchmark blade section design in Part III to design a blade section featuring straight-fibre variable stiffness laminates in its facesheets, to maximise buckling performance under a deflection requirement. An outlook on the results and the performance achieved by the blended blade section for various design concepts will be provided. Finally, recommendations for further research will be provided in Part IV.

Part I

Literature Study

2

Context and Challenges of Wind Turbine Blade Design

The present chapter is intended to provide background knowledge on the topics of wind turbine blade design, and composite laminates designs. The present review does not aim to be exhaustive, rather to provide an overview on the key concepts and the context in which the present project will be developed.

Section 2.1 will contextualise the design trends for wind turbine blades, namely providing details on typical blade components, materials used, and design approaches, particularly on aeroelastic tailoring. Aeroelastic rotor design will be further discussed in Section 2.2, with a focus on the benefits and challenges of bend-twist coupling.

2.1. Wind Turbine Blade Design Drivers

The available power P that a horizontal-axis wind turbine can extract from the wind is proportional to the square of the rotor radius R and the cube of the free-stream wind speed V, as defined in Equation 2.1 (M. O. L. Hansen, 2015). The wind resource and air density, captured by V and ρ, respectively, are factors that are dependent on the site at which a turbine is implemented. A wind turbine designer does not have control over those. Therefore, to increase power production, a wind turbine would benefit from a larger rotor radius R, and improved aerodynamic performance, as captured by the power coefficient C_P.

$$P = \frac{1}{2}\rho R^2 V^3 C_P \tag{2.1}$$

Increasing the rotor radius, however, induces challenges such as an increase in blade mass and material usage. Mølholt Jensen and Branner (2013) have shown through historical data that wind turbine blade manufacturers achieved more efficient blades than one would have obtained through simple linear scaling. Historically, blade mass can be shown to have increased with blade length with a power of 2.3. Through simple linear scaling of a blade structure, blade mass would have increased instead with the power of three. Continuous effort in improving aerodynamical, structural and control performances are three reasons suggested to drive down mass. A larger rotor usually correlates with a heavier rotor. Heavier rotors suffer from increased gravitational and inertial loads. Mishnaevsky et al. (2017) and Mølholt Jensen and Branner (2013) even suggested that those loads tend to dominate over aerodynamic ones. Hence, achieving lighter blades is paramount in limiting gravitational and inertial loads. Besides, lighter blades also benefit other components supporting the rotor, such as the nacelle and tower. Reduction in load requirements on those structures entails benefits in production and operation cost reduction for the entire wind turbine (Jureczko & Mrówka, 2022).

Regarding the design drivers of blades, an increase in energy capture and load mitigation are fundamental objectives (Griffin, 2004). One can argue the equivalence of those two objectives. In fact,

through load alleviation, one can design a larger rotor experiencing equivalent loads as the baseline. In turn, such a larger rotor extracts more energy from the wind compared to the baseline. Other objectives relate to the minimisation of the Cost of Energy (COE) (Jureczko & Mrówka, 2022). The cost of energy in the context of wind energy is the ratio of the total cost of a wind turbine to the annual energy production. The Annual Energy Production (AEP) is a metric that captures the yearly power yield of a turbine, typically measured in MWh or GWh, while accounting for the wind speed probability distribution specific to a given site.

The main structural design objectives are maximum stiffness and minimum blade mass (Söker, 2013). Maximum stiffness can be related to another important constraint which is tip deflection. In fact, sufficient clearance between a blade and a tower shall be ensured. Other structural requirements relate to fatigue loads, structural integrity such as maximum strain and buckling, and dynamic stability. As such, additional objectives could be related to the optimisation of those structural performances (e.g. stresses in the structure, root bending moments, eigenfrequencies), with constraints on fatigue damage allowed, buckling performance, and logistic constraints (e.g. maximum component size) (Chetan et al., 2019). Overall, the certification design requirements of wind turbines are presented in the IEC 61400-Series.

In general, two regions can be defined over a blade span. The inboard blade section, extending to approximately a third of a blade span, is usually designed dominantly for structural considerations. For the remaining two-thirds outboard, aerodynamics typically dominates over structural requirements (Mølholt Jensen & Branner, 2013). Blade cross-sectional design can generally be categorised in two topologies, as reported by Ashwill (2010b): either as a spar-shell configuration, where the spar is the primary structure and the aerodynamic profile is provided as a secondary structural element, which is illustrated in Figure 2.1a; or as a stressed-shell configuration, where the aerodynamic shell becomes a primary structure, as illustrated in Figure 2.1b.

(a) Traditional blade section topology. Spar-shell blade architecture. Retrieved from B. F. Sørensen et al. (2004).

(b) Modern blade section topology. Stressed-shell blade architecture. Adapted from Ashwill (2010b)
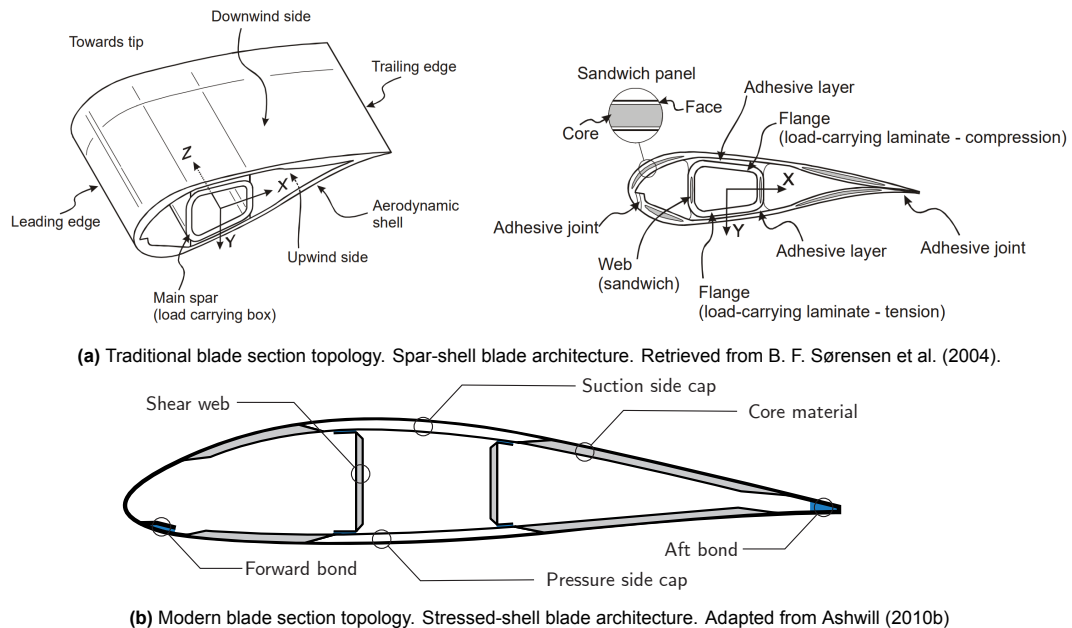
Figure 2.1: Wind turbine blade section topologies.

Modern blades commonly feature a stressed-shell configuration. In fact, this topology has a higher structural efficiency compared to the simpler spar-shell architecture, and it is therefore preferred for large rotors. A blade is generally a hollowed, thin-walled structure. Typically two shells are used to characterise the aerodynamic profile, one for the suction side (i.e. down-wind, also referred to as leeward shell) and one for the pressure side (i.e. up-wind, also referred to as windward shell). The load-carrying elements typically consist of two spar caps, each infused in the suction and pressure side shells for the stressed-shell architecture, combined with one or multiple shear webs connecting the suction and pressure side shells. The critical structural elements are commonly the spar caps (Chetan

et al., 2019; Nijssen & Brøndsted, 2013) because these elements carry the normal loads generated due to the flapwise bending of the blade. Flapwise and edgewise bending moments are moments that deform the blade out of the rotor plane and within the rotor plane, respectively (M. O. L. Hansen, 2015). Flapwise deformation can be understood as a deformation perpendicular to the chord line of a blade airfoil section, whereas edgewise deformation is a deformation parallel to the chord line of a blade airfoil section (Griffin, 2004). The flapwise bending direction is illustrated along with the edgewise one in Figure 2.2.

Figure 2.2: Edgewise (left) and flapwise (right) blade deformations. Retrieved from Barnes et al. (2015).

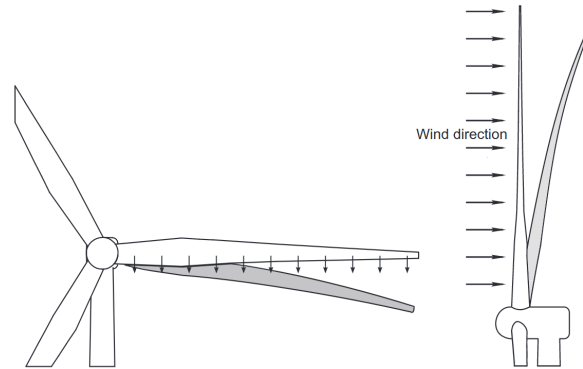Regarding the material used, the shells and shear webs are usually sandwich materials, with a core made out of balsa wood or foam, and facesheets out of composite laminates. The aerodynamic shells are primarily designed against buckling (Mishnaevsky et al., 2017). The spar caps are typically monolithic laminates of unidirectional material in the spanwise direction. The spar laminates are generally tapered towards the blade tip, with most plies running from the root partly all the way to the tip, following the aerodynamic bending moment distribution (Mishnaevsky et al., 2017; Nijssen & Brøndsted, 2013).

With respect to manufacturing techniques, resin infusion is generally preferred, especially for increasingly large modern blades. Lately, automated tape lay-up and fibre placement are considered to achieve cost reduction and quality improvements (Mishnaevsky et al., 2017). Related to manufacturing, Nijssen and Brøndsted (2013) estimated the cost of a composite blade to be 5-10 €/kg. An estimate of a typical blade material cost breakdown showed that the spar caps amount to more than 60%, and skin laminates to about 16% of the total material cost (Nijssen & Brøndsted, 2013). Therefore, optimisation of the material used in skins and spar caps can lead to cost reduction as those regions amount to the majority of the total material cost of a blade.

The typical wind turbine blade failure modes of interest are buckling and material failure. Nevertheless, for modern blades, due to important bending moments, large deformations of a blade cross-section are critical. This flattening effect of a hollow structure under crushing pressure is referred to as the Brazier effect (Mølholt Jensen & Branner, 2013).

2.2. Aeroelastic Rotor Design

Composite materials show numerous benefits in wind turbine blade design. Those materials allow for superior fatigue characteristics compared to metals, higher stiffness-to-weight ratio, and potential for aeroelastic tailoring. The potential for aeroelastic tailoring is explained by the anisotropic properties of composite materials. In fact, the stiffness of a blade can be adapted over both its cross-section and along its span by selecting appropriate ply angles, thicknesses, and lay-up sequences. This characteristic allows the introduction of aeroelastic tailoring in a blade. Aeroelastic tailoring is formulated as the approach exploiting the elastic deformation of a blade under aerodynamic loads (Ashwill, 2010a; Barr & Jaworski, 2019; Lobitz et al., 2001). Lobitz et al. (2001) namely stated that Bend-Twist Coupling (BTC) can be introduced to leverage aeroelastic coupling, to enable blade deformation that would dampen fluctuating and extreme loads.

Adaptive wind turbine blade design can be categorised into two approaches, as follows:

- **Through material design |** Also referred to as elastic coupling or material BTC; by exploiting material anisotropy, blade twist under bending loads can be achieved namely by placing fibres off-axis relative to the blade axis (Bottasso et al., 2013; Veers et al., 1998).

- **Through geometric design |** Also referred to as geometric coupling; by sweeping the blade planform, aeroelastic coupling can also be achieved. In fact, twist can be achieved from the additional moment generated by the swept shape (Ashwill, 2010b; Zuteck, 2002).

Anisotropy can namely be induced through the design of Variable Stiffness (VS) composites, as will be introduced in Chapter 3. With variable stiffness, fibre orientation in a laminate is spatially varied over the composite. With a spanwise variation of blade stiffness, blade twist can be affected, which in turn directly influences the loads and generated power, through a change in angle of attack. For large angle of attack gradients, average loads, power, as well as load oscillations are affected. The amplitude and frequency of those oscillations affect in turn the fatigue loads (Lobitz et al., 2001; Nijssen & Brøndsted, 2013).

Among others, Bottasso et al. (2013), Lobitz et al. (2001), McWilliam et al. (2018), and Zahle et al. (2016) discussed that aeroelastic tailoring is by definition a multidisciplinary problem, as aeroelasticity considers the interaction of elastic structures in an airflow. Lobitz et al. (2001) recognised that this multi-disciplinary problem shall accommodate for conflicting demands such as enhanced energy yield, vibratory response, and load reduction, while considering constraints on aeroelastic stability, resonances, blade mass and aerodynamic profile.

Through adaptive blade design, passive load mitigation can be achieved. Passive load mitigation is shown to be an attractive strategy as it does not require actuation systems. As mentioned by Bottasso et al. (2013), the cost of wind energy benefits from simplicity, low maintenance and high availability of the system. In contrast to pitch actuation, BTC is capable of reacting to sudden gusts as sudden flapwise deflection would induce twisting that can reduce the loads. Reduction in both fatigue and extreme operating loads can be achieved through adaptive designs as demonstrated by Ashwill (2010a).

Conversely, passive load mitigation strategies often suffer from an increase in blade mass, an increase in manufacturing complexity, and thereby an increase in cost (Bottasso et al., 2013). Furthermore, regarding material-adaptive blade design, the presence of anisotropy in the blade materials can be shown to reduce flapwise bending stiffness as fibres are purposely placed off of the blade axis. This reduction in flapwise stiffness often increases maximum blade tip deflection and shifts the placement of the flapwise natural frequency with respect to operational frequencies, which can induce resonance issues (Bottasso et al., 2013).

3

Composite Laminate Design Concepts

Composite materials benefit other engineering materials from their anisotropy, high stiffness-to-weight ratio, high strength-to-weight ratio, and tailoring opportunities. As discussed in Chapter 2, composite laminates have mechanical properties that are loading direction dependent. Those structures can therefore be tailored by adjusting the geometrical and mechanical properties of the laminates.

In a laminate, each lamina can take any orientation, that is to be set by the designer. A lamina, also referred to as a ply, is said to be orthotropic as there exist three orthogonal axes with distinct mechanical properties. It is common practice to prefer the use of $\{0°, \pm45°, 90°\}$ ply orientations, namely due to certification and manufacturing constraints (Stanford et al., 2014). Such laminates are referred to as conventional composite laminates.

Conventional laminates however suffer from a limited design space, due to the limited set of fibre orientations. Non-conventional composite laminates allow to further exploit the tailoring potential of composite materials. Tailoring of non-conventional laminates can be achieved in several approaches, defined as follows:

- **Constant stiffness non-conventional laminate |** By extending the set of fibre orientation angles, a laminate can feature additional fibre angles, thus widening the design space. This category specifies "constant stiffness" as one assumes the fibre angle is kept constant in each ply, hence giving the laminate a constant stiffness.

- **Variable stiffness non-conventional laminate |** In contrast to the previous category, "variable stiffness" is specified, as the fibre angle is allowed to spatially vary throughout the laminate, thus producing a variable stiffness laminate. Two methods achieving this variable stiffness concept are fibre steering (i.e. continuous fibre angle variation), and laminate blending (i.e. multi-patch laminate), as illustrated in Figure 3.1. The former allows fibre orientations to continuously vary in a laminate. The latter consists in partitioning a laminate, with each section having its own stiffness characteristics. The regions are then blended in a coherent laminate. Laminate blending refers to the process of restoring continuity between adjacent stacks in a multi-sectional composite laminate, as first introduced by Zabinsky (1994). This blending is paramount to ensure manufacturability and structural integrity of the structure.

The advantage of variable stiffness laminates lies in a higher achievable degree of tailoring in a structure compared to conventional laminates. Considering aerospace structures, such as wind turbine blades or aircraft wings, uniform load distributions are rarely experienced. Instead, those structures are often subjected to varying loads, namely in spanwise direction (Söker, 2013). Therefore, stiffness and strength requirements throughout a structure vary, making the use of conventional laminates an over-conservative design, and in most cases, a heavier design. Alternatively, variable stiffness laminates can satisfy the local stiffness and strength requirement, hence achieving further tailoring, and allowing load redistribution within a laminate. Even though most design approaches currently use fibre steering as a mean to apply in-plane stiffness variation, laminate blending suggests attractive characteristics as
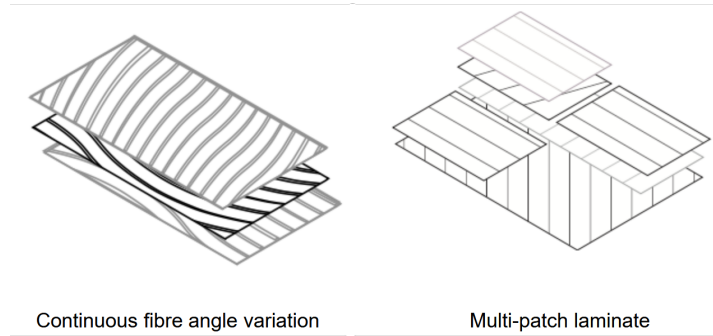
| Continuous fibre angle variation | Multi-patch laminate |

Figure 3.1: Variable stiffness non-conventional laminates. Retrieved from van den Oord and van Campen (2020).

will be discussed in Section 4.3.2.

The challenge with multi-patch laminates lies in finding the optimal blending configuration that will ensure stacking sequence compatibility, manufacturability, and structural integrity of the structure. The objective of multi-patch laminate design is to achieve the lowest mass laminate by establishing the stacking sequences of discrete design regions while complying with structural and manufacturing constraints. This is however a complex problem due to the global constraint induced by the fact that the optimal stacking sequence of a given patch in the blended laminate depends on that of the adjacent design regions. Furthermore, laminate blending suffers from the curse of dimensionality as, for increasing number of design regions, the number of design solutions increases exponentially (van den Oord, 2018). Therefore, the author argued that for an increasing number of regions, the effectiveness of the blending algorithm is critical to achieve a locally optimal blended laminate. Complex structures can require a large amount of design regions.

Since the introduction of the concept of laminate blending by Zabinsky (1994), several blending rules and approaches have been proposed in the literature. Two blending rules defined by van Campen et al. (2008) allow for a wider design space compared to previous formulations, without the need to adjust manufacturing methods:

> **Generalised blending definition:** *"We consider two adjacent panels completely blended if all the layers from the thinner panel continue in the thicker one regardless of their position along the thickness of the laminate."* (van Campen et al., 2008)
> **Relaxed generalised blending definition:** *"We consider two adjacent panels completely blended if there are no dropped edges in physical contact."* (van Campen et al., 2008)

An illustration of those two blending definitions is provided in Figure 3.2. The generalised blending rule namely specifies that plies occurring in the thinner of two segments shall also occur in the thicker segment. Essentially, this statement specifies that only plies in the thickest of two sections can be terminated. The relaxed generalised blending rule expands further the design space and specifies that a laminate is blended for ply-drops in any of two adjacent segments considered, with the only requirement being that a ply drop is always left open or covered by a continuous ply. This statement essentially enforces that no butted edges shall be present. In the present report, butted edges characterise lamina edges that are in physical contact.
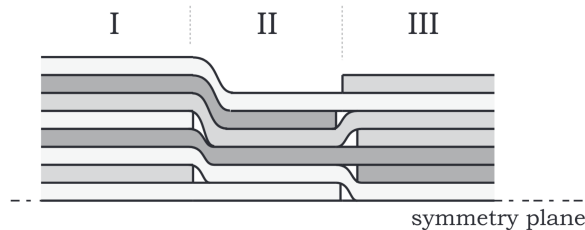
Figure 3.2: Example of generalised (segment I-II) and relaxed generalised (segment II-III) blending definitions. Retrieved from van Campen (2011).

Top-view of a 3x4 regions laminate

Cross-sectional view (Section A-A)
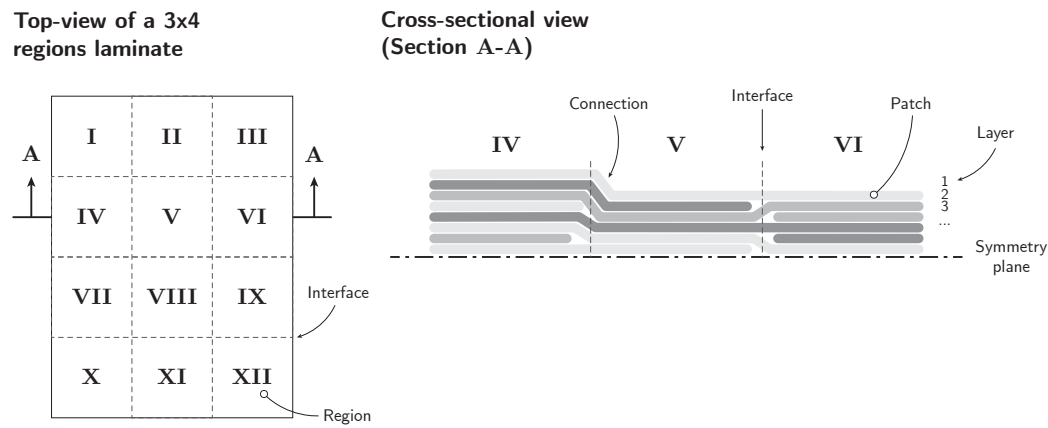
Figure 3.3: Illustration of the top view (left) and cross-section (right) of a three-by-four regions laminate, highlighting the terminology used for Straight-Fibre Variable Stiffness laminates.

Provided with the main concepts related to variable stiffness non-conventional laminates, one can introduce the concept of Straight-Fibre Variable Stiffness (SFVS) laminates. This type of variable stiffness laminate can be defined as a multi-patch laminate following the relaxed generalised blending rule. The terminology used in the design of such structures is illustrated in Figure 3.3, based on the terminology defined by Roepman (2021). The following nomenclature will be relevant in the subsequent analyses:

Region   Portion of a laminate that features a constant stacking sequence.

Layer   Smallest entity of a laminate region that has a constant fibre angle.

Patch   A set of layers that are connected together as they share a common fibre orientation. Patches define how layers from a region are connected to other regions.

Interface   Transition area among adjacent regions. An interface is the location between regions where a layer either stops or connects to another region to form a patch.

Connection   Interface of two layers belonging to the same patch.

Guide   A stacking sequence that is unique in a laminate and which can be applied to at least one laminate region.

State-of-the-Art on Aeroelastic Blade Design and Straight-Fibre Variable Stiffness Design Frameworks

With some background on the design drivers for wind turbine blade design, and on the opportunity to exploit further the potential of composite materials through variable stiffness approaches, the concepts and approaches currently used for blade aeroelastic tailoring will be reviewed in Section 4.1. A distinction can be made between literature that performed parametric studies, and those which developed optimisation frameworks to tackle Bend-Twist Coupling (BTC). Table 4.1 provides a schematic representation of the belonging of the cited references to each category. It is argued in the literature that to fully understand the effect of variable stiffness laminates in wind turbine blade design, Multidisciplinary Design Optimisation (MDO) shall be preferred, due to the nature of aeroelastic tailoring. McWilliam et al. (2018) argued that optimal blade design can only be achieved by evaluating a combined set of interacting constraints, namely through MDO. The present literature study will therefore focus on several MDO approaches. In the subsequent paragraphs, the optimisation objective is specified preceding the appropriate research. Aside from aeroelastic tailoring approaches, literature investigating alternative blade topologies are presented in Section 4.2. Finally, in Section 4.3.2, the approach developed to achieve laminate blending for a large number of design regions will be introduced, along with experimental results of a multi-patch laminate demonstrator.

Table 4.1: Aeroelastic tailoring literature matrix. MA stands for Material Adaptive coupling; GA stands for Geometrical Adaptive coupling.

Coupling Type	Parametric Study	MDO
MA	Capellaro (2012), Griffin (2002), and Stanford et al. (2014)	Barr and Jaworski (2019), Bottasso et al. (2013), and Scott et al. (2017)
GA	-	Ashwill (2010b) and Zahle et al. (2016)
Combined	-	Abdalla et al. (2017), Ashwill (2010a), Capuzzi et al. (2015), McWilliam et al. (2018), and Scott et al. (2017)

4.1. Multidisciplinary Design Optimisation for Aeroelastic Tailoring

The concepts and benefits of aeroelastic tailoring of wind turbine blades were introduced in Section 2.2. In the present section, several approaches developed to achieve such adaptive designs are presented.

A review on the research conducted prior to 2001 on composite coupling in wind turbine blade for enhancing the performance of Horizontal Axis Wind Turbine (HAWT) was provided by Lobitz et al. (2001). The authors outlined that passive load mitigation through composite coupling can mitigate
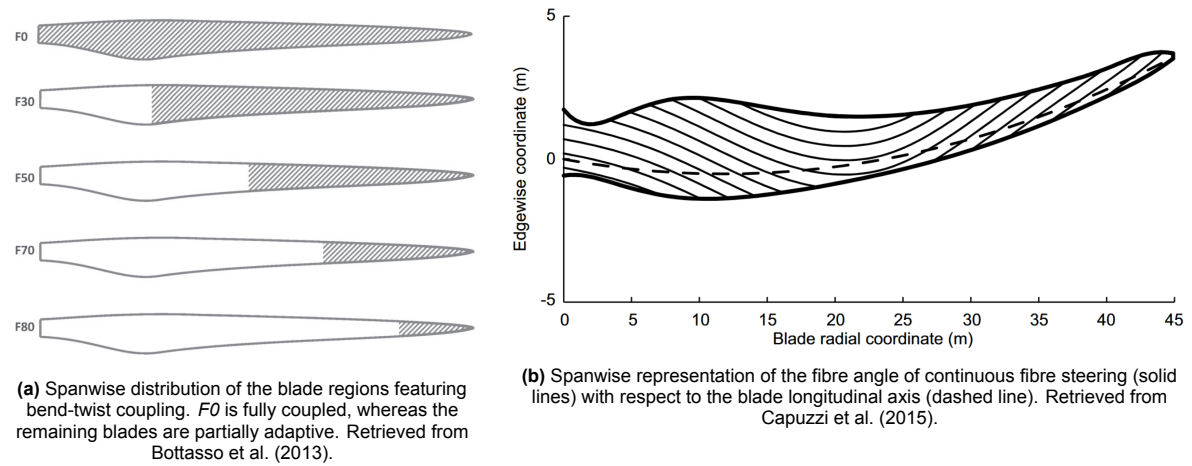
(a) Spanwise distribution of the blade regions featuring bend-twist coupling. *F0* is fully coupled, whereas the remaining blades are partially adaptive. Retrieved from Bottasso et al. (2013).

(b) Spanwise representation of the fibre angle of continuous fibre steering (solid lines) with respect to the blade longitudinal axis (dashed line). Retrieved from Capuzzi et al. (2015).

Figure 4.1: Spanwise representation of bend-twist coupling and steered fibre angle along a wind turbine blade.

aerodynamic loads by twisting towards feather (i.e. a twist motion unloading a blade), without reducing the average power. This results in substantial reductions in both extreme and fatigue loads by reducing the cyclic blade loading (especially for variable-speed pitch-controlled rotors). Besides, divergence and classical flutter are shown to become less stable for twist-coupled blades.

Blade Mass Minimisation

Bottasso et al. (2013) contributed to understanding the effect of material BTC in blade design through an MDO approach. The objective of the optimisation is the minimisation of the total blade mass, as it is argued by the authors to be a good overall indicator of cost, as a reliable cost model was not available to them. To benefit blade mass, the authors showed that fibre rotations in both skin and spar caps should be preferred. Besides, to reduce blade mass, partial BTC is suggested over fully anisotropic blades (i.e. avoiding fibre rotations from the blade root to about the span of maximum chord, as illustrated in Figure 4.1a). This can be explained as the design drivers for the considered blade are maximum tip deflection and blade natural frequency, both of which depend on the blade stiffness. Stiffness reduction is induced by off-axis fibre placement required to achieve BTC. In addition, it is argued that the thickest sections typically suffer from fatigue damage, thus promoting bending stiffness rather than BTC performance close to the root is reasoned to be beneficial to comply with fatigue constraints without the need for increased laminate thickness. Therefore, limiting fibre rotation in selected spanwise sections is preferred to mitigate these effects. Finally, the multidisciplinary design optimisation showed that, through BTC, mean and fatigue load reduction is achieved. Besides, reduced pitch actuation was achieved. The authors argued that, from the load reduction achieved through BTC, a larger rotor design could be considered, hence achieving an increase in AEP. This potential increase in energy production was however not investigated. They also recognised that there is an interest in investigating the optimisation of the spanwise distribution of couplings (i.e. to adjust the fibre orientations in different blade segments). In fact, the authors conclude that the use of spanwise varying fibre angles could benefit further the performance of wind turbines. Finally, the need to further research the performance of BTC while accounting for manufacturing constraints was recommended. Those manufacturing constraints were however not specified by the authors.

Cost of Energy Minimisation

Abdalla et al. (2017) recognised that BTC has the benefit of reducing the cost of wind energy by removing rotating parts (i.e. pitch control), thus reducing operational and maintenance costs. The authors therefore developed an aeroelastic optimisation framework to investigate the aerodynamic performance for power regulation of a stall-regulated wind turbine blade using variable stiffness laminate design, both along blade span and cross-section. The objective function of the optimisation was the cost of energy (COE), based on an adapted cost model of the National Renewable Energy Laboratory (NREL), with constraints on maximum power, tip deflection, strain and buckling. The NREL-5MW blade design was used as the baseline design. The authors have shown that, depending on the maximum power require-
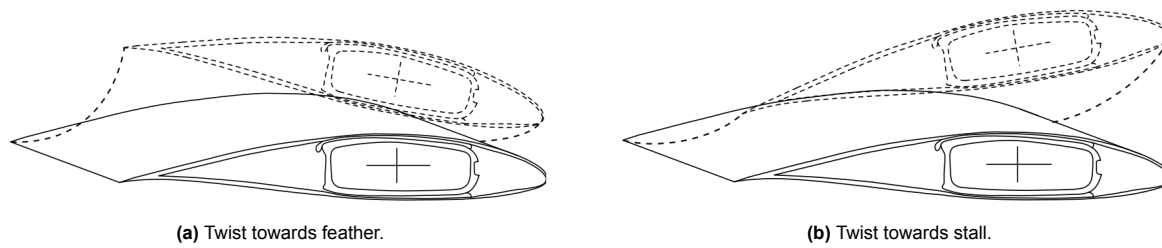
(a) Twist towards feather.   **(b)** Twist towards stall.

Figure 4.2: Bend-twist coupling response of a wind turbine blade. Retrieved from Fedorov (2012).

ment, a decrease in COE and blade mass is achieved. In fact, despite a decrease in AEP, a reduction in blade mass and in Initial Capital Cost (ICC) is achieved with variable stiffness laminate along the blade span. The reduction in mass is argued to originate from a reduction in lift which is driven by an increase in angle of attack due to the aeroelastic response of the blade. Even though the reduction in lift allows for a lighter design, it also has the downside of reducing the AEP. The authors recommend the development of a more elaborate cost model to evaluate the ICC.

Annual Energy Production Maximisation

Following on the recommendation made by Bottasso et al. (2013) to investigate the benefit on AEP, McWilliam et al. (2018) developed an MDO to investigate the combined effect of BTC on blade design. A 100kW pitch-regulated turbine is considered in their study. The optimisation aims for maximising AEP while avoiding load increase. The authors have shown that, while excluding manufacturing constraints (i.e. limits for sweep and prebend), material-adaptive designs must decrease the flapwise stiffness to increase the coupling, whereas geometric-adaptive design (i.e. sweep) achieves an increase in coupling without this trade-off. As such, the authors quantify that, for the considered blade, sweep is 59% more efficient than material coupling to achieve greater AEP. While considering manufacturing constraints, the optimal design achieved lower improvements compared to the unconstrained designs relative to manufacturing considerations, yet improved compared to the baseline.

Barr and Jaworski (2019) considered a static aeroelastic optimisation of the fibre orientation distribution in the blade skin and spars. With the NREL 5MW wind turbine blade as a baseline, fixing the blade geometry, mass distribution, and material properties, the spanwise distribution of variable stiffness composite fibres was optimised at discrete wind speed below rated condition. The objective is to maximise the aerodynamic torque, hence increasing energy capture, by twisting the blade towards stall. The authors have shown the potential of variable stiffness composite fibres in wind turbine blades in improving power extraction while avoiding stall at higher wind speeds with spanwise variable stiffness blades. This was achieved with the spanwise variation in fibre angle relative to the blade axis, twisting the inboard section towards stall, while twisting the outboard blade towards feather, thus avoiding stall in the most productive region of a blade, being the outboard section. Twisting towards stall and feather is namely illustrated in Figure 4.2. Recommendations are made by the author to improve the representation of the internal structure of the blade and material properties, specifically to account for structural constraints such as buckling and ultimate strains.

Several authors have investigated bend twist coupled blade optimisation by performing the aerodynamic and structural design separately, namely as performed by Capuzzi et al. (2014a) and Capuzzi et al. (2014b), respectively. The former research focused on evaluating target twist distributions that maximise power yield at different operating conditions. Then, the latter research focused on the structural design of an adaptive blade, through the blade spar design, that achieves the target elastic twist distribution aligning the blade for the ideal aeroelastic response, while also providing gust load alleviation capability. The blade adaptive behaviour is designed into the spar, through the use of material (i.e. off-axis fibres) and geometric (i.e. swept planform) adaptive techniques. The structural analysis included a detailed strength and buckling design, which was carried out in a later research by Capuzzi et al. (2015). In all those studies, the authors have improved on the research by Bottasso et al. (2013), namely by investigating the use of variable stiffness composite fibres, as illustrated in Figure 4.1b, rather than maintaining constant spanwise fibre orientations.

Multidisciplinary optimisation allows to systematically evaluate and balance conflicting objectives, which

is relevant for aeroelastic blade design. An optimisation framework that allows such concurrent design of the internal and outer geometry of a blade was developed by Zahle et al. (2016), Zahle et al. (2015) and is referred to as *HawtOpt2*. This MDO framework was developed based on the open-source optimisation framework *OpenMDAO* (Gray et al., 2019) to couple aeroelastic and structural solvers. The finite-element cross-sectional analysis tool BECAS (Blasques, 2012) is used as the structural solver, to evaluate the mass and structural section properties, and the material failure due to fatigue and extreme loads. Besides, *HAWC2S* (Larsen & Hansen, 2007) and *HAWC2* (M. H. Hansen et al., 2018) are used for steady-state and time-marching aeroelastic calculations, respectively. The capabilities of the developed methodology were demonstrated by the aeroelastic tailoring of the DTU 10MW reference wind turbine to achieve maximum AEP while constraining the design loads to the baseline load envelop. An increase of more than 8% in AEP is achieved for the tailored blade.

4.2. Alternative Blade Topologies

Besides the conventional blade structural architecture introduced in Section 2.1, research has been performed on alternative wind turbine blade topologies. Several alternative designs were deemed relevant to the present research, namely for their improved structural performance.

4.2.1. Spanwise Material Variation

As previously argued, for increasingly large rotors, blade mass becomes an important design driver. This was especially observed by Joosse et al. (2002), who considered alternative blade design for cost-effective application of carbon fibre in rotor design, as this material was expected to achieve cost-effective mass reduction and stiffness improvements. The authors have shown, using the rotor design optimisation software *BLADOPT*, for minimisation of COE, that a carbon fibre spar could achieve 38% reduction in mass and a 14% decrease in cost relative to the baseline 120 m glass fibre blade.

Since carbon fibre used in the spar of the blade was identified to achieve cost-effective weight reductions and stiffness improvements, Griffin and Ashwill (2003) performed a parametric study to investigate the sensitivity of blade root moments and tip deflection to the spanwise extend of carbon fibre in the spar structure. The authors showed that edgewise Blade Root Moment (BRM) reduction is most effectively achieved for carbon fibre placement in the outer blade span. This result can be explained as, when carbon fibre use is further extended inboard, even though further mass reduction is achieved, the moment arm to the blade root section reduces, hence rendering diminished effects on the gravity-induced moment reductions (i.e. edgewise BRM). Similar results were obtained while considering normalised tip deflection with mass increase, where greater tip deflection reduction is achieved for carbon fibre use solely in the outer part of the blade. In fact, the gravity-induced moments are shown to be more effectively reduced by mass reduction on the outer part of a blade. Griffin (2004) further argued that mass reduction in the outboard region of a blade is most effective on gravity-induced bending moments rather than an absolute blade mass reduction.

The use of carbon fibre on the outboard span of a spar is shown to be beneficial for gravity load reduction and tip deflections. Nevertheless, challenges in the transition from glass fibre to carbon fibre, such as mismatch in stiffness and strain-to-failure, are argued. The transition region was not designed in the research by Griffin (2004) and Griffin and Ashwill (2003), only candidate test coupons were proposed to understand the structural behaviour of glass fibre to carbon fibre laminate transition, and a four-point bending test setup was proposed to experimentally benchmark spar cap configurations.

4.2.2. Cross-sectional Material Variation

Besides the use of monolithic laminates in spar caps as introduced in the conventional blade cross-section (c.f. Section 2.1), the use of sandwich structures and other topologies are considered by Berggreen et al. (2007), Rosemeier and Bätge (2014), and Thomsen (2009) for blade spar caps. The interest in introducing sandwich panels in down-wind spar caps (i.e. mainly under compression) rather than conventional laminates is driven by the interest to improve spar cap buckling resistance for the increasingly large rotors (Thomsen, 2009).

Driven by the interest to investigate the potential improvement in buckling performance, the implementation of sandwich structure in spar caps design was analysed by Berggreen et al. (2007) through a parametric finite element model. A significant weight reduction and increased buckling performance
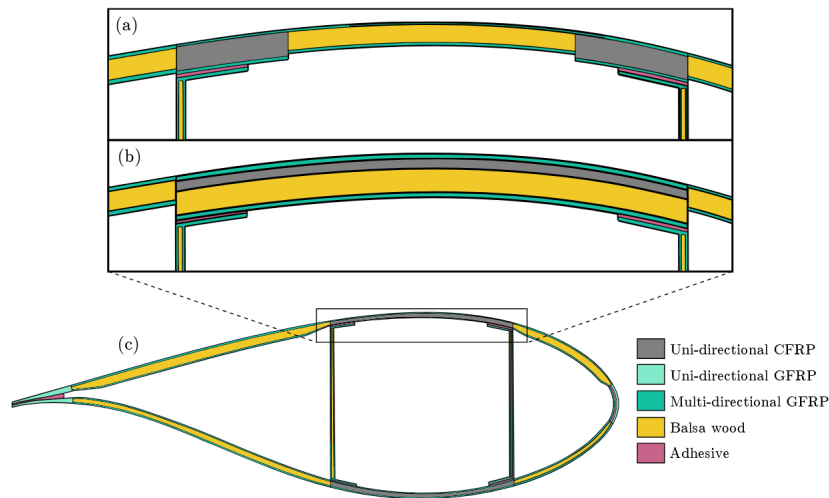
Figure 4.3: Spar cap topologies considered by Rosemeier and Bätge (2014): a) Split Spar Cap (SSC), b) Continuous Spar Cap (CSC), c) monolithic spar cap (baseline). Retrieved from Rosemeier and Bätge (2014).

were achieved with a sandwich concept compared to monolithic composite designs. The downside of a sandwich is a decrease in global bending stiffness induced by the sandwich spar, as stiff composite materials shift towards the section neutral axis due to the bottom facesheet, hence reducing the section bending stiffness. The benefit of increased buckling performance comes at the expense of reduced global stiffness, thus rendering further critical tip deflection.

Rosemeier and Bätge (2014) studied the influence on blade performances of various spar caps topologies to improve buckling stability. Conventional monolithic laminate spar cap is compared to a split spar cap concept, as illustrated in Figure 4.3, both of which use hybrid carbon glass fibre and sandwich structures. The blade properties considered were mass, tip deflection, and modal properties (i.e. first flap- and edgewise frequencies). The split spar concept was shown to achieve favourable results, with the lowest mass relative to other concepts, and increased edgewise stiffness, due to further material reinforcement achieved with unidirectional composites towards leading and tailing edges. The authors argued that from this improved edgewise stiffness, there is potential for material saving in leading and trailing edges.

4.2.3. Trailing Edge Reinforcement & Offset Spar Caps

Driven by the motivation to achieve mass reduction and cost-effective wind turbines, Buckney, Green, et al. (2013) have performed a topology optimisation to explore alternative structural configurations that would improve the structural efficiency of blades. Two distinct objectives were considered for the optimisation of a 45 m blade: either minimising the structural volume with a stress constraint, or minimising its compliance. The topology optimisation was performed under static failure, and maximum twist and deflection constraints. Both objectives display similar trends in the blade topology, which is illustrated in Figure 4.4 for the compliance minimisation objective. Through this topology optimisation, a spanwise varying blade structure was achieved, with a Trailing Edge Reinforcement (TER) inboard transitioning to an offset spar caps configuration. In fact, spar caps are shown to run along the span of the blade as in conventional design. However, the spar caps differentiate from conventional design as they are first located near the maximum thickness region inboard, then the suction-side cap shifts towards the trailing edge on the outboard blade section. Besides, TER is revealed at the trailing edge, which tapers towards the tip. The spanwise change in topology can be understood from the substantial changes in blade geometries (i.e. large changes in twist and relative thickness). The introduction of TER can be reasoned to improve edgewise stiffness, and shifting the section centroid towards the trailing edge, thus bringing the neutral axis closer to the reinforcement and thus reducing the stresses under edgewise loading. Furthermore, under flapwise and combined loading, the presence of TER is argued to increase the product moment of inertia, thus further aligning the neutral axis with the airfoil chord under flapwise and combined loading. With this change in neutral axis placement, the
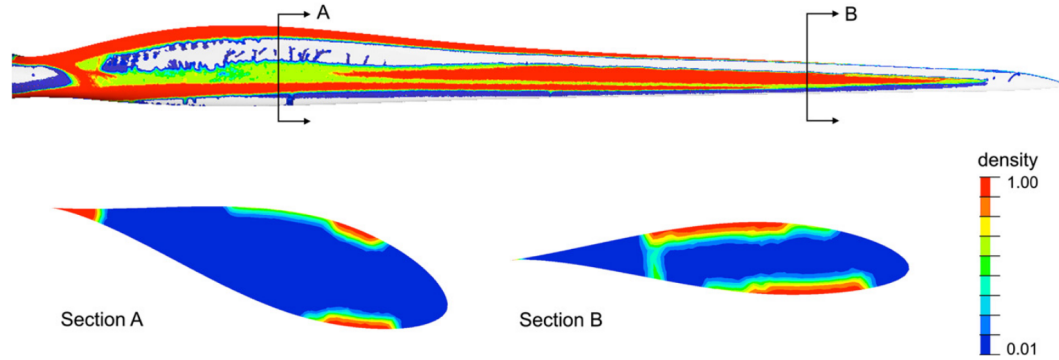
Figure 4.4: Result of the compliance minimisation topology optimisation by Buckney, Green, et al. (2013) showing the material density distribution. Spanwise view with density less than 0.05 hidden (top), and cross-sections at 25% (Section A) and 75% (Section B) radial positions. Retrieved from Buckney, Pirrera, et al. (2013).

bending stresses in the spar caps are reduced due to the reduced distance of the caps to the neutral axis. Two main regions are highlighted over the span: a stress-driven region inboard, with the TER achieving further strength-efficient design on the inboard first half of the blade (due to large thickness and twist); a stiffness-driven region outboard, with the offset cap topology on the remaining outer half of the blade (due to slender airfoil profiles). Besides topology optimisation, the authors performed a structural sizing optimisation to quantify the performance of TER design, with the objective to minimise mass under several constraints (static failure, fatigue failure, buckling, and deflection). In comparison to a conventional blade topology, the addition of a TER feature, in the form of a C-section web at the trailing edge, achieves more than 13% mass reduction in the modelled blade section. It was argued that such mass reduction was achieved due to the stabilisation of the spar caps thanks to the trailing edge reinforcement.

The offset spar cap topology as observed by Buckney, Green, et al. (2013) was previously discussed, namely in a parallel work by Pirrera et al. (2012). The authors have performed a structural optimisation on the topology of a spar-box configuration to achieve the lightest configuration at several radial positions. The spar section was set to be a quadrilateral section with corners placed along the aerodynamic profile, that shall accommodate for input aerodynamic loads while fitting in a given aerodynamic profile. The structural constraints considered are buckling and allowable strains. Each spar wall was assumed to be symmetric and the ply content was an additional design variable. The results presented were comparable to those of Buckney, Green, et al. (2013), where spar caps are located at the maximum thickness inboard, and then gradually offset from each other towards the tip. In fact, the webs are seen to lean towards the direction of maximum load, which is argued to maximise the moment of inertia of a blade section, and thus increasing its load-bearing capabilities. Two spanwise regions are defined by the authors, namely a strength-driven region outboard (as argued previously by Buckney, Green, et al. (2013)), and a buckling-driven region inboard.

4.3. Variable Stiffness Laminate Design Approaches

The formulation of variable stiffness composite structures, as introduced in Chapter 3, requires capturing the spatial variation of the structural properties in the problem parametrisation. If this spatial variation in structural properties is performed independently, impractical structures featuring discontinuities would be achieved. Based on the review by Ghiasi et al. (2010) on the design approaches for variable stiffness laminates, such a problem can be parameterised continuously or discretely. The former parametrisation for instance relies on the definition of fibre path as a continuous function and is referred to as curvilinear parametrisation. This approach is disregarded in the present report as the aim is to consider the design of variable stiffness laminates with the use of constant orientation plies, rather than continuously steered fibres.

4.3.1. Discrete Material Optimisation

The parametrisation of a structure in discrete regions is namely the focus of the Discrete Material Optimisation (DMO) developed by Lund and Stegmann (2005). This design approach for general laminated composite shell structures is based on the multi-phase topology optimisation approach. The mechanical property of each layer, namely their constitutive matrix, is evaluated as a weighted sum of those from a set of candidate materials. This formulation allows the definition of weight functions for these constitutive matrices as design variables, rather than controlling directly the fibre orientation. The design variables can thus be controlled as continuous variables for a set of materials, for which efficient gradient-based optimisation schemes can be applied. Besides, hybrid material structures can be achieved as both isotropic and orthotropic candidate materials can be specified. To steer the optimisation in the selection of distinct candidate materials, penalisation is originally used on the design variables to drive to zero all but one candidate to identify unique materials per layer. Further research performed by Hvejsel (2011) extends the discrete material selection through the definition of linear equality constraints.

The DMO approach is a single monolithic optimisation problem. This approach can therefore be argued to reach greater constraint satisfaction compared to a multi-step optimisation. Despite allowing for the optimisation of hybrid material variable stiffness laminates, the DMO approach suffers from a limitation in enforcing region continuity. It is recognised by S. N. Sørensen et al. (2014) that even though manufacturing constraints are enforced, adjacent layers with different fibre orientations are assumed perfectly bounded. The structure obtained through DMO can therefore suffer from discontinuity, among regions not sharing plies.

The design framework for straight-fibre variable stiffness laminates as presented hereafter enforces such continuity through blending constraints. A multi-step design approach is applied, allowing to tailor the parametrisation and optimisation scheme at each design stage. The parametrisation used in the straight-fibre variable stiffness tool essentially corresponds to that of the DMO approach, with regions within a structure of constant stacking sequence. The evaluation of the local optimal stacking sequence uses lamination parameters as design variables, which differs from the DMO method.

4.3.2. Straight-Fibre Variable Stiffness Laminate Design

Following the introduction of Straight-Fibre Variable Stiffness (SFVS) in Chapter 3, methods and potential for the use of laminate blending in aerospace structures are briefly reviewed hereafter. As discussed by van den Oord (2018), the challenge of laminate blending lies in minimising the number of design variables while keeping a reasonably large design space.

Several methods have been proposed to achieve laminate blending, but van den Oord (2018) was the first to propose a laminate blending algorithm capable of blending laminates with a large number of sections while satisfying the relaxed blending definition. The method proposed is a two-step approach defined as follows: first, the structure is subdivided into cells, also referred to as design regions, and a multi-chromosomal Genetic Algorithm (GA) (McMahon et al., 1998) is used to locally optimise the stacking sequence of each cell, with genotypes describing the stacking sequence of the patches. This step produces what is referred to as a local optimal design, as illustrated in Figure 4.5. In a second step, the locally optimised regions are fed through a Cellular Automaton (CA) to blend them and make a coherent structure, hence achieving a locally blended SFVS laminate, as illustrated in Figure 4.5.

Following with the model proposed by van den Oord (2018), Gomaa (2019) demonstrated that it is possible to manufacture a blended laminate that satisfies the relaxed generalised blending definition using a hand lay-up technique. The author experimentally showed the potential for blended laminate to have a significantly improved pre-buckling stiffness and critical buckling load when compared to a homologous constant stiffness panel, by achieving around 93% higher stiffness and about 81% higher critical buckling load. However, the author recommends improvements on the method, namely on the CA algorithm to guarantee locally blended configurations by further accounting limitations in manufacturing. This recommendation was also mentioned by van den Oord (2018). Furthermore, both authors recommended evaluating the method on more complex structures than plates under compression loads. In fact, since the relaxed generalised blending rule is implemented, a larger design space compared to alternative state-of-the-art methods is achieved, which may lead to an increase in the number of patches in a structure. The increasing number of patches and their distribution is expected to have an effect on
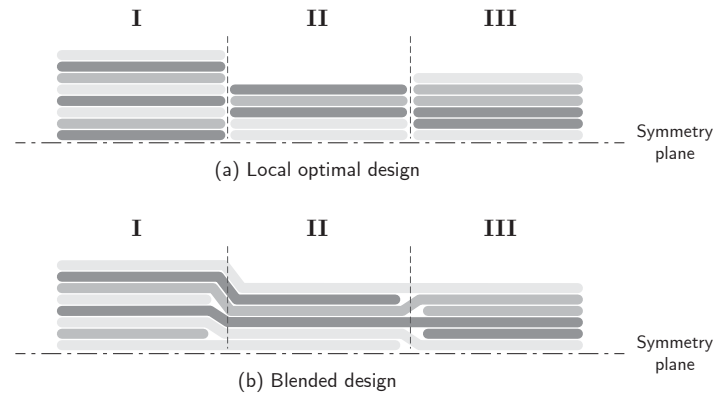
Figure 4.5: Illustration of a laminate cross-section at two stages of the blending process. Adapted from van den Oord (2018).

structural integrity, namely due to the increase in the number of ply drops. Ply drops affect structural integrity in several aspects. First of all, external ply drops shall be avoided as uncovered terminated plies are prone to delamination. In case ply drops are present within a laminate, those should be as close to the mid-plane of the laminate as possible, as recommended in the design practices defined by Kassapoglou (2013). Besides, the number of consecutive ply drops shall be limited, as they are a source of interlaminar stresses. Finally, the distance between successive ply drops is also critical as stress enhancement can occur among nearby ply drop sites. An illustration of various ply drop structures is provided in Figure 4.6.

Roepman (2021) further improved the design methodology to achieve manufacturable SFVS laminates with an automated framework. The four-step methodology gradually introduces blending and manufacturing constraints. The author has defined certain terminology for SFVS laminate design, which was introduced previously in Chapter 3, and illustrated in Figure 3.3. In the first stage, the stiffness of the individual regions of a laminate is optimised using lamination parameters, for instance for improved buckling performance. In the second step, the optimised stiffness distribution is converted from lamination parameters to stacking sequences for each region, using a genetic algorithm. Blending is introduced in the third step using a CA to connect the locally optimised regions. This CA extends the work by van den Oord (2018) and is segmented in three stages: 1) layers in neighbouring regions are first rotated to form patches; 2) then minimum cutting size constraints are defined to account for minimum manufacturable patch sizes; 3) lastly the number of butted edges is minimised by limited layer changes. Finally, once the locally blended design is achieved, the fourth step converts it to a globally blended one through global interpretation. The global interpretation approach forms patches, for which the stacking sequence and assembly sequence are characterised such that the laminate can be manufactured using current manufacturing techniques. The current manufacturing techniques considered are automated fibre placement, automated tape laying or manual pick and place.
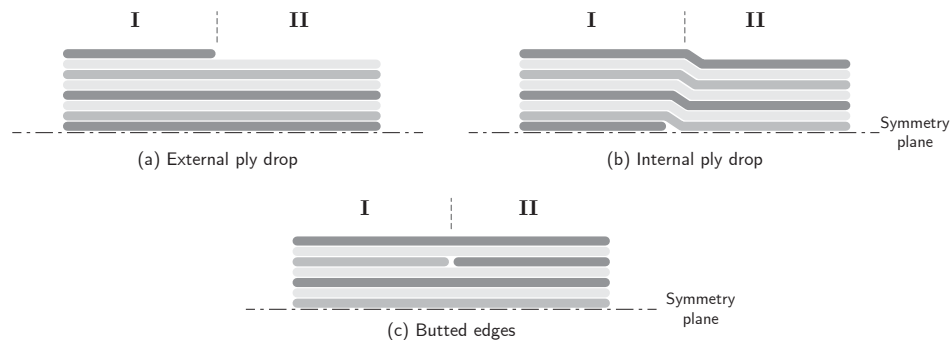

Figure 4.6: Ply drop configurations between neighbouring regions. Adapted from van den Oord (2018).

This novel methodology was then applied to maximise the buckling performance of plates under uniaxial compression and cylinders in bending. The author assumed the use of balanced and symmetric

laminates to reduce the complexity of the problem. With SFVS, load redistribution within the laminate enabled an estimated 42% increase in buckling performance, and an 11% decrease in mass, for the optimised plate compared to a conventional constant stiffness design. Regarding the laminated cylinder under bending, a 30% increase in buckling performance, and a 7% decrease in mass, were modelled compared to a constant stiffness laminate cylinder, which is an improvement of 1% in buckling performance relative to the current optimal design reported in the literature which uses fibre steering. The author recognised that improvements on the framework are required, namely on the convergence of the global interpretation. Besides, variable region layouts are recommended to be investigated to further provide freedom to the blending algorithm to limit losses in structural performance while converting lamination parameters to stacking sequence. With variable region layouts, one can understand the partitioning of a design in non-uniform regions. Finally, the author recognised the interest in applying the developed methodology to more complex configurations and multiple load cases, for instance in the design of aircraft structures such as wingbox and fuselage sections.

5

Scope and Aims of the Research

Based on the current knowledge gaps and research interests in the field of wind turbine blade design that were presented in the preceding sections, a research objective can be formulated. The present research is centred on straight-fibre variable stiffness laminates and undertakes the evaluation of their possible application in wind turbine blade structures. This study endeavours a wider adoption of such variable stiffness laminate design technique. The research objective is formally formulated as follows:

> *The research objective is to investigate the structural performance potential for straight-fibre variable stiffness laminates in wind turbine blade design by extending and coupling existing frameworks to incorporate these laminates at a large scale.*

In order to achieve this research objective, a collection of research questions was established. The main research question is formulated as follows:

> *How do straight-fibre variable stiffness laminates perform in wind turbine blade design depending on their location within the structure, namely in trailing edge panels?*

A set of sub-questions supporting the research objective are defined as follows:

- **Methodology |** How to couple the existing design framework for straight-fibre variable stiffness laminates with a wind turbine blade design tool? What iteration scheme is applicable to couple these frameworks?

- **Laminate Blending Algorithm |** How to expand the existing design framework for straight-fibre variable stiffness laminates for complex geometries?
    - How to formulate an optimisation problem to design a structure with variable stiffness to maximise the buckling load under a deflection constraint?
    - How to parameterise a blade structure for straight-fibre variable stiffness laminate design?
    - How to adapt the existing blending algorithm such that a multi-material stacking sequence can be defined?

- **Evaluation of blade performance |** What are the benefits of straight-fibre variable stiffness in a wind turbine blade section design?
    - Which blade component shall feature straight-fibre variable stiffness laminates?
    - Which reference turbine blade should be used?
    - Why could straight-fibre variable stiffness benefit trailing edge panel design?
    - Which blade performance metrics are relevant to benchmark the implementation of straight-fibre variable stiffness design?
    - What are the leverage points and challenges of the implementation of straight-fibre variable stiffness to blade design?

Part II

Method | Blade Patching Framework

6

Aero-Structural Optimisation Framework

In developing a framework to perform the design of an aeroelastic blade design with variable stiffness laminates, The coupling of two frameworks is considered. The first one enables the conceptual aeroelastic design of wind turbine blades. The second deals with the structural design of straight-fibre variable stiffness laminates. Prior to the definition of the coupling approach, the two tools considered in such coupling will be introduced. This chapter will provide further information on the aeroelastic blade design tool, referred to as the Aero-Structural Optimization Framework (AESOpt).

The AESOpt framework is a research tool developed at the DTU Wind Energy Department. This framework makes use of the open-source optimisation framework *OpenMDAO* by Gray et al. (2019) to set up the workflow. An overview of the full aero-structural optimisation methodology following the extended design structure matrix guidelines defined by Lambe and Martins (2012) is provided in Figure 6.1.
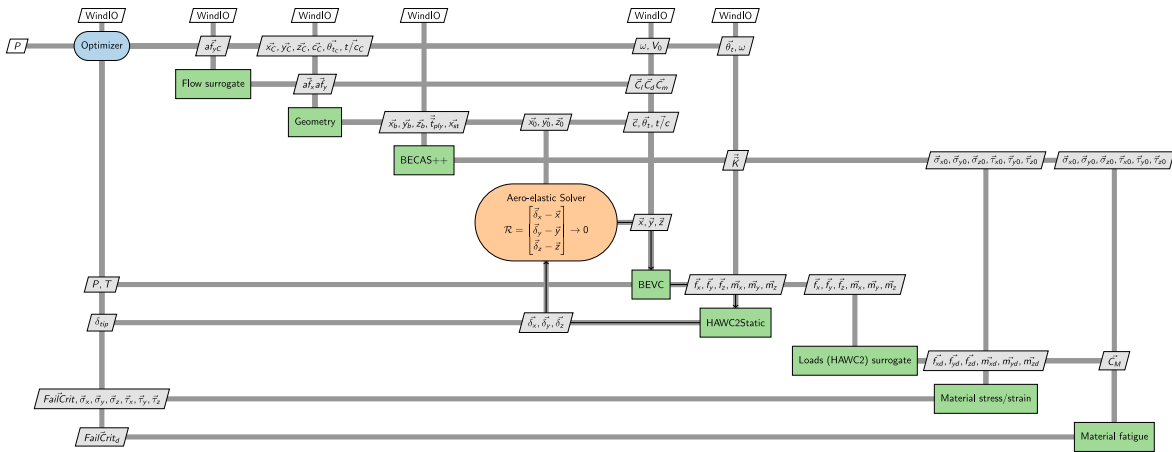
Figure 6.1: Extended design structure matrix of the full Aero-Structural Optimization Framework. Retrieved from the AESOpt documentation.

In the present study, structural design will be the main focus, and aerodynamic design is disregarded. The main reason is to limit the scope of the research. In fact, this research is a preliminary attempt to evaluate the performance of straight-fibre variable stiffness laminates when introduced to blade structures. Hence, to achieve a tractable design framework, pure structural optimisation is considered. This will further be discussed in Chapter 8. Following this simplification, several analysis blocks from the full AESOpt framework are disregarded. For instance, the wind turbine rotor aerodynamics solver (i.e. Blade Element Vortex Cylinder model, abbreviated as BEVC) is not considered, as well as the aeroe-

lastic solver, and flow surrogate model. As such, a simplified workflow is considered in the present research, which is presented in Figure 6.2 as a blade mass minimisation problem. The flowcharts presented in this report all comply with the convention presented at the beginning of this report.

Figure 6.2: Structural analysis workflow defined in the AESOpt framework.

The optimisation framework starts by retrieving the problem definition provided in an input file. The format used in the AESOpt framework is referred to as a WindIO file. This format is a recent ontology defined by the Interna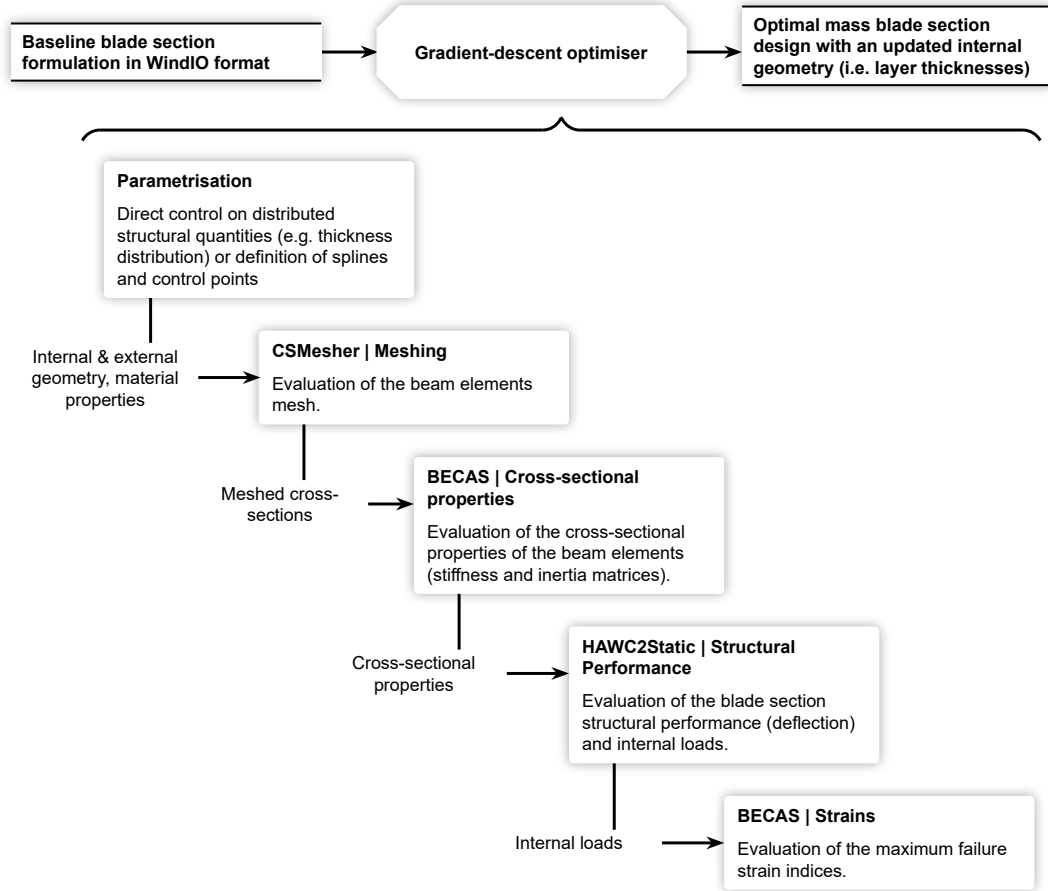tional Energy Agency Wind Task 37, namely to standardise the definition of wind turbine designs in the context of multi-disciplinary design and optimisation (Bortolotti et al., 2022). This WindIO format defines a common input-output data structure as a yaml file.

Once a baseline design is formulated, the loading condition, meshing options and optimisation settings are to be defined. The structural solver used in the AESOpt framework is a beam element model. As such, the beam element properties are to be evaluated. The stiffness and inertia matrices are computed with the cross-sectional analysis tool BECAS, which stands for BEam Cross-Section Analysis Software. Provided with a list of coordinates of a cross-section (e.g. airfoil coordinates), layup description and material properties, a cross-sectional mesher, referred to as CSMesher is used. CSMesher is tailored to feed cross-sectional mesh properties to BECAS. The latter then provides the stiffness properties of the cross-section considered, while accounting for geometrical and material coupling (Blasques, 2012).

The need to evaluate the beam element properties originates from the fact that wind turbine aeroelastic codes commonly rely on beam models. Beam models benefit from an attractive balance between computational efficiency and accuracy. The structural solver used in the AESOpt framework is that of the aeroelastic tool HAWC2, and is referred to as HAWC2Static. In such a solver, the blade is assumed to be a flexible body, and the nonlinear statics problem is solved as a beam model to characterise the deflection and twist under a prescribed aerodynamic loading. Regarding the aero-elastic solver used in AESOpt, it is a non-linear aero-elastic solver that converges the steady state between such beam

model structural solver, with an aerodynamic solver based on the beam element vortex cylinder method. In the present analysis, the aerodynamic solver will not be considered, as was introduced in Chapter 8. In fact, a blade section problem will be considered, and an aerodynamic loading will be frozen.

With a baseline problem defined and a structural solver setup, the design properties can be optimised. In this report, the optimisation has for objective to minimise the mass of a blade section. A gradient descent optimisation scheme is used, which is programmed with the SciPy Sequential Least Squares Programming (SLSQP) method. Gradients of the design variables are computed through finite differences, even though current efforts are made for the framework to support analytical gradients throughout.

The design variable is the thickness of each layer in all regions. The fibre orientation of the plies was also considered as a design variable, namely as it is expected to provide more design freedom. However, as an idealised flapwise bending-driven problem is considered, off-axis fibre orientations were not expected to be favoured. Besides, it was currently not possible to set fibre orientation as a design variable and only layer thickness was considered. Working in the OpenMDAO framework allows declaring splines that attach to inputs defined in the WindIO dictionary. Rather than modifying the thickness of each region individually, attaching a spline to parameters defining the distributed properties has the benefit of reducing the number of design variables, as well as producing smoother solutions. The layer thickness of each region was defined as a linear spline, with two control points defined over the span of the structure, one at the root, and the other at the tip. Design constraints were set on the minimum and maximum thicknesses that a layer can adopt. The objective of the optimisation is formulated in Equation 6.1. In this formulation, x is the design vector, which defines the layer thickness of each region of interest. Besides, m represents the structural mass evaluated for a given thickness distribution.

$$\min_{\boldsymbol{x}} \quad m(\boldsymbol{x})$$

$$\text{subject to} \quad \text{constraints on thickness bounds;} \tag{6.1}$$
$$\text{constraints on maximum strain failure indices;}$$
$$\text{constraints on tip deflection;}$$

Further design constraints were specified to render a reasonable design space. First, each layer is limited to a maximum strain failure index lower than one. The use of maximum strain failure theory was selected for its straightforward implementation. Besides, a constraint on the tip displacement of the structure is specified. In the present analysis, a constraint for the flapwise displacement is set to not exceed the baseline displacement in that direction, under the same loading, as introduced in Chapter 9.

The optimisation is terminated if the deflection of the optimum design is within a user-defined threshold. In order to further bound the design search, the number of iterations is tracked and a constraint is set on the maximum number of iterations that can be performed.

<div style="text-align: right">

7

</div>

Straight-Fibre Variable Stiffness Laminate Design Framework

This chapter will provide further information on the Straight-Fibre Variable Stiffness (SFVS) laminate design tool, also referred further to as the SFVS framework. An overview of the methodology is first provided, followed by a description of each step of the process.

7.1. Blending Design Framework

The design framework for straight-fibre variable stiffness laminates presented in this analysis is based on the work from Gomaa (2019), Roepman (2021), and van den Oord (2018). Extensions made to their tools will be the primary focus of discussion in the present report. For the design of SFVS structures, a four-step method was proposed by Roepman (2021). A schematic representation of this multi-step framework is presented in Figure 7.1.

The design framework is initiated by the definition of a problem. One should define the geometry as well as the loading condition and material distribution as a parametric finite element model. Once the problem is formulated, the first step is to evaluate the local stiffness requirement per region. In the present research, the local stiffness optimisation evaluates the set of lamination parameters for a given structural performance. Buckling load maximisation was the objective of the local stiffness optimisation by Roepman (2021). The framework has now been extended to minimise the structural deflection to a target level, while ensuring a positive buckling margin. Further discussion on the setup of the local stiffness optimisation approach is reported in Section 7.2.

Provided with an optimal set of lamination parameters for each region of the design, the second optimisation step is to retrieve discrete stacking sequences matching the lamination parameters design for each region. This conversion step uses a genetic algorithm based on the research of van Campen and Gürdal (2009). Further discussion on this second optimisation step is provided in Section 7.3. The stacking sequences retrieved in each region are evaluated for fitness compared to the optimal lamination parameter set. The fittest layups of each region are joined into a locally optimal stacking sequence design.

The locally optimal stacking sequence design obtained from the second step lacks structural integrity as ply continuity between the regions has not been enforced. To resolve this continuity issue, a cellular automaton based on the work of Roepman (2021) and van den Oord (2018) is employed to impose local blending constraints. Compliance with the relaxed blending guideline formulated by van Campen et al. (2008), and introduced in Chapter 3, is established. Further details on this local blending approach are discussed in Section 7.4.

Finally, from this locally blended design, a fourth and final optimisation step is undertaken. The objective is to provide a globally blended design, meaning a design complying with the relaxed blending guideline, as well as being manufacturable using current manufacturing techniques, either manual or automated,

such as automated fibre placement as well as pick-and-place techniques. The approach to enforce such global blending was developed by Roepman (2021), and relies on a connection search algorithm that formulates patches among plies that can be stacked monotonically. A description of this fourth step is provided in Section 7.5.

The result of this global interpretation step, and as such of the whole SFVS framework, is the definition of a straight-fibre variable stiffness laminate design complying with the relaxed blending guidelines. The globally blended design has a defined stacking sequence for each of its regions, patches are identified and the order of patch assembly is described.

<div style="text-align:center">

Problem Formulation

Geometry, material properties,
loading condition

↓

**Step 1 | Local Stiffness
Optimisation using Lamination
Parameters (LPs)**

Optimal local
LPs design

↓

**Step 2 | Local Stacking
Sequences (SS) Retrieval from
Optimal Lamination Parameters
Design**

Optimal local SS
design

↓

Step 3 | Local Blending Process

Locally blended
design

↓

Step 4 | Global Blending Process

Globally blended
design

↓

**Straight-fibre variable stiffness
laminate design**

</div>

Figure 7.1: Overview of the multi-step optimisation process for SFVS laminates design.

7.2. Step 1 | Local Stiffness Optimisation Process

The local stiffness optimisation is the first step in the formulation of a straight-fibre variable stiffness laminate design. To support the description of this optimisation step, Figure 7.2 is provided. The first step in the local stiffness optimisation is the definition of a parametric finite element model.
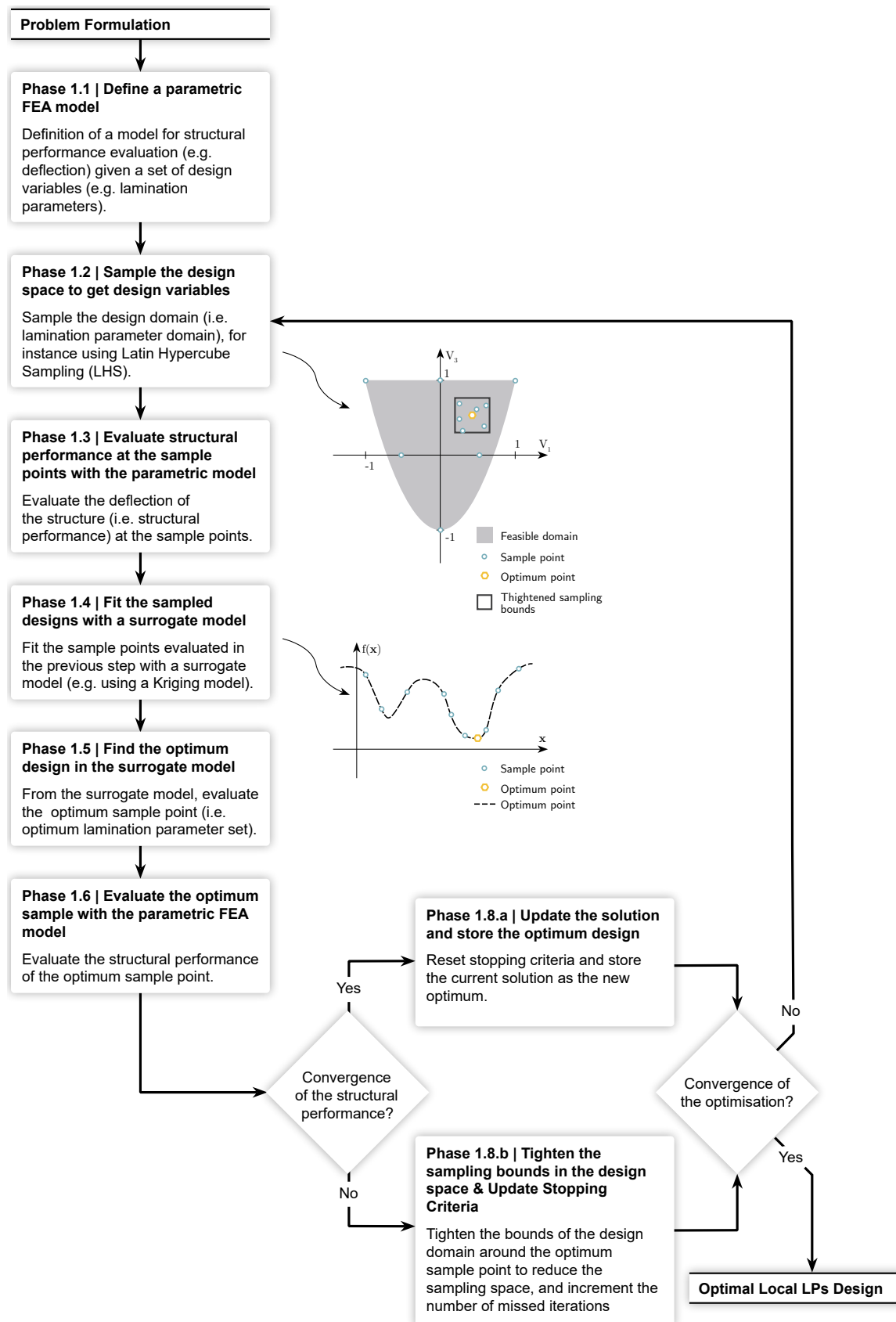
Problem Formulation

Phase 1.1 | Define a parametric FEA model

Definition of a model for structural performance evaluation (e.g. deflection) given a set of design variables (e.g. lamination parameters).

Phase 1.2 | Sample the design space to get design variables

Sample the design domain (i.e. lamination parameter domain), for instance using Latin Hypercube Sampling (LHS).

Phase 1.3 | Evaluate structural performance at the sample points with the parametric model

Evaluate the deflection of the structure (i.e. structural performance) at the sample points.

Phase 1.4 | Fit the sampled designs with a surrogate model

Fit the sample points evaluated in the previous step with a surrogate model (e.g. using a Kriging model).

Phase 1.5 | Find the optimum design in the surrogate model

From the surrogate model, evaluate the optimum sample point (i.e. optimum lamination parameter set).

Phase 1.6 | Evaluate the optimum sample with the parametric FEA model

Evaluate the structural performance of the optimum sample point.

Phase 1.8.a | Update the solution and store the optimum design

Reset stopping criteria and store the current solution as the new optimum.

Yes

No

Convergence of the structural performance?

Convergence of the optimisation?

No

Yes

Phase 1.8.b | Tighten the sampling bounds in the design space & Update Stopping Criteria

Tighten the bounds of the design domain around the optimum sample point to reduce the sampling space, and increment the number of missed iterations

Optimal Local LPs Design

Feasible domain
○ Sample point
○ Optimum point
□ Thightened sampling bounds

○ Sample point
○ Optimum point
--- Optimum point

Figure 7.2: Overview of the local stiffness optimisation process.

7.2.1. Parametric Finite Element Model

Pursuing the work by Roepman (2021), the use of a commercial finite element analysis tool is made to evaluate the structural performance of a given structure for a set of design variables. Abaqus was selected as this tool allows the use of Python to set up input files, as well as submitting, running and post-processing structural analysis results. This makes Abaqus ideal to define parametric finite element models that can conveniently be generated for a given set of design variables. In the present section, the problem formulation used to generate buckling and displacement analyses in Abaqus will be introduced.

Regarding the mesh element selection, a four-node shell element is used, denoted as S4 in Abaqus. Even though shell elements were shown to over-predict the torsional response of beams featuring bend-twist coupling (Fedorov et al., 2010), they are shown to perform well relative to continuum shell elements for buckling performance (Roepman, 2021). Furthermore, as for the DTU 10MW reference wind turbine, the reference surface for the shell elements was defined as the blade outer surface. In fact, as the profile geometry defines the outer surface of the blade, the shell elements have to be placed towards the inside of the section, to avoid changing the actual geometry of the airfoil.

In the current framework, the parametric model is to be defined for both a lamination parameter design and a stacking sequence design. This can be achieved in Abaqus through the definition of the element stiffness matrix for the former, and through the definition of a composite layup for the latter. In fact, for the lamination parameters design, the stacking sequence is yet unknown, and the general stiffness of elements can be provided as an input to the stiffness of a composite shell. The general stiffness matrix of a lamination parameter set is equivalent to the ABD matrix of this laminate, as provided by Equation 7.1 (Gürdal et al., 2010).

$$
\begin{aligned}
\boldsymbol{A} &= h\left(\boldsymbol{\Gamma_0} + \boldsymbol{\Gamma_1} V_1^A + \boldsymbol{\Gamma_2} \boldsymbol{V_2^A} + \boldsymbol{\Gamma_3} V_3^A + \boldsymbol{\Gamma_4} V_4^A\right) \\
\boldsymbol{D} &= \frac{h^3}{12}\left(\boldsymbol{\Gamma_0} + \boldsymbol{\Gamma_1} V_1^D + \boldsymbol{\Gamma_2} V_2^D + \boldsymbol{\Gamma_3} V_3^D + \boldsymbol{\Gamma_4} V_4^D\right)
\end{aligned}
\tag{7.1}
$$

The A, and D matrices are the laminate in-plane, and out-of-plane stiffness matrices, respectively. Please note that the coupling stiffness matrix B is not formulated here as balanced and symmetric laminates are considered, hence rendering this matrix to be zero. In Equation 7.1, h denotes the laminate thickness, $\boldsymbol{\Gamma_i} \ \forall \ i = [1, 2, 3, 4]$ denote the material invariant matrices. The formulation of these matrices of material invariants is namely provided by IJsselmuiden et al. (2010). Finally, $\boldsymbol{V_i^A}$, and $\boldsymbol{V_i^D}$ are the in-plane, and extension lamination parameters, respectively.

The benefit of using lamination parameters as a design variable in laminate stiffness optimisation lies in the linear dependence of the ABD laminate stiffness matrix on these material invariant matrices, scaled by continuous lamination parameters (Gürdal et al., 2010). The lamination parameters hold information on the fibre orientation, whereas information on the material properties is captured by the material invariant matrices.

7.2.2. Progressive Detailing Algorithm

A progressive detailing scheme, inspired by the work of Rouhi et al. (2017), is defined to optimise the local stiffness requirement per region. The optimisation consists in sampling a design space and evaluating the performance of those sample points. In the present case, the design space is the feasible domain for the four lamination parameters considered. In fact, the laminate design considered in the present report is limited to balanced and symmetric laminates. This assumption allows to reduce the number of lamination parameters from 12 to 4, being V_1^A, V_3^A, V_1^D, and V_3^D, and thus reduce the number of design variables. This can be explained as the four lamination parameters defining the coupling of the in-plane and out-of-plane behaviour become zero (i.e. $\boldsymbol{V_i^B} = 0 \ \forall \ i = [1, 2, 3, 4]$), the second and fourth component of the in-plane lamination parameters drop out (i.e. $V_2^A = V_4^A = 0$), and the second and fourth component of the out-of-plane lamination parameters become negligible (i.e. $V_2^D \approx 0$ and $V_4^D \approx 0$) (van Campen, 2011).

The sampling of the lamination parameter space is performed using Latin hypercube sampling, as was defined by Roepman (2021). This sampling approach allows to explore the design space equally.

Since the selection of samples forms the basis of the whole optimisation process, it is paramount for the sampling approach to be robust and cover equally the design space.

The evaluation of structural performances at each sample is carried out using the commercial finite element analysis Abaqus, which was further detailed in Section 7.2.1. Due to the computationally expensive nature of structural evaluation through finite element analysis, a Kriging surrogate model is used to predict the structural performance fitting the sample points evaluated.

Once the surrogate model for the structural performance of interest is defined, that is either buckling or deflection, a constrained gradient descent optimisation is used to drive the optimisation. The present extension to the framework is the definition of an augmented objective function that tailors a design to match a given deflection target, while maximising its buckling load. A detailed description of the formulation of this optimisation problem is provided in Section 7.2.3.

Once the optimal structural performance is evaluated, a first decision node is entered. In case the optimal structural performance is better than the previous sample set, the new optimal design is saved, and the number of missed iterations is reset. Otherwise, the sampling bounds in the design space are tightened around the current best solution. A second decision node is then checked, which evaluates the convergence of the optimisation. In case the maximum number of iterations is reached, or the number of consecutive iterations that do not achieve a better design is reached, then the design search is stopped, and an optimal lamination parameters design is assumed to be achieved. Otherwise, a new set of samples is taken within the sample bounds, and the loop is covered once more.

Evaluating the structural performance of each sample point with the finite element solver represents the most computationally expensive part of the local stiffness optimisation. Each buckling and deflection analysis takes on average about 6 and 9 seconds, respectively, for a given blade section model when running on a high-performance computing cluster. Please note that in the mesh convergence study that will be reported in Figure 11.2, the run time reported is relatively longer. This can be explained as the mesh convergence study was performed on a mobile workstation rather than on the high-performance computing cluster. Typically, less than 100 iterations are required to achieve convergence of a locally optimal design. In case 100 iterations are to be performed, with for instance a population size of 20 samples, the local stiffness optimisation would approximately take 8 hours of computational time.

7.2.3. Optimal Design of Variable Stiffness Laminates for Displacement under a Buckling Constraint

The local stiffness optimisation was extended to consider deflection as a design objective. The objective of the optimisation is defined as an augmented objective function, as formulated in Equation 7.2. The augmented objective function, based on the formulation presented in van Campen (2011), allows considering both deflection and buckling to evaluate the performance of a given design.

$$\min_{\boldsymbol{x}} \quad \Phi(\boldsymbol{x}) = \begin{cases} f(\boldsymbol{x}) - \varepsilon g_{max} & \text{if } g_{max} \geq 0 \\ f(\boldsymbol{x}) + \beta g_{max} & \text{if } g_{max} < 0 \end{cases}$$

$$\text{subject to} \quad \text{constraints imposed by the lamination parameter design space} \tag{7.2}$$

$$\text{with} \quad \text{Objective function: } f(\boldsymbol{x}) = |\|\delta(\boldsymbol{x})\| - \|\delta_0\||$$

$$\text{Buckling constraint: } g(\boldsymbol{x}) = \left(\frac{B(\boldsymbol{x})}{B_0} - 1\right) \geq 0$$

In Equation 7.2, $\boldsymbol{x}$ is the design vector. This design vector contains the lamination parameters set per region. In the present research, as laminates are limited to balanced and symmetric configurations, four lamination parameters are considered per region. The augmented objective function, represented by $\Phi(\boldsymbol{x})$, is an extension to the objective function $f(\boldsymbol{x})$ as it differentiates two cases. In the case the buckling constraint, denoted by $g(\boldsymbol{x})$, is valid, namely that it is greater or equal to unity, then the objective function is reduced by the product of a bonus term ε and the magnitude of this buckling margin.

Conversely, in the case the buckling constraint is violated, namely that $g_{max} < 0$, then the objective is penalised by the product of a penalty term with the buckling constraint violation.

As recommended by Haftka and Gürdal (1992), to prevent ill-conditioning of the augmented objective function, the design variables are normalised such that they have comparable values at comparable levels of criticality. For instance, a buckling constraint $g_{max} = 0.10$ would represent a 10% buckling margin, which compares to an objective value $f = 0.10$, which represents a 10% difference in deflection compared to the target level.

The objective function $f(x)$ is defined as the absolute value of the difference of the norms of the design deflection, denoted as $\|\delta(x)\|$, with a target deflection $\|\delta_0\|$. With deflection, the tip displacement of the structure is to be understood. This formulation allows to steer the optimisation towards the compliance of a design to a set deflection limit. One should note that, by taking the norm of the deflection vector, information on the direction of displacement is however not captured.

The buckling constraint $g(x)$ is to be greater than or equal to zero as the design buckling load $B(x)$ is to be greater than the applied load B_0. Otherwise, buckling would occur prior to the applied load, which is not desired in the present research, as the structure is not to operate in post-buckling regime. The design buckling load is understood to be the buckling load of the structure defined by the design vector x. The buckling load is evaluated based on an eigenvalue analysis and is further discussed in Section 7.2.4.

Finally, the bonus and penalty terms, ε and β, respectively, are arbitrary factors that were experimentally tuned. Values of $\varepsilon = 1.0$ and $\beta = 50.0$ were shown to lead to stable optimisation results for the blade section analysis considered in the present report, and provided in Chapter 11.

The design buckling load is evaluated from a parametric finite element model developed in Abaqus and solved using the eigenvalue buckling analysis presented previously. The design deflection of the model was assessed from an analogous parametric finite element model developed in Abaqus and solved as a static perturbation analysis, with non-linear geometric analysis enabled.

7.2.4. Buckling Analysis Formulation

In the present analysis, post-buckling regime is not considered, and the loading of a structure past its buckling load is assumed to lead to its failure. In fact, a structure is assumed not to retain its load-bearing potential past the buckling load.

To evaluate the buckling load of a structure, a linear buckling analysis was defined. An incremental loading pattern, denoted as Q, is defined with a unit load magnitude. This unit loading pattern is then scaled by a load multiplier, denoted as λ_i and also referred to as the ith eigenvalue, through a static perturbation analysis. The critical load is found for the increment at which the tangent stiffness matrix of the model becomes singular. The eigenvalue problem is formulated in Equation 7.3.

$$\left(K^{mat} + \lambda_i K^{geo}\right) v_i = 0 \tag{7.3}$$

In the eigenvalue problem formulation, K^{mat} is the base state matrix, K^{geo} is the geometrical stiffness matrix, and v_i is the ith eigenvector. The base state matrix represents the stiffness matrix of the system under the effect of a preload, defined as P. The geometric stiffness matrix relates to the change in the tangent stiffness matrix resulting from the unit incremental load Q.

With the ith eigenvalue solved, the critical load is evaluated as provided in Equation 7.4. In fact, the critical load is the sum of the preload value P with the product of the eigenvalue of interest λ_i and the unit increment load pattern Q. The definition of a preload value is of interest for buckling analyses of variable stiffness structures. This can be understood as these structures, due to their spatially varying stiffness properties, will display a lower buckling load in a particular direction. The application of a preload value therefore allows nudging the buckling analysis in a direction of interest. The use of preload will be further highlighted in the result discussion.

$$P_{crit} = P + \lambda_i Q \tag{7.4}$$

A remark should be made regarding the shortcomings of the eigenvalue buckling analysis. In fact, the critical load evaluated through linear buckling analysis often overestimates the buckling load of a structure as imperfections are not accounted for. Besides, linear behaviour is assumed before buckling occurs, and non-linear deformations are therefore neglected. Nevertheless, in the present work, the critical load is assumed to be the buckling load of the structure.

7.3. Step 2 | Stacking Sequence Retrieval Process

Even though the conversion of a stacking sequence to a lamination parameter set is a trivial process, the contrary translation is not. In fact, provided with a given lamination parameters set for each laminate region, retrieving a distinct stacking sequence is not a straightforward approach. The retrieval process can be expressed in an optimisation formulation, as in Equation 7.5.

$$\min_{\boldsymbol{\theta_i}} \left(\boldsymbol{V_i^*} - \boldsymbol{V}(\boldsymbol{\theta_i}) \right)^2 \tag{7.5}$$

In Equation 7.5, the objective function is formulated as the squared distance between the optimal lamination parameter set, denoted as $\boldsymbol{V_i^*}$, and a lamination parameter set evaluated for a given stacking sequence $\boldsymbol{V}(\boldsymbol{\theta_i})$. This squared difference can also be referred to as the L2 error and represents the squared distance between a target value and an actual value. The design variable in this formulation is the stacking sequence of a given region i, denoted by $\boldsymbol{\theta_i}$. The asterisk indicates an optimal value, in this case, the optimal lamination parameter set of a region i, denoted by $\boldsymbol{V_i^*}$.

A genetic algorithm based on the work from van Campen and Gürdal (2009) is used to find the stacking sequence for each region that best matches the lamination parameter set of such region. As no further extension has been made in the present research regarding the retrieval algorithm, readers interested in further details are referred to Roepman (2021) and van Campen and Gürdal (2009).

7.4. Step 3 | Local Blending Process

Receiving locally optimised stacking sequences for each region from the second step, the design would most likely not be manufacturable nor have structural integrity due to discontinuity between regions. To provide a first fix to this locally optimal design, local blending is applied. This optimisation approach was developed by Roepman (2021) and van den Oord (2018), and is organised in two main phases.

In the first phase, labelled as patch foundation, layers of neighbouring regions are connected. A patch is defined as the connection of layers sharing a common fibre orientation and spanning over multiple regions. The approach to form those initial patches is to rotate some layers incrementally until they join. Convergence of this first phase is achieved when any layer rotation would break a patch, or would not improve the cohesion of neighbouring plies. Evolution of layers is done in a pattern as developed by Roepman (2021), which can follow any of the two principles: 1) *"cells evolving at the same time shall not be in each other neighbourhood"*; 2) *"cells evolving at the same time shall not share neighbours"* Roepman (2021). The former resembles a chequerboard pattern, whereas the latter evolution pattern is based on the Latin hypercube sampling structure.

In the context of a blade section analysis, the layup over the circumference of the airfoil can experience radical changes in thicknesses, namely as it is the case for the much thicker cap laminates (c.f. Table 9.1). This large difference in laminate thickness can be a source of ply removal when applying local blending constraints. In fact, as the thick cap laminates are bounded by relatively thinner ones, the patch foundation process removes the plies in excess as they are bounded by empty regions. This removal of the extra plies in the caps leads to a degradation of the structural performance. To alleviate such effect of the patch foundation, a neighbouring connection matrix can be passed on that defines which regions should be connected, and which are not enforced to. A representation of this region connectivity is shown in Figure 7.3. Besides, in the context of wind turbine blade design, the layup at the trailing edge is not required to be blended going from the suction to the pressure side. In fact, as the trailing edge panels of blades are usually bonded by an adhesive, the laminates on the suction and pressure sides of the trailing edge do not have to be matched. As such, connectivity of the two trailing edge regions (i.e. between the tail A regions on the suction and pressure sides) is also disabled.
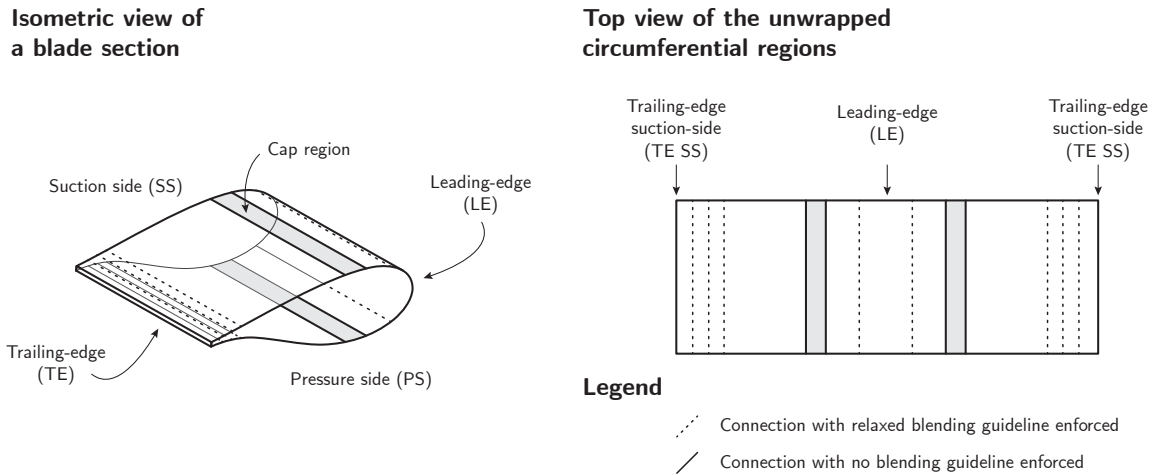
Figure 7.3: Illustration of the region connection rule applied to a blade section with equivalent region distribution as the DTU 10MW reference blade, illustrated in Figure 9.1.

Another connectivity approach will be preferred, which allows continuity of the skin laminates around the full blade circumference. This neighbouring connection defines that the trailing-edge and leading-edge panels shall be blended. This definition differs from the one shown in Figure 7.3 as laminate continuity is achieved despite the presence of spar caps. Further discussion on this neighbouring connection approach will be presented in Section 11.4.

Once preliminary patches are formed, the second phase consists in enforcing the relaxed blending guidelines formulated by van Campen (2011). To enforce this compliance, butted edges that may be present in the design are to be removed. Butted edges are defined as the interface between two plies present at the same level and that do not share the same fibre orientation. These butted edges are to be avoided as they introduce manufacturing complexity. In fact, it is a challenging process to accurately place two plies abreast without leaving a gap, or generating an overlap between the two plies, both of which would affect the structural performance of the manufactured laminate. The butted edges removal process was formulated by Roepman (2021) and van den Oord (2018) as an optimisation problem by finding modifications of single layers in each region that would minimise the number of butted edges in a design. Readers interested in further information on the cellular automaton developed for local blending are invited to consult the latter two research.

7.5. Step 4 | Global Blending Process

The fourth and final step of the straight-fibre variable stiffness design is the global blending process, also referred to as global interpretation. This final algorithm strives to define a manufacturable design from the locally blended design. The outcome of the global interpretation is the identification of patches, as well as the assembly sequence required to manufacture such laminate.

The formation of patches and assembly assignment is evaluated through a connection search algorithm developed by Roepman (2021). The aim of this process is to minimise the number of remaining butted edges and push those as close to the laminate symmetry plane. The author argued that bringing butted edges closest to the mid-plane would have less impact on the flexural performance of the modified design. In fact, flexural stiffness is not only sensitive to the fibre orientation content of a laminate but also to its stacking sequence, namely on the location of plies within the laminate (Kassapoglou, 2013). As no further extension on this global blending process has been made in the present research, readers are recommended to consult the work by Roepman (2021) for further details.

8

Frameworks Coupling

Two methodologies will be introduced in this section, for the different structural scales considered. First, the framework considered for the aeroelastic design of a blended blade is presented. Then, the framework defined for an aeroelastic blended blade section design is presented. The latter differs from the former as it only considers a spanwise section of a full blade design.

8.1. Full Blade Design

The full blended blade design approach is illustrated in Figure 8.1. This method starts with the definition of a baseline structure. For this structure, the blade planform (i.e. chord, twist and thickness distribution) shall be available. Besides, the loading condition of interest shall also be specified, as it will influence the loading distribution on the structure.

In the second step, the structural performance of such a baseline blade is assessed. For this assessment, the reference load distribution and displacement field are characterised and set as targets for the optimisation process. In fact, once a convergence of the load envelopes is achieved, the iterative design approach for a blended blade will be terminated.

Once a baseline displacement field and applied loading is retrieved, one can feed the baseline design in the Aero-Structural Optimization Framework (AESOpt) tool for mass minimisation. Further information on this particular optimisation tool is provided in Chapter 6. The main output from this first optimisation tool is an updated internal geometry of the blade, where the thickness and fibre orientation of each layer has been optimised to shave-off weight, while still complying with deflection and strain constraints.

From this updated internal geometry of the blade design, the thickness distribution is set in the blade. The only variables that are selected for optimisation are the fibre orientation and stacking sequence. The material distribution over the blade section is set in that the number of plies is considered fixed from the previous step. However, the stacking sequence can still be optimised per region, and blended into manufacturable laminates. The process of variable stiffness optimisation and blending is performed by the SFVS Framework. This framework will further be presented in Chapter 7.

After these two optimisation steps, where both mass and stiffness have been optimised, an updated blade internal geometry is obtained. Due to aeroelastic effects, the change in the internal properties of the structure will result in a change in the loading and deformation of the structure under operational conditions. After the evaluation of the aeroelastic response of the updated blade structure, a convergence assessment is made. In case the loading distribution over the blade is drastically different from the reference frozen loads, the optimal design needs to be iterated. An additional condition is set such that the number of iterations and missed updates are tracked. In case a design has not been improved over several consecutive iterations, one can assume that an optimal design was found and the whole framework is completed. Otherwise, the current optimal design is set as the baseline design and the optimisation is iterated.

In the state-of-the-art review of aeroelastic blade design reported in Section 4.1, it was suggested that
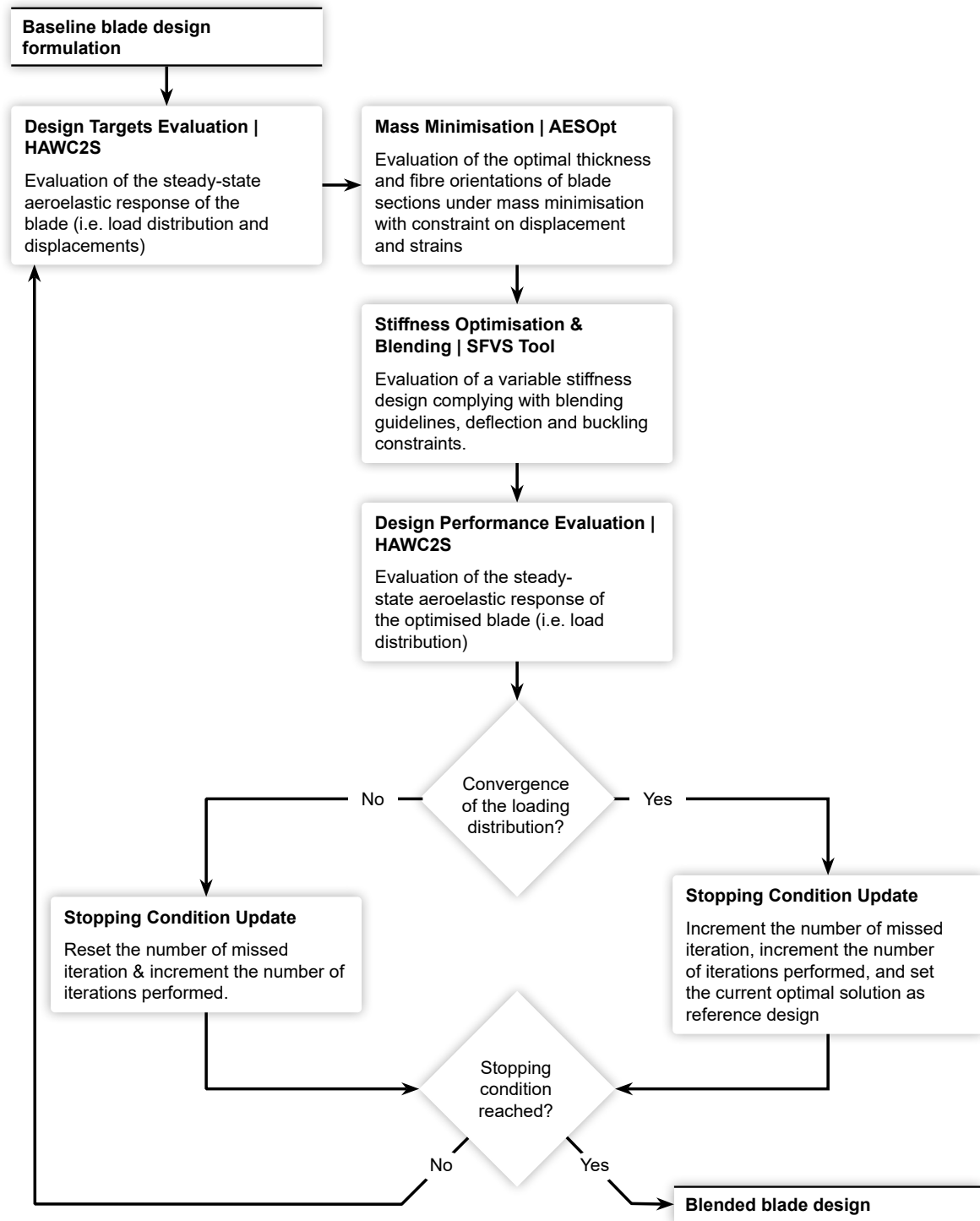
Figure 8.1: Full blade blended aeroelastic design framework overview.

a fully coupled aero-structural optimisation is preferable to properly design for aero-elastic tailoring. The separate optimisations between mass minimisation with the AESOpt framework and the stiffness optimisation performed in the SFVS tool should thus preferably be integrated as a single monolithic optimisation problem. This separation is initially proposed in the present research as it allows working with these independent tools in a manageable approach. Involving AESOpt and SFVS in a single optimisation tool is proposed for further studies.

8.2. Blade Section Design

To achieve the full blade design approach described in the previous section, significant computational resources and coding complexity would be required, and therefore a simplified workflow was defined. This intermediate design approach allows to achieve a tractable design methodology by working on a sub-scale of the larger problem. This workflow considers the design of a blade section, for mass minimisation, while constraining deflection and targeting maximum buckling performance.

The simplified methodology is represented in Figure 8.2. As for the full blade design approach, the definition of a baseline structure is the first step of the approach. Provided with both internal and external geometry of a blade section, as well as the design loading condition, the first step of the design approach is to minimise the mass of the structure by optimising the thickness distribution. As discussed in the full blade design workflow, this first optimisation is performed in the AESOpt framework, which will be further presented in Chapter 6.

Once an optimal thickness distribution is defined for the considered blade section, the internal geometry of the structure is assumed to be fixed, and one will aim to maximise the buckling performance while complying with a deflection constraint. The second optimisation step will call on the straight-fibre variable stiffness laminate design tool, which will be covered in greater depth in Chapter 7.

As a blade section is considered rather than a complete blade, the aeroelastic response for the updated structural design cannot be assessed, and load re-distribution cannot be evaluated. Therefore, there is no iteration loop from the SFVS to the AESOpt framework. Hence, the design obtained after the second optimisation step consists of the final design of the workflow.
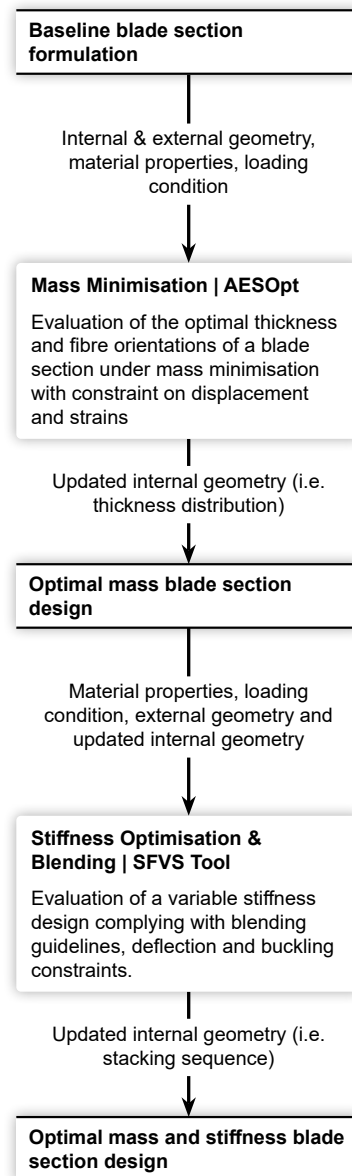
Figure 8.2: Blended blade section design framework overview.

Part III

Results | Blade Section Analysis

9

Benchmark Design

In the conceptual phase of wind turbine blade design, reference turbines can play an important role as baseline design for a redesign. One of the widely used referenced turbines is the DTU 10MW. The DTU 10MW reference wind turbine is selected as a baseline for the investigation of the use of straight-fibre variable stiffness laminates in blade design. This wind turbine was chosen as data is readily available for it, and a wide amount of research has used it as a reference. The description of this reference turbine is provided by Bak et al. (2013).

As will be discussed later in this report, the analysis performed in the present research is limited to the consideration of a blade section, rather than a full blade design. The blade section chosen for the present analysis is taken approximately at the third of the blade span. This region was deemed relevant for analysis for two main reasons: first, on the inner third part of the blade span, structural considerations lead over aerodynamic design (Mølholt Jensen & Branner, 2013); second, for the DTU 10MW reference blade, the maximum chord is observed at 27% of the blade span. At the maximum chord span, the largest trailing edge panels are observed, making it a region prone to trailing edge buckling. In fact, this can namely be verified from the buckling analysis performed on the reference blade, where the ratio of buckling load to applied load approaches one, indicating a small buckling margin (Bak et al., 2013). Hence, the blade section at the maximum chord location is selected, which is located at 27% of the blade span, or 24.2 m from the rotor hub centre.

The external geometry of the blade at this spanwise location is defined by the FFA-W3-360 airfoil. The blade chord at the maximum chord location is 6.2 m. A buckling analysis of the reference turbine is reported in the description report. The approach used by the author is to partition the blade into 27 blade sections, with an aspect ratio of 1.2 of the local chord length. To match the analysis performed on the DTU 10MW reference wind turbine, a blade section of 7.44 m will therefore be considered.

The internal geometry of a section of the reference blade is defined by 11 regions as illustrated in Figure 9.1. Those regions include skin laminates (e.g. trailing edge panels, caps, etc.) as well as webs. Each region is composed of the material stacking sequence as defined in Table 9.1, given specifically at the section of interest, from the outermost layer given in the first column to the innermost layer in the last column. The material properties of these layers are also provided in Bak et al. (2013), and are summarised in Table 9.2.

In Figure 9.1, the material regions are defined over the circumference of the airfoil profile based on the following metrics. The cap width is defined as the distance between the shear webs (i.e. web A and B). The caps are placed at the maximum thickness of the airfoil, as to maximise the flapwise bending stiffness as argued by the authors. The cap centre, denoted as CC, is defined as a distance b from the pitch axis, denoted as PA in the figure. For the blade section of interest in the present report, the airfoil internal geometry metrics are summarised in Table 9.3. Finally, the shear webs are oriented at an angle of 90° relative to the global x-axis. Besides the definition of the keypoints for the caps, the remaining regions are defined at the perpendicular of the fractions of the chordline. For instance, tail A extends from 0 to 7% of the chord length, followed by tail B from 7% to 13%, etc., as illustrated in
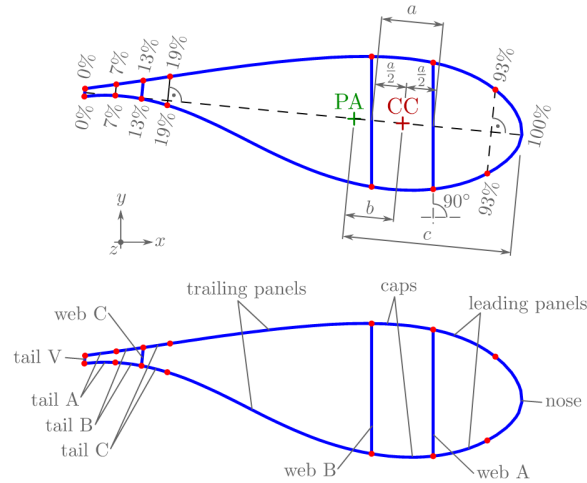
Figure 9.1: Internal geometry definition and circumferential regions definition of the DTU 10MW. Retrieved from Bak et al. (2013).

Table 9.1: Layup definition for the 24.2 m blade section of the DTU 10MW reference blade.

		Triax [mm]	Uniax [mm]	Biax [mm]	Balsa [mm]
Skin	Cap	0.0	37.5	0.0	0.0
	LE panels	3.0	0.9	0.0	35.0
	Nose	3.0	2.1	0.0	35.0
	Tail A	3.5	5.4	0.0	65.0
	Tail B	3.5	5.4	0.0	70.0
	Tail C	3.5	0.9	0.0	70.0
	Tail V	3.5	0.9	0.0	70.0
	TE panels	3.5	0.9	0.0	70.0
Web	Web A	0.0	0.0	3.8	50.0
	Web B	0.0	0.0	3.8	50.0
	Web C	0.0	0.0	3.0	15.0

Figure 9.1. Keypoints are the region division points, namely the coordinates that define the boundaries between regions.

As will become apparent later, in the current analysis, the definition of the region keypoints is more conveniently specified as a percentage of the perimeter of the airfoil section, rather than as a percentage of chord length. As such, the retrieved circumferential region definition as a percentage of the section perimeter is provided in Table 9.4.

Finally, the loading condition considered in the present report is based on the extreme loads analysis reported in Bak et al. (2013). The extreme loads reported were evaluated using the aeroelastic code HAWC2 for a range of design load cases, which are described in the IEC61400-I standard. In the present report, the focus will be kept on a simple loading condition. As was highlighted in the previous chapters, blade tip deflection is an important constraint in the design of wind turbine blades. Therefore, a simplified loading case is considered in this report where a blade section is loaded by a tip moment, loading the suction side (i.e. down-wind) under compression. At the section of interest, the extreme flapwise moment loading the suction side of the blade in compression is about 40.52 MNm. An illustration of the loading condition and coordinate system is defined in Figure 9.2. The root is considered to be clamped, and the tip moment is applied at the elastic centre of the section, with all nodes of the tip section constrained to deform as a rigid body with the applied load.

**Table 9.2:** Materials properties for the DTU 10MW reference wind turbine.

Property	Symbol	Unit	UD lamina	Uniax	Triax	Balsa
Longitudinal Young's modulus	E_1	[GPa]	43.05	41.63	21.79	0.050
Transverse Young's modulus	E_2	[GPa]	13.43	14.93	14.67	0.050
Poisson's ratio	ν_{12}	[-]	0.268	0.241	0.478	0.50
Shear modulus	G_{12}	[GPa]	5.05	5.05	9.41	0.017
	G_{23}, G_{13}	[GPa]	5.05	5.05	4.54	0.150
Mass density	ρ	[kg/m^3]	1915.5	1915.5	1845.0	110.0

Table 9.3: Internal geometry properties for the 24.2 m blade section of the DTU 10MW reference blade.

Property	Symbol	Unit	Value
Chord length	c	[m]	6.2
Relative thickness	t/c	[-]	0.41
Cap width	/	[m]	0.94
Distance between PA and CC	/	[m]	0.42
Distance between PA and LE	/	[m]	2.38

Table 9.4: Circumferential region keypoints definition as a percentage of the airfoil perimeter.

Region		Start [%]	End [%]
SS	Tail A	0.0	0.03
	Tail B	0.03	0.06
	Tail B	0.06	0.09
	TE	0.09	0.27
	Cap	0.27	0.34
	LE	0.34	0.43
	Nose	0.43	0.57
PS	LE	0.57	0.64
	Cap	0.64	0.70
	TE	0.70	0.91
	Tail C	0.91	0.94
	Tail B	0.94	0.97
	Tail A	0.97	1.0
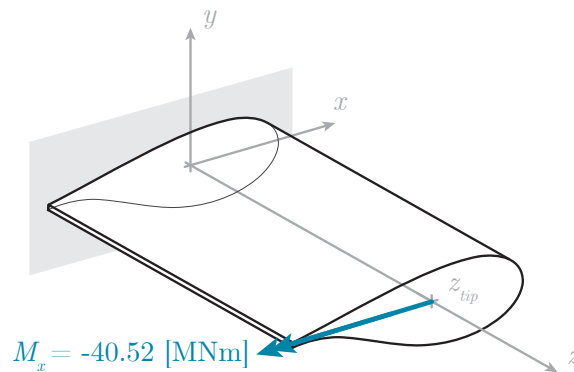
Figure 9.2: Loading condition considered for a blade section problem of the DTU 10MW turbine.

10

Blade Section Mass Optimisation

The evaluation of the minimum thickness required per region of a blade section will be presented in this chapter. More specifically, the thickness optimisation workflow presented in Chapter 6 and defined in the AESOpt framework will be applied on the baseline blade section introduced in Chapter 9.

10.1. Blade Section Formulation

The blade section problem considered for the mass minimisation optimisation is based on the baseline blade section. The structure consists of 13 constant laminate regions along the circumference of the airfoil profile, which all run from root to tip of the blade section.

The loading case considered is illustrated in Figure 10.1. For pure thickness optimisation, a tip bending moment M_x is considered such that the trailing-edge suction side panel is loaded under compression. To match the design capabilities of the parametric finite element model used in the SFVS framework, the presence of the shear webs is neglected in the present case. As such the extreme load of -40.52 MNm described in the DTU 10MW report was reduced to -19 MNm. At this load, the maximum failure strain indices in all regions and for all strain components remain below one. For the presented loading case and baseline blade section structure, the following structural performances are expected: a tip deflection of 63 mm is evaluated, and the baseline mass of the structure is 4091.54 kg.
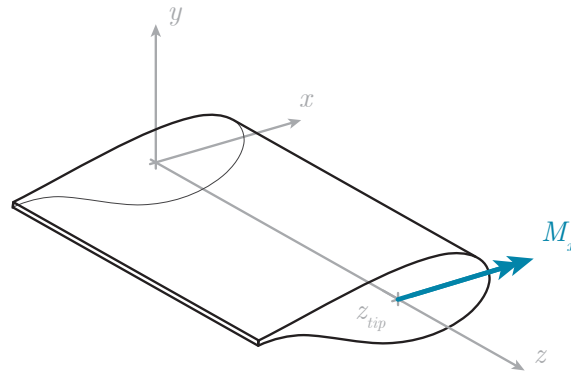
Figure 10.1: Coordinate system and loading condition considered for the blade section problem.

A convergence study is performed on the tip deflection of the baseline structure for different mesh configurations. In the cross-sectional mesher, the number of elements in the circumferential direction and in the surface normal direction are to be defined. For a number of mesh elements around the circumference between 50 and 200, a convergence of the deflection was observed for a minimum of 100 elements as presented in Figure 10.2a. Besides, for a number of through-the-thickness elements

ranging from 5 to 25, a convergence of the deflection was observed for a minimum of 15 elements. The final mesh arrangement is chosen to be 200 elements in the chordwise direction and 15 elements in the thickness direction. A convergence study on the number of beam elements, or referred to as sections in Figure 10.2 was also performed. These elements are defined in the spanwise direction. A minimum of 5 sections are to be defined in the spanwise direction to achieve convergence of the tip deflection. In the following analysis, a number of 15 sections were chosen.
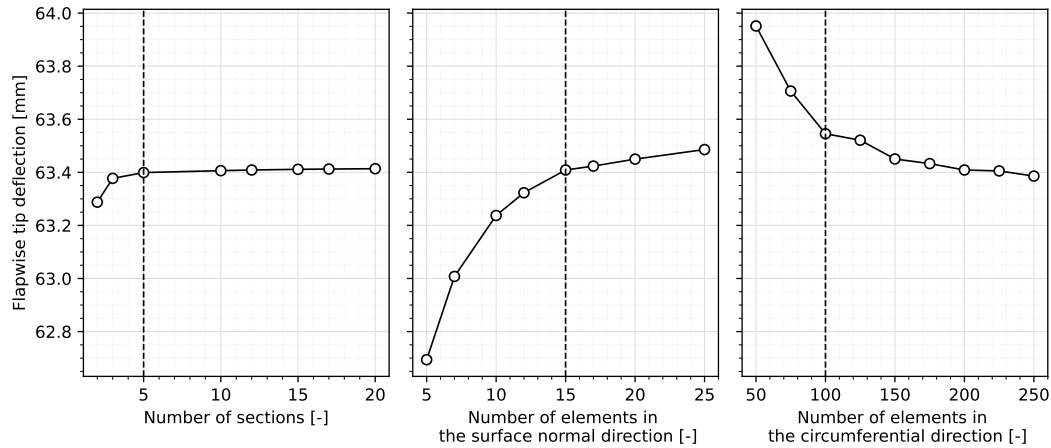
(a) Convergence study on the flapwise tip deflection of the blade section problem considered.
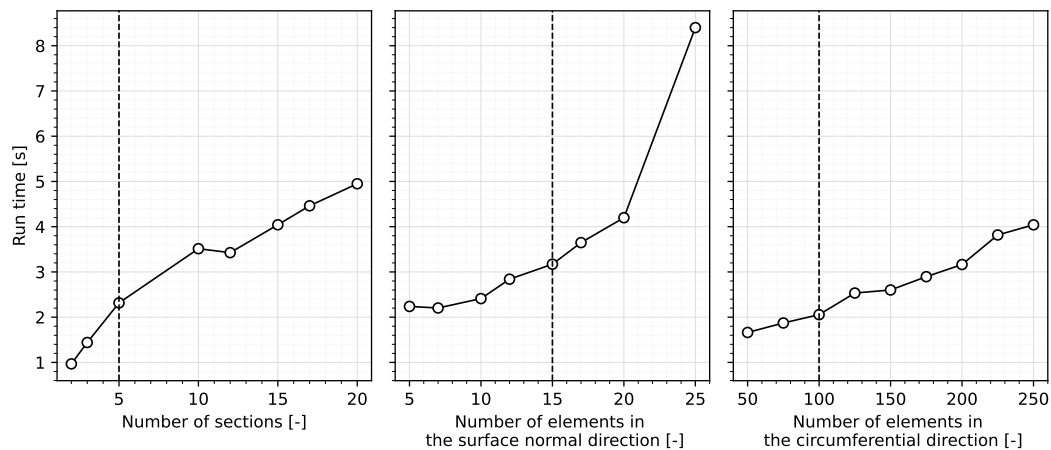
(b) Run time in the convergence study of the blade section problem considered.

Figure 10.2: Mesh convergence study on the blade section problem. The vertical dashed-line represents the minimum number of elements to achieve convergence of the tip deflection.

10.2. Layer Thickness Optimisation

As presented in Chapter 6, the optimisation approach defined in the AESOpt framework strives for mass minimisation under a deflection and maximum strain failure index constraint. In the present section, the design variable is the layer thickness. More precisely, the thickness of the uniax material is chosen to be optimised as the loading condition defines a pure bending moment in the flapwise direction. As such, one can argue that to resist this bending, laminates with fibres aligned in the spanwise direction should be preferred. Considerations such as buckling which mainly affect the use of balsa and triax material will be considered in the second optimisation tool, where stiffness will be optimised.

To analyse the results of the thickness optimisation, the total region thicknesses achieved are first reviewed. The baseline and optimal design region thicknesses are reported in Figure 10.3. The spar caps experience the largest change in thickness, with the pressure side cap increasing by approximately 7 mm in thickness, whereas the suction side cap thickness is reduced by 14.5 mm. Regions closer to the

x-axis, thus closer to the moment axis have their thickness reduced. Those regions are for instance the nose and tail A and B regions. This result is expected as regions closer to the moment axis contribute less to resisting bending. Regions furthest away from the x-axis carry a greater part of the flapwise moment and as such experience an increase in thickness. It is however remarkable that the suction side cap has a reduction in thickness. This could be explained as the thickness of the leading edge region is increased. In fact, even though material is removed on the suction side cap, the leading edge on that side has its thickness increased by 6 mm, thus carrying part of the load. Overall, the blade section achieves a mass reduction of 3.86%, therefore reaching a total mass of 3932.98 kg.

(a) Baseline and optimised total region thicknesses.

(b) Difference between the optimised and baseline region thicknesses.
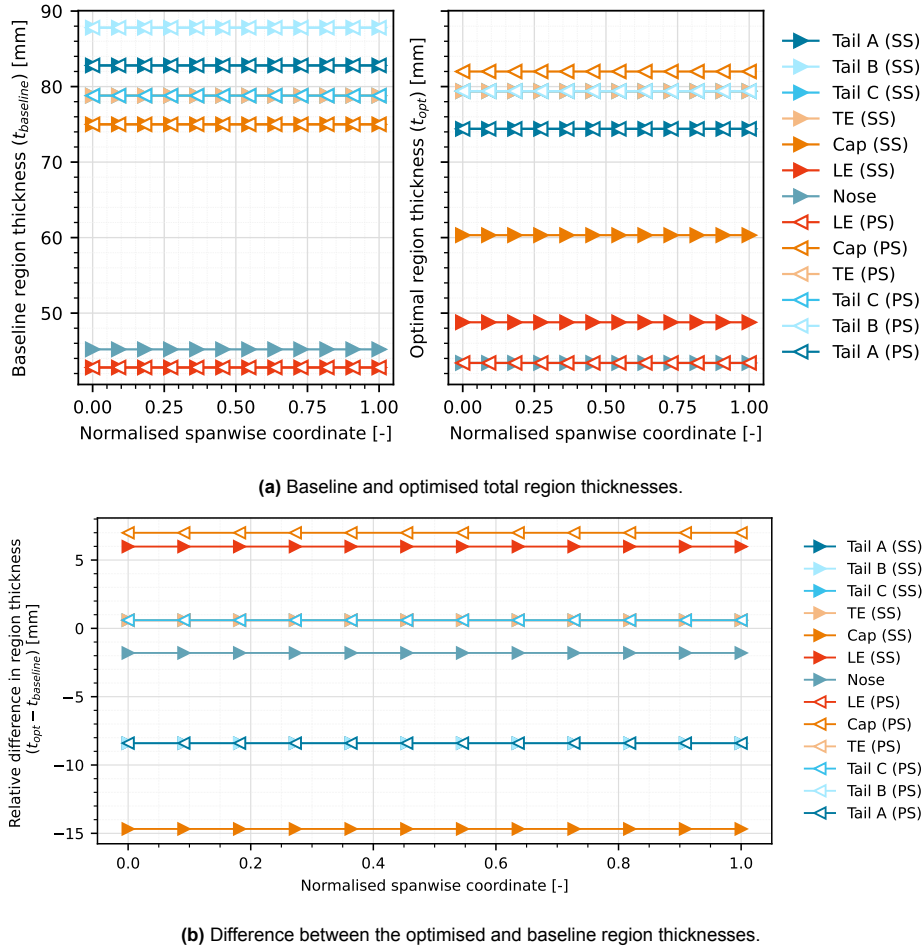
Figure 10.3: Total region thicknesses for the blade section problem.

Regarding the deflection of the structure, the optimised blade section complies with the deflection target specified. In fact, as illustrated in Figure 10.4, the tip deflection in the flapwise direction (i.e. in the y-direction) matches the baseline deflection of 63 mm. The constraint on deflection is therefore satisfied.

Besides deflection, constraints on the maximum strain failure indices were specified. Material failure is assumed when any of the six independent strain components exceeds their allowable thresholds, in which case the strain failure indices exceed one. Therefore, those six failure indices were constrained to remain below one throughout the optimisation. This is indeed achieved in the optimal blade section design, where all maximum strain failure indices remain below 0.9, as reported in Figure 10.5. The strain failure index for the ε_{11} component, which is aligned with the spanwise direction, is displayed over a cross-section of the blade in Figure 10.6. This strain failure index reaches its maximum in the suction side cap, as well as in the uniax material of the leading edge panel on the suction side, as highlighted by the red zones in Figure 10.6b. As the suction side is loaded under compression, and since the allowable compression strain is lower than the allowable tension strain for the uniax material considered, those regions are expected to have a critical strain failure index in the spanwise direction.
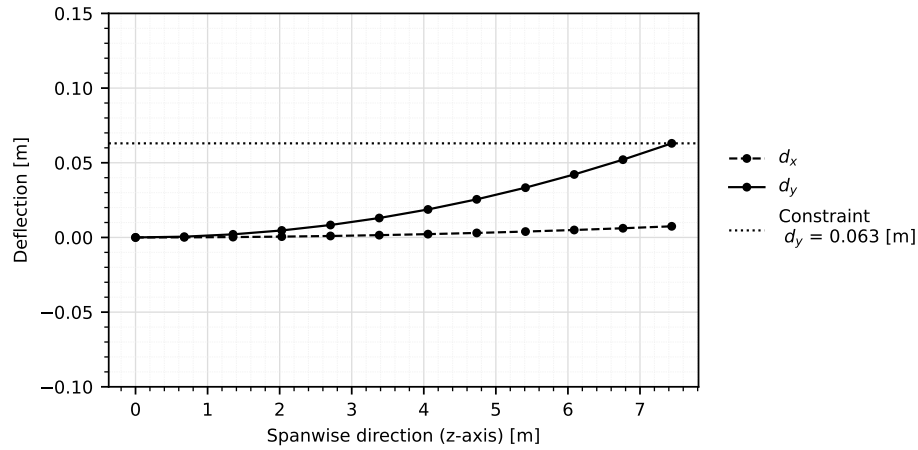
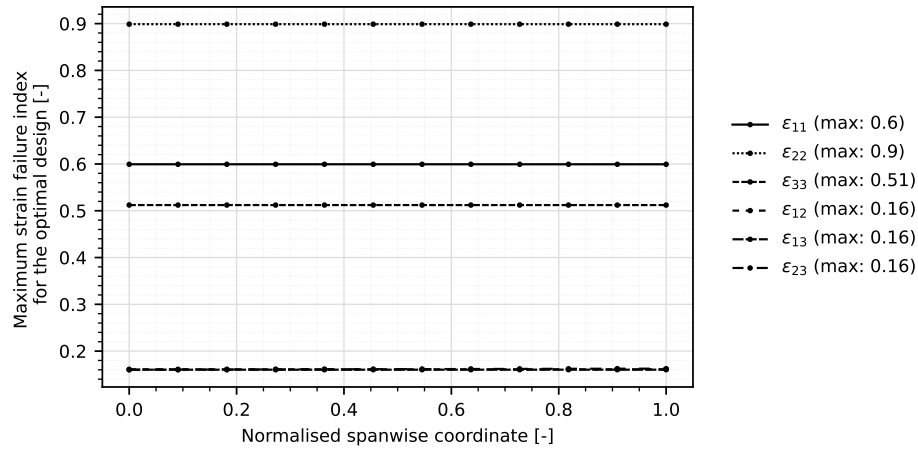**Figure 10.4:** Deflection profile of the optimal blade section design.

Figure 10.5: Maximum strain failure indices for the optimal blade section designs.

Finally, one can review the change in cross-sectional stiffness from this change in material distribution. The cross-sectional stiffness matrices K are evaluated from BECAS and the following convention is used in this software. The first three stiffness components on the diagonal of a cross-section stiffness matrix (i.e. K_{11}, K_{22}, K_{33}) relate to the resistance to forces in the x-, y-, and z-axes, respectively. Comparatively, stiffness components K_{44}, K_{55}, K_{66} relate to the resistance to moments in the x-, y-, and z-axes, respectively. In Figure 10.7, the ratio of those six stiffness components between the optimal and baseline blade section designs are presented over the normalised span of the structure. First of all, the stiffness components remain constant along the span as the thickness of each region remains constant too. Furthermore, it is interesting to note that K_{44} remains unchanged (i.e. $K_{44,\text{opt}}/K_{44,\text{baseline}} = 1$). This indicates the bending stiffness in the flapwise direction has not been changed. This result is expected as the optimised design is constrained to achieve the same flapwise deflection as the baseline design under the same loading condition. Reduction in the K_{33} stiffness is argued to be the consequence of the overall reduction in material used. In fact, as region thicknesses have overall been decreased, the optimal blade section design has a lower cross-sectional area, thus observing a stiffness decrease in the spanwise direction.
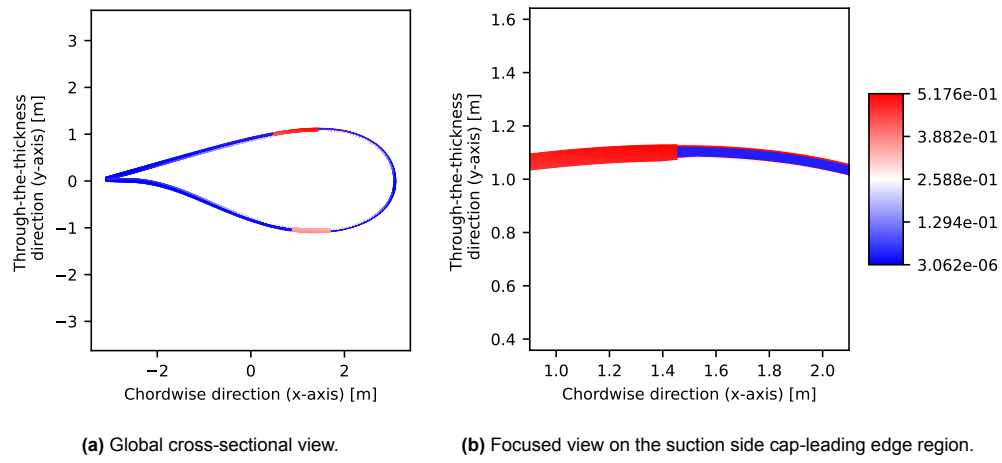
(a) Global cross-sectional view.

(b) Focused view on the suction side cap-leading edge region.

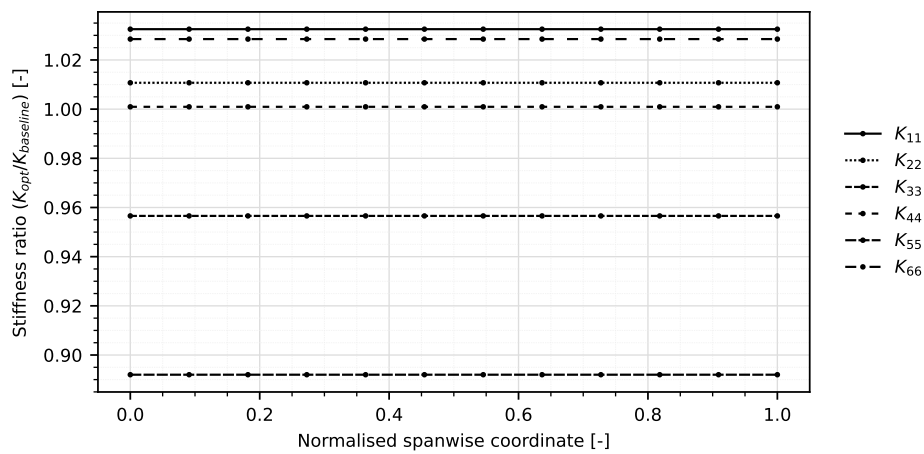**Figure 10.6:** Maximum strain failure index for the ε_{11} strain component.

Figure 10.7: Stiffness ratio between the optimal and baseline blade section designs.

11

Blade Section Blending

The optimal design of a blade section through laminate patching will be presented in this chapter. More specifically, the use of straight-fibre variable stiffness on a section of the DTU 10MW reference wind turbine blade will be made. Based on the benchmark blade section introduced in Chapter 9, the blending optimisation tool is used to maximise the buckling performance of the blade section, while complying with a deflection target. The results of the analysis for several region definitions is presented in this chapter.

11.1. Blade Section Formulation

The structure considered in the present chapter is that of the baseline blade section introduced previously. Reflecting on the research question posed in Chapter 5, the performance of straight-fibre variable stiffness laminate design approach on the trailing edge panel design of a turbine blade is to be investigated. As such, three blade section concepts are considered for laminate patching, having a distinct number of constant laminate regions over their trailing edge panels. Those three concepts are labelled as follows: concept 1x13, with one region in each trailing edge panel; concept 1x17, with three regions in each trailing edge panel; and concept 1x24, with six regions on the suction side trailing edge panel and seven regions on the trailing edge panels. An illustration of those three blade sections is provided in Figure 11.1. This partitioning was done arbitrarily, namely to investigate the structural performance achieved by an increasing number of constant laminate regions on the trailing-edge panels. Please note that concept 1x24 has one more region on its pressure trailing edge panel than the one on its suction side. This is merely due to the fact that the pressure side trailing edge panel spans 21% of the airfoil circumference (i.e. between 70 and 91% arc length of the airfoil perimeter, c.f. Table 9.4) making this section separable in seven regions of 3% of the profile circumference.
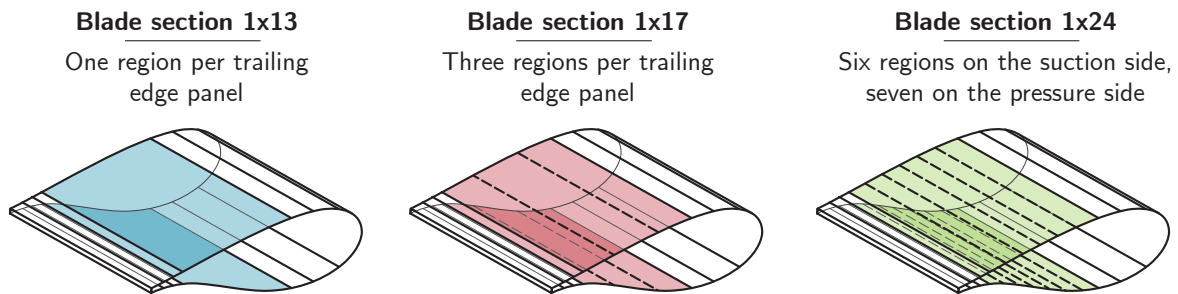
Blade section 1x13
One region per trailing
edge panel

Blade section 1x17
Three regions per trailing
edge panel

Blade section 1x24
Six regions on the suction side,
seven on the pressure side

Figure 11.1: Illustration of the three blade concepts considered for laminate blending

The convention used in the naming of the concepts is the following. The first digit relates to the number of regions in the axial direction (i.e., in the spanwise direction of the blade), and the second digit relates to the number of regions over the circumference of the profile (i.e., in the chordwise direction). For instance, concept 1x13 has 1 region in the axial direction and 13 regions defined over its airfoil profile,

meaning that all circumferential regions run from the root to the tip of the section.

A limitation of the tool in its current form is the use of a single material definition. In fact, once a lamination parameter distribution is evaluated in the first step of the design process, a discrete stacking sequence is retrieved to match those lamination parameters. This retrieval process, as discussed in Figure 11.6a, is a complex process when considering a given ply material, and is especially challenging when mapping lamination parameters to a hybrid composite material, such as a sandwich layup. An attempt was made to extend the retrieval process to hybrid composite layups, but due to time constraints, this has not been included in this research. Hence, a further simplification of the structure has to be made compared to the structure optimised with the AESOpt framework. Sandwich panels from the blade section are converted to monolithic panels, by neglecting the presence of the core material. In fact, only the facesheet layups of the sandwich structures were considered.

The loading condition is a bending moment introduced by a tip moment in the flapwise direction, causing the suction side of the blade section to be loaded in compression, as illustrated in Figure 10.1. The applied load was evaluated for the three concepts to -5.0 MN, based on a buckling eigenvalue analysis. In fact, for those concepts in their baseline configuration, the buckling load was evaluated to about -5.11 MN. For the applied load, a tip deflection of approximately 12.4 mm in magnitude was recorded, and a target tip deflection of 12.5 mm was therefore chosen. The deflection and buckling performance of the baseline design were taken from the convergence study reported hereafter.

Each region was assigned its own guide. Following the terminology introduced at the end of Chapter 3, this means that each region is allowed to have its own stacking sequence. The original design had symmetric layups between suction and pressure sides, as presented in Chapter 9. Actual blade designs do not require such symmetry. Therefore, the present study considers each region to have its own guide to explore achievable designs with further design freedom.

The thickness, and as such the number of plies, in each region is received from the baseline blade section presented in Chapter 9. The laminate of each region is defined with material thickness rather than a stacking sequence of discrete plies. Since the SFVS tool handles discrete stacking sequences, a conversion from the baseline internal geometry received as continuous layup thicknesses is required. In the present analysis, triax layup was considered to be a $[\pm 45/0_2/\pm 45]_T$ layup, and uniax material was assumed to be $[0_2]_T$ layup, both of which are assumed to be made out of glass-epoxy Unidirectional (UD) lamina, with properties as reported in Table 9.2. A ply thickness of 1.2 mm was assumed based on material properties available for the unidirectional lamina used (Mandell et al., 2016). This conversion was selected in accordance with the material definition used on the DTU 10MW reference turbine (Bak, 2013), as well as complying with the assumption made that all laminates used in the SFVS framework are balanced and symmetric. Based on the continuous material layup defined in Table 9.1, and following the conversion presented here, the baseline stacking sequence of each region is summarised in Table 11.1.

Table 11.1: Baseline stacking sequence definition for a blade section of the DTU 10MW reference blade taken at a span of 24.2 m.

Region	Layup [°]	Total laminate thickness [mm]
Tail A	$[\pm 45/0_2/\pm 45/0_6]_S$	28.8
Tail B	$[\pm 45/0_2/\pm 45/0_6]_S$	28.8
Tail C	$[\pm 45/0_2/\pm 45/0_2]_S$	19.2
TE panels	$[\pm 45/0_2/\pm 45/0_2]_S$	19.2
Cap	$[0_{32}]_S$	76.8
LE panels	$[\pm 45/0_2/\pm 45/0_2]_S$	19.2
Nose	$[\pm 45/0_2/\pm 45/0_2]_S$	19.2

A mesh convergence study was conducted on each of the three blade section concepts. In Figure 11.2a, the convergence of the buckling load is shown for a wide range of mesh configurations. For the same mesh configurations, a convergence study on the tip deflection was also performed which is reported in Figure 11.2b. A number of 15, 20 and 30 mesh elements were tested in the axial direction, and

a number n of mesh elements per region, ranging from 3 to 9, in the circumferential direction was taken. Please note that the number of elements in the circumferential direction is defined as a number of mesh elements per region to ensure that a discrete number of elements fall within a design region. Convergence was assumed when the structural performance (i.e., buckling load or tip deflection) for a given mesh arrangement is less than 1% different relative to the performance of the previously evaluated mesh arrangement. The present convergence study highlights that 7 mesh elements per region circumferentially are required for a convergence of the buckling load, regardless of whether 15, 20, or 30 elements are taken axially. Similarly, 4 mesh elements per region circumferentially are required in the axial direction for a convergence of the tip deflection. Hence, and to limit the run time required per finite element evaluation, a number of 15 elements axially and 7 elements circumferentially per region are selected.
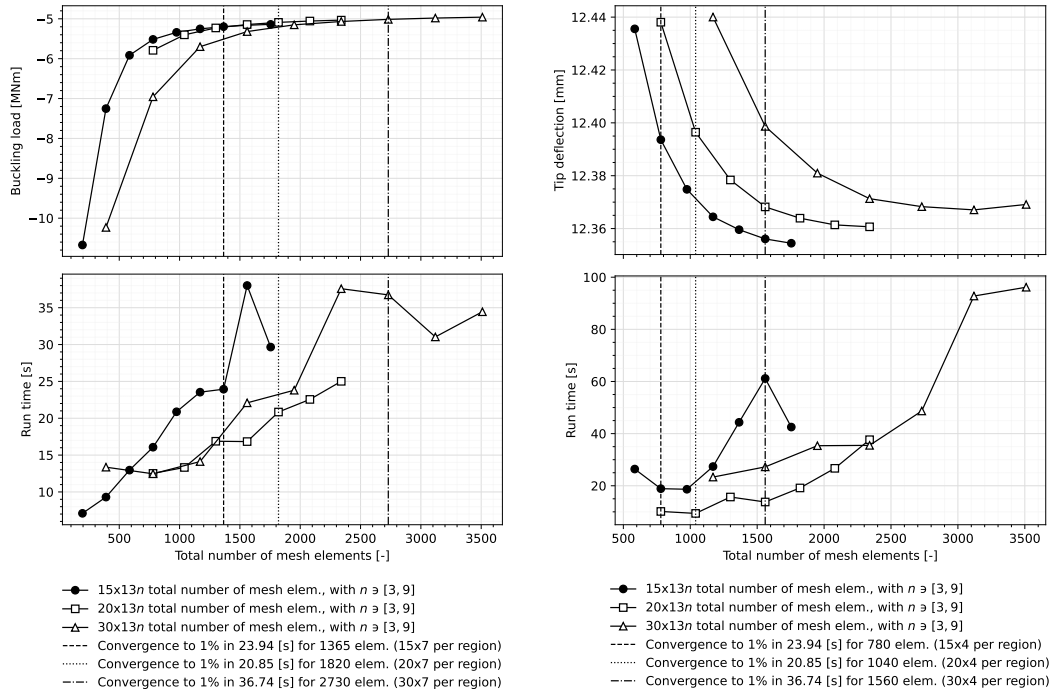
(a) Mesh convergence study on the buckling performance.

(b) Mesh convergence study on the deflection performance.

Figure 11.2: Mesh convergence study performed on the 1x13 region blade concept with 15, 20, and 30 mesh elements in the axial direction, and a varying number of mesh elements in the circumferential direction.

11.2. Local Stiffness Optimisation

The first step in the straight-fibre variable stiffness design optimisation framework is the evaluation of the optimal local stiffness. By local stiffness, it is understood to be the stiffness of a given region.

The lamination parameter distribution for the 1x13 regions blade section is provided in Figure 11.3. The distribution is shown for the four lamination parameters considered in the present research, namely the two in-plane (V_1^{A*} and V_3^{A*}) and out-of-plane (V_1^{D*} and V_3^{D*}) components. The asterisk indicates that those components are the optimal values. The distribution is shown on the horizontal axis from root to tip, and on the vertical axis for each circumferential region, going from the Trailing Edge (TE) Suction Side (SS) to the Trailing Edge Pressure Side (PS). From this distribution, one can namely highlight the presence of the caps as the white regions. It is remarkable that those regions feature unity lamination parameters as this indicates a purely unidirectional layup, which corresponds to the initial layup in these cap regions.

The stacking sequence retrieved for the lamination parameter sets introduced hereinabove is presented in Figure 11.6a. The stacking sequence is shown only for the upper half of the laminates as they are all symmetric. Hence, layers 1 to 16 represent the layup from the outermost to the innermost ply. On
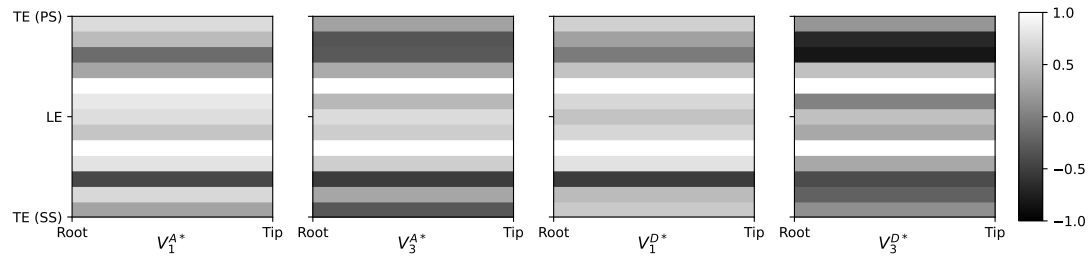
Figure 11.3: Optimal lamination parameter set for the 1x13 blade section design

the horizontal axis, the regions run from root to tip, highlighting the fact that a singular region is used over the full span of the blade. On the vertical axis, the ply orientation of each region circumferentially is provided, where the abbreviations introduced previously hold, and LE stands for Leading Edge.

The performance of the retrieval process going from lamination parameters to a discrete stacking sequence can be evaluated in several ways. Here two performance metrics are used. First, the L2 error can be evaluated between the optimal lamination parameter set, and the lamination parameter set of the stacking sequence retrieved. This is visually represented in Figure 11.4 for the 1x13 blade section. The difference in the optimal and retrieved lamination parameters is arguably low, and slight differences are observed in the regions about the caps. The second metric used to assess the performance of the retrieval process is the comparison of the ABD matrix of both designs.
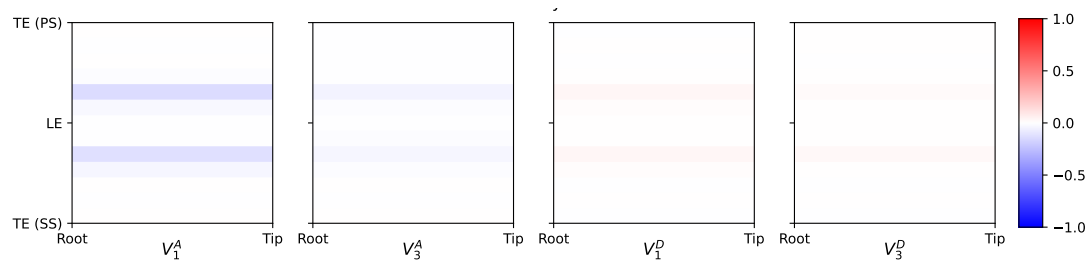
Figure 11.4: L2 error between the optimal and retrieve lamination parameter sets for the 1x13 blade section design

In Figure 11.5, a comparison of the ABD matrices for the optimal lamination parameter design, and the design with retrieved stacking sequence is compared. The fourth region, namely the trailing-edge panel region, is the one displaying the greatest L2 error in Figure 11.4, and thus was used here. Good agreement between the two matrices is argued as the difference in stiffness does not exceed 5.3%.
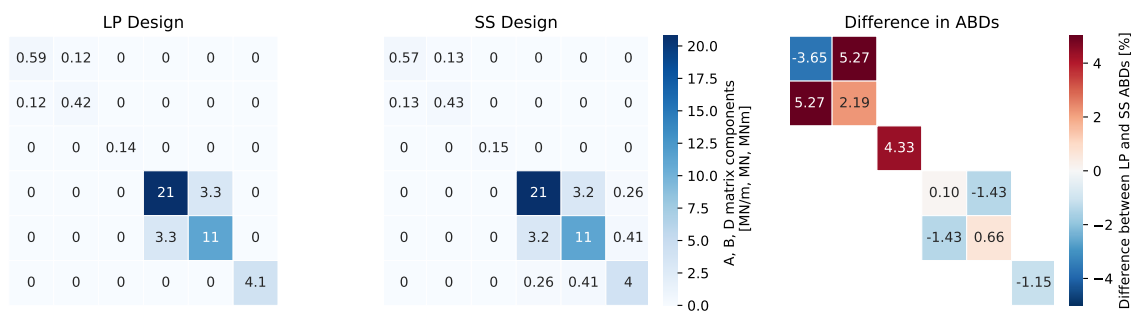

Figure 11.5: Comparison of the ABD matrix for the suction side trailing-edge panel of the 1x13 blade section design

11.3. Enforcing Blending Constraints

When introducing local blending, the local optimal stacking sequence shown in Figure 11.6a evolves into the stacking sequence provided in Figure 11.6b. In this conversion, the stacking sequence gets noticeably simplified, namely as isolated plies tend to be replaced by plies similar to their neighbours.

More interestingly, when focusing on the 12th layer, an additional ply is introduced in the 3rd and 11th regions, being the trailing-edge panels regions. These additional plies are introduced to comply with the local blending rules. This introduction of two additional plies in regions such as the trailing edge panel will have an influence on the structural performance of the whole structure, as will be highlighted in Section 11.5.

(a) Retrieved locally optimal stacking sequence.   **(b)** Locally blended stacking sequence
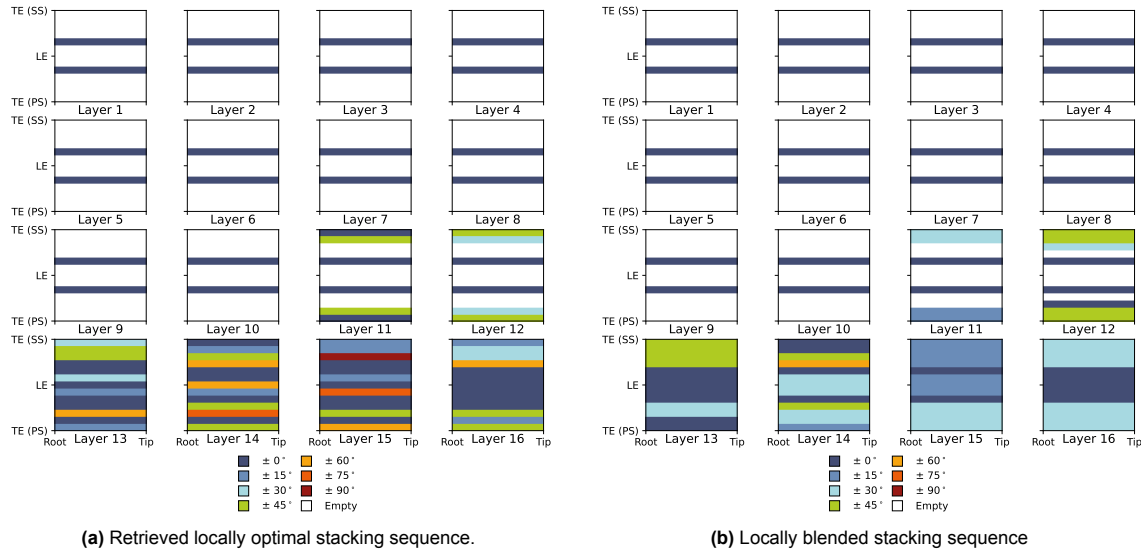
Figure 11.6: Locally optimal and blended stacking sequence for the 1x13 blade section design.

The decision was taken to not blend the caps with their neighbouring regions, as discussed in Section 7.4, and illustrated in Figure 7.3. This can also be visible in Figure 11.7a as the thick cap laminates do not have plies continuing in the trailing and leading edge panels. Due to their relatively thicker layup, the local blending process removed the plies in excess in those cap regions, making the design violate the deflection and buckling requirement specified. Hence, it was chosen to not enforce blending rules around the cap regions.
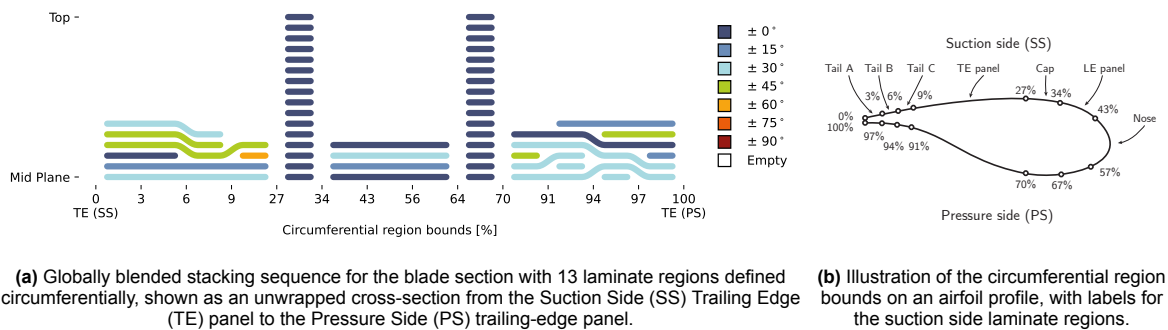

(a) Globally blended stacking sequence for the blade section with 13 laminate regions defined circumferentially, shown as an unwrapped cross-section from the Suction Side (SS) Trailing Edge (TE) panel to the Pressure Side (PS) trailing-edge panel.

(b) Illustration of the circumferential region bounds on an airfoil profile, with labels for the suction side laminate regions.

Figure 11.7: Globally blended stacking sequence of the 1x13 blade section design, with an illustration of the circumferential region bounds definition.

It is interesting to note that the laminate present on the suction side does not mirror that of the pressure side. This could be argued from the non-symmetry of the cross-section, but most importantly it can be explained by the loading condition. As a tip moment is applied that loads the suction side under compression, its regions will be prone to buckling, rather than the pressure side. The fact that the

suction side shall resist buckling can be observed from the stacking sequence of the suction side which tends towards a quasi-isotropic layup (i.e., more $\pm 45°$ and $\pm 60°$ plies). Furthermore, those off-axis plies are placed furthest away from the laminate symmetry plane in order to benefit the bending stiffness (Kassapoglou, 2013).

11.4. Enforcing Blending Constraints Between Trailing-Edge and Leading Edge Panels

The result presented previously, namely in Figure 11.7a, features a crucial flaw: the skin laminates do not feature continuity around the caps. As previously stated, blending the spar caps with trailing-edge and leading-edge panels is hindered by the relatively large thickness gradients. However, it is paramount to restore continuity across those regions to achieve a manufacturable and integral structure.

To resolve this continuity, in the blending process, the trailing-edge and leading-edge panels were enforced as neighbouring regions. This approach is illustrated in Figure 11.8. Essentially, the blending process is applied to the facesheets of the skin laminate of a blade. The caps laminates are considered to be encompassed by those facesheets, in a similar fashion as facesheets envelop a core material in a sandwich material. In this manner, the laminate over the circumference of a blade section is continued across spar caps.
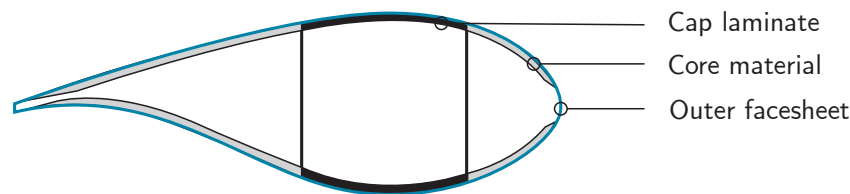

Figure 11.8: Illustration of the main material components in wind turbine blades, highlighting the presence of a cap laminate, core material, and laminate facesheet.

Applying this continuity rule between the trailing-edge and leading-edge panels for the 1x13 blade section problem returns the globally blended facesheet laminate as presented in Figure 11.9a. It is namely remarkable that continuity is achieved across the full laminate, meaning over the full circumference of the blade section. For reference, a comparable laminate cross-section is shown in Figure 11.9b for the baseline layup considered, which is the stacking sequence of the DTU 10MW.
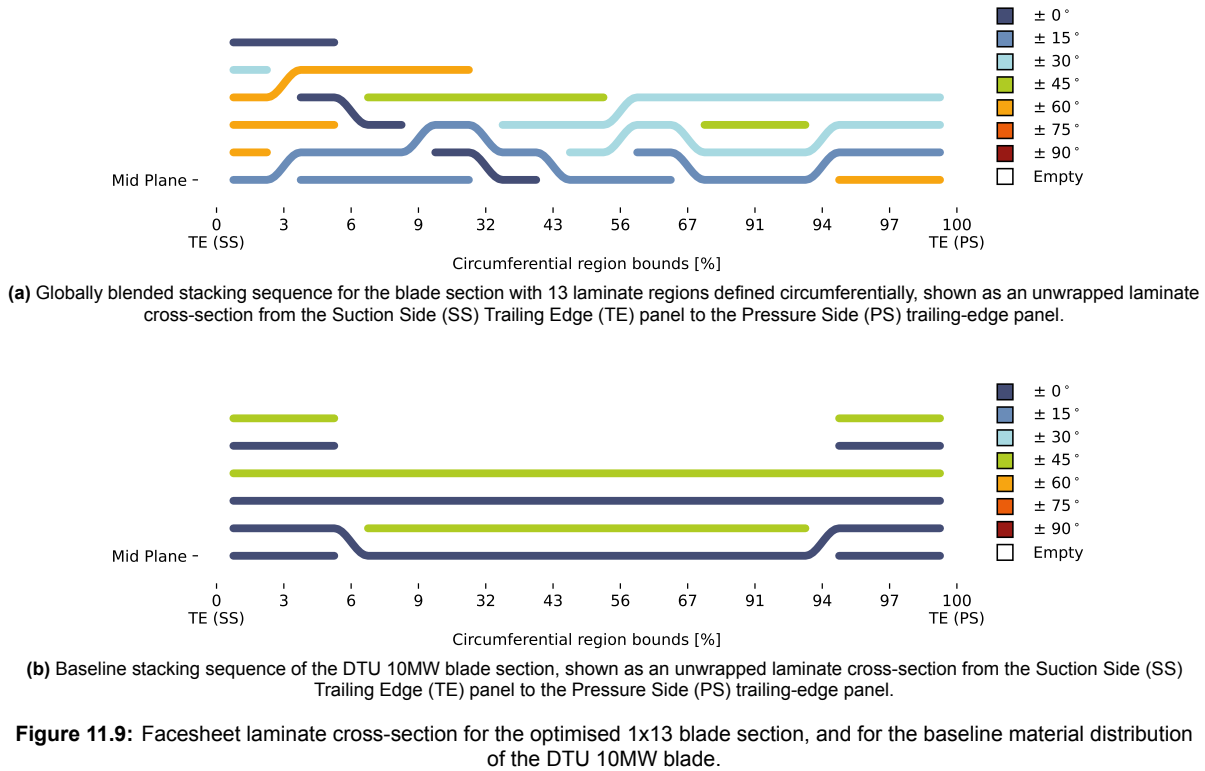
11.5. Evolution of the Blended Blade Sections Performances

Provided with insights on the results achieved in the local stiffness and blending optimisations for the 1x13 blade section problem, it is relevant to compare the overall performances achieved for the three blade section concepts considered. The evolution of the performance will be reported for each concept and for each step of the straight-fibre variable stiffness laminate optimisation.

The evolution of the structural performance for the three blade concepts considered is presented in Figure 11.10. In the top figure, the evolution of the tip deflection is shown, with the target deflection highlighted by the dotted horizontal line. In the bottom diagram, the design buckling loads are reported, along with the baseline buckling load shown as a dashed horizontal line. Please note that here-above, the results for the 1x13 regions blade section were discussed. Nonetheless, readers interested in reviewing the results for the 1x17 and 1x24 regions blade sections are referred to Appendix A.

Regarding the deflection, step 1 of the optimisation process overall achieves a deflection for all concepts around the target value. One can argue that the deflection does not exactly lie on the target threshold value because of the bonus given to designs with higher buckling margins. In fact, a design with a deflection further away from the target, yet with an increase in buckling performance is preferred through the use of the augmented objective function.

In the conversion of a design with lamination parameters to a stacking sequence design (i.e. going from step 1 to step 2), the buckling performance is less affected by this conversion than the deflection. For

(a) Globally blended stacking sequence for the blade section with 13 laminate regions defined circumferentially, shown as an unwrapped laminate cross-section from the Suction Side (SS) Trailing Edge (TE) panel to the Pressure Side (PS) trailing-edge panel.

(b) Baseline stacking sequence of the DTU 10MW blade section, shown as an unwrapped laminate cross-section from the Suction Side (SS) Trailing Edge (TE) panel to the Pressure Side (PS) trailing-edge panel.

Figure 11.9: Facesheet laminate cross-section for the optimised 1x13 blade section, and for the baseline material distribution of the DTU 10MW blade.

instance, for the 1x13 blade section, the difference in deflection going from a lamination parameters design to a stacking sequence design is about 7%, while the difference in buckling load is about 3%. Yet, reductions in deflection and buckling performances remain consistent for all concepts, indicating that the stacking sequence retrieval process is independent of the problem size. This result is expected as the retrieval approach is a local process, thus not affected by the increase in the number of regions.

For all blade section concepts, the buckling performance evolution seems unexpected going from step 2 to step 3. In fact, when going from local optimal designs to locally blended designs, the buckling load increases. This result is unexpected as, when applying blending constraints, the design space is reduced, rendering a decrease in structural performance. However, for all blade section concepts, an improved buckling performance is achieved when applying local blending constraints. Investigating the stacking sequence at those steps could explain the improved performance. For instance, for the 1x13 blade section, the stacking sequences for the local optimal and locally blended design are reported in Figure 11.11a and 11.11b, respectively. In the 12th layer, additional plies are introduced in the 3rd region (i.e. suction side cail C), in the 4th region (i.e. suction side trailing edge panel), and in the 11th region (i.e. pressure side tail C). These additional plies are introduced to ensure the local blending of those regions with their neighbours. The blending guidelines ensure that no dropped edges are in contact. The introduction of these additional plies, especially in crucial regions such as the suction-side trailing edge panel, can explain the buckling performance increase of the design going to a locally blended design. In fact, as buckling occurs on the blade suction side, towards the trailing edge, the introduction of plies in those regions allows to resist greater buckling instabilities.

The introduction of these additional plies enables improved structural performances that were not accessible in the local stiffness optimisation with lamination parameters. The reason is that the local stiffness optimisation is constrained to a given number of plies. In the blending process (i.e. step 3), this constraint on the number of plies available is no longer enforced, thus allowing the algorithm to introduce additional plies, if need be, to comply with the blending guidelines. The hypothesis that the local stiffness optimisation did not explore the full design space is unlikely. The reason is that, for all concepts, the number of consecutive misses was the cause for the convergence of the local stiffness optimisation. As such, one can assume that the optimal lamination parameter sets were then achieved.
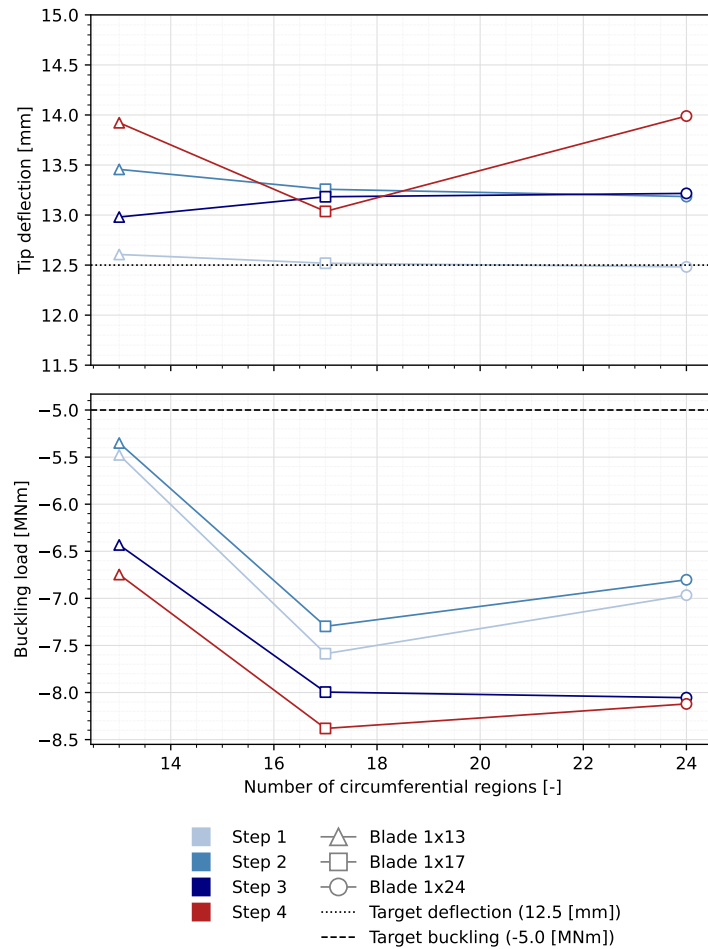
Figure 11.10: Performance of the blade section optimisation with straight-fibre variable stiffness.

With respect to the evolution in tip deflection going from step 2 to step 3, an improved tip deflection is achieved for all designs. In fact, deflections closer to the threshold value are achieved. This improvement, despite the enforcement of blending constraints, can also be linked to the introduction of additional plies. As for the buckling improvement, the introduction of these plies stiffens the structure, thus reducing the tip deflection.

The globally blended blade section designs all achieve an improved buckling performance, while suffering from an increase in the tip deflection relative to the threshold value. The 1x17 regions design achieves the best performance, with a buckling load of -8.4 MNm, which is an increase of 68% compared to the baseline value, and a tip deflection of approximately 13.1 mm (4.8% increase relative to the target value). The 1x24 regions design however achieves the best deflection performance with a tip deflection of 13.2 mm, which is in best agreement with the target value. The 1x24 regions design achieves a great tip deflection, to about 14 mm, which is 12% greater than the target value. Nevertheless, this concept allows for a 63% increase in buckling performance.

Curiously, the performance of the 1x24 regions concept is lower than that of the 1x17 regions. This result is unexpected as one would anticipate that a structure with more design regions, thus more design freedom, could be further tailored. However, the 1x17 regions blade section manifestly achieves better deflection and buckling performances compared to the 1x24 regions concept. Roepman (2021) reported similar results, where the buckling performance of a straight-fibre variable stiffness shaft under bending achieved no further buckling performance improvement past a given number of design regions. It was therefore suggested that the blending optimisation converged, and that the region layout provides sufficient design freedom to increase the maximum achievable performance.
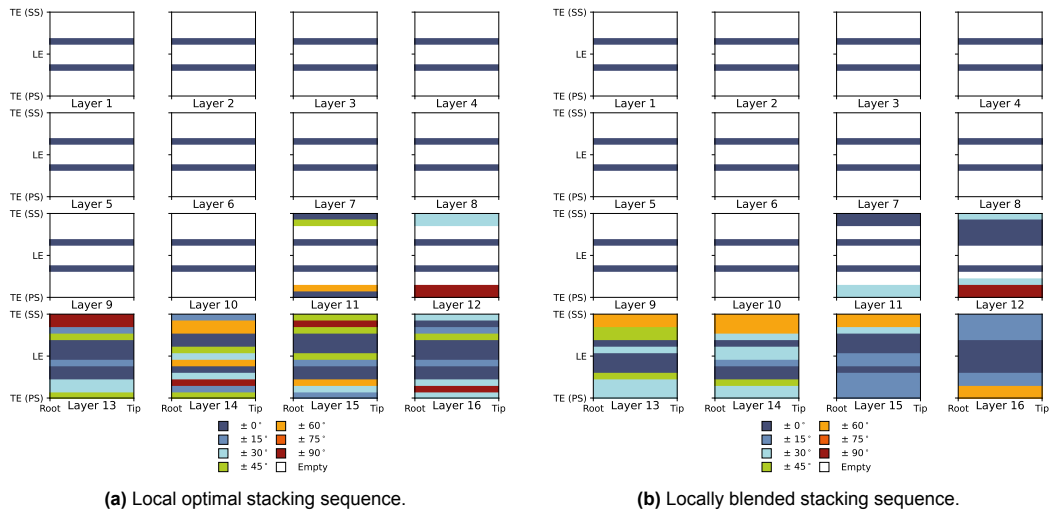
(a) Local optimal stacking sequence.

(b) Locally blended stacking sequence.

Figure 11.11: Locally optimal and blended stacking sequence for the 1x13 blade section design with continuity enforced between trailing-edge and leading-edge panels.

Investigating the buckling mode of the blade sections considered, a comparison between the first mode shape for the baseline section and for the 1x17 regions concept is provided in Figure 11.12. The buckling mode observed matches the trailing-edge buckling mode reported in the documentation of the DTU 10MW reference turbine (Bak et al., 2013). It is interesting to note that the buckling mode achieved by the blended blade design, shown in Figure 11.12b, resembles that of the baseline structure, shown in Figure 11.12a. In fact, under the idealised flapwise bending moment, buckling remains localised on the suction-side trailing edge panel.

(a) First buckling mode of the DTU 10MW reference blade section.

(b) First buckling mode of the 1x17 regions blade section.
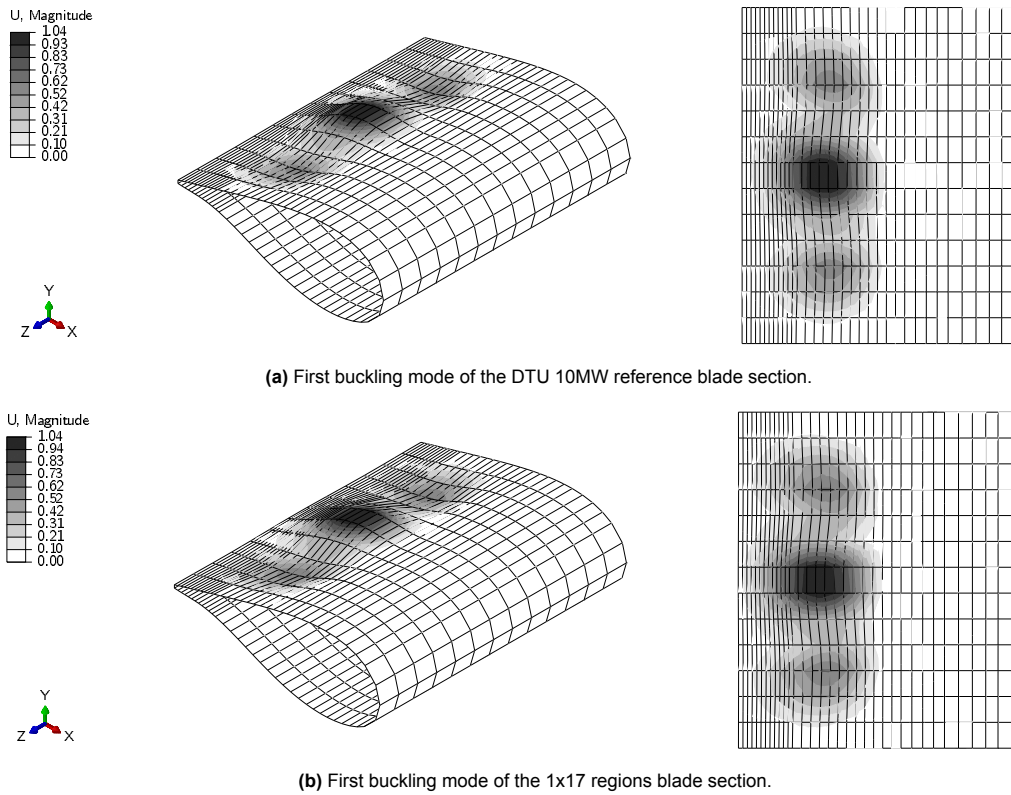
Figure 11.12: Isometric (left) and suction-side (right) views of the first buckling mode for the baseline and 1x17 blade section concept. The contour plot shows the magnitude of the deflection.

11.6. Mesh Convergence Study Post-Optimisation

A mesh convergence study was performed on one of the final blade section designs. As the internal structure of the blade section has been drastically revised through the laminate blending optimisation, it is relevant to assess whether the mesh convergence study performed on the baseline design holds for the globally blended design obtained.

The globally blended blade design with 1x13 regions was selected for this post-optimisation mesh convergence study. The number of mesh elements in the spanwise direction was kept to 15 elements as this corresponds to the figure used during the optimisation. Comparably to the mesh convergence study performed previously, convergence is assumed when the structural performance for a given mesh arrangement is less than 1% different relative to the performance of the previously evaluated mesh arrangement. Reported in Figure 11.13a is the buckling performance convergence, highlighting that a minimum of 6 elements per region in the circumferential direction are required. The deflection convergence study, presented in Figure 11.13b underlines that a minimum of 4 elements per region in the circumferential direction are required. Hence, the mesh configuration chosen in the straight-fibre variable stiffness laminate optimisation, namely with 15x7 elements per region, is reasonable.

(a) Mesh convergence study on the buckling performance.   (b) Mesh convergence study on the deflection performance.
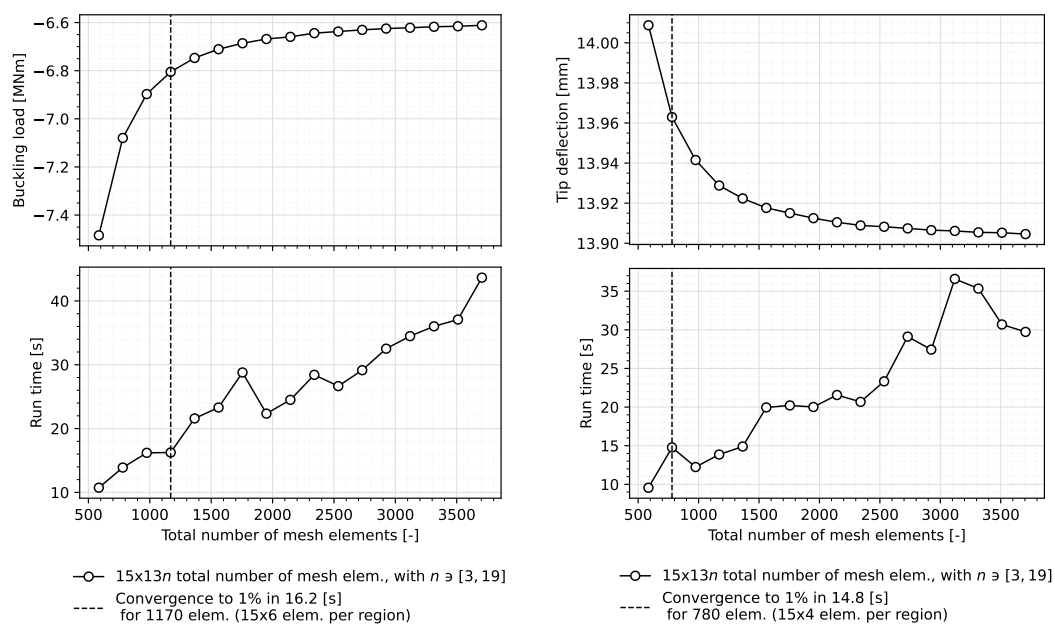
Figure 11.13: Mesh convergence study performed on the 1x13 region globally blended blade design with 15 mesh elements in the axial direction, and a varying number of mesh elements in the circumferential direction.

11.7. Outlook on Straight-Fibre Variable Stiffness Sandwich Structures

In the literature study reported in Section 2.1, sandwich structures were shown to be essential components in the design of wind turbine blades. Monolithic laminates were considered in the present research, with a unique unidirectional material as lamina for the straight-fibre variable stiffness laminates of the blade sections. The question remains regarding whether straight-fibre variable stiffness laminates benefit sandwich structures in blade design.

A preliminary approach to answer such a question is proposed here-after. The baseline core material distribution reported for the DTU 10MW structure (c.f. Table 9.1) is added at the symmetry plane of the globally blended laminate obtained previously. Considering the 1x17 regions concept, a buckling performance under the idealised flapwise bending moment achieves a critical load of 40.06 MNm. This buckling performance exceeds by 21.36% the performance of the baseline blade section with core material. In fact, the baseline DTU 10 MW blade section with core material achieves a buckling load of

33.01 MNm.

The first buckling mode of both baseline and 1x17 regions blade sections fitting core material is sensibly identical, and it is reported for the 1x17 concept in Figure 11.14. It is interesting to note that, with the presence of core material, the buckling mode shifts over the suction side trailing-edge panel towards the leading-edge, compared to the behaviour observed in Figure 11.12b. Due to the addition of core material, the bending stiffness of the suction side trailing edge panels is improved, allowing to extend the buckling behaviour towards the thick unidirectional spar cap.
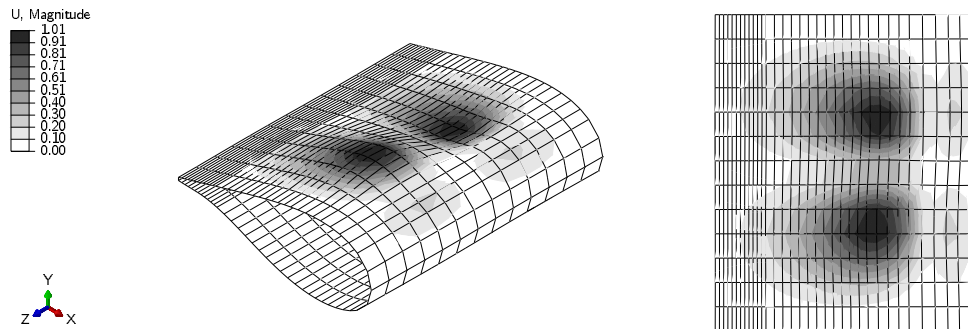
Figure 11.14: Isometric (left) and suction-side (right) views of the first buckling mode for the 1x17 blade section concept fitted with core material. The contour plot shows the magnitude of the deflection.

Even though the improvement for the blade section with core material is lower than the 68% increase achieved with monolithic blended blade designs, these preliminary buckling suggests the potential for the use of straight-fibre variable stiffness laminates when used in sandwich structures. Further research is however required to assess the full potential of straight-fibre variable stiffness laminates applied to the facesheets of sandwich panels.

Part IV

Highlights & Further Research

12

Discussion

Two frameworks, referred to as AESOpt and SFVS, were selected to perform a variable stiffness laminate design of a wind turbine blade section. These two tools are research codes developed on one hand at DTU Wind Energy Department, and on the other hand from the effort of Gomaa (2019), Roepman (2021), and van den Oord (2018). After a familiarisation phase with each tool, the following contributions to each framework were made.

Regarding the blade design tool, the main effort was provided in defining a workflow to achieve a structural optimisation where the mass of a structure is minimised under a set of design constraints, such as deflection, strain and stiffness. Regarding the straight-fibre variable stiffness laminate design tool, coding effort was provided in setting up a Python script to generate parametric Abaqus simulations for prismatic beam structures for both non-linear static analyses and linear buckling studies. This parametric finite element model has also been extended to define variable region sizes and mesh distributions. The problem formulation partially relies on the WindIO problem definition from Bortolotti et al. (2022) to conveniently interface with the AESOpt framework. A converter was also developed to export the results from the AESOpt optimisation to the SFVS tool. The SFVS framework was further extended to perform local stiffness optimisation with lamination parameters for a buckling maximisation problem under a deflection constraint. This contribution extends on the work of Roepman (2021), through the use of an augmented objective function.

Based on these extensions, the investigation into the application of straight-fibre variable stiffness laminates to blade structures was performed on a reference blade section. Refinement in the number of design regions over the trailing-edge panels highlighted improvements in buckling performance at the cost of an increase in deflection. The improvement in buckling for globally blended laminates ranges from 34 to 68% greater than the baseline critical load. These improvements were attributed to the local stacking sequence optimisation, tailoring the stiffness of a blade around its circumference. Deflection increase was however observed, ranging from 4.8 to 12% larger than the baseline target value. This discrepancy was attributed to the fact that the deflection constraint is solely enforced in the first stage of the optimisation. As the stacking sequence gets blended, the deflection target is no longer tracked and is therefore subject to increase. Further research could consider tackling this issue, for instance by iterating the laminate blending process to adjust the constraints and achieve a design satisfying the targets.

Due to time constraints, some analyses were not performed. For instance, spanwise stiffness variation was not assessed as constant region laminates were considered to extend from root to tip. Load redistribution could benefit from such spanwise stiffness variation, and remains to be investigated. Furthermore, the definition of core material within the parametric finite element model would allow to further evaluate the performance of straight-fibre variable stiffness laminates when introduced in the facesheets of sandwich structures. These additional analyses are part of the recommendations suggested at the end of the present report.

13

Conclusion

The research objective set out in this report was to investigate the structural performance potential for straight-fibre variable stiffness laminates in wind turbine blade design, by extending and coupling existing frameworks. Two methodologies were proposed to achieve a laminate blending design in a wind turbine blade structure. The first method defines the approach for a full design of a blended blade, which includes aeroelastic response analysis for load redistribution evaluation. The second methodology considers a small scale of the full blade design. This small-scale design is the blending of a section of a blade. With these two workflows defined, the first sub-research question on the methodology was then tackled.

To apply the design approach of straight-fibre variable stiffness laminates to a large-scale structure such as a wind turbine blade, a contribution was made by the definition of a parametric finite element model capable of defining a blade geometry as a stacking sequence design, as well as a lamination parameters design. Two main limitations of the current definition however are that the definition of shear webs and sandwich materials, which were not implemented. Furthermore, the local stiffness optimisation of a multi-region laminate was further extended by the definition of a detailing scheme approach to maximise the buckling performance of a structure while ensuring its compliance with a target deflection requirement. This contribution tackles the second sub-research question about the extension of the variable stiffness laminate design for blade structures.

The extended laminate blending framework was then applied to a benchmark blade section design. The DTU 10MW reference wind turbine blade was selected as the baseline structure. A section of this blade taken at the maximum chord location, was considered for laminate blending. Three concept variants of this blade section were examined to assess the influence of laminate blending on the buckling performance of the trailing edge panels. These three alternative concepts differed in the number of regions featured on their trailing-edge panels.

The evolution of the blended blade section performance was evaluated for these three concepts. The local stiffness optimisation was shown to achieve designs complying with the target deflection while improving the buckling performance between 10% to 52% relative to the reference blade section. With an increasing number of regions on the trailing edge panels, the change in structural performance going from step 1 to step 4 of the blending framework returns less variation for the 1x17 regions design, than for the coarser (1x13 regions) or finer (1x24 regions) designs. In fact, for the 1x17 regions blade section, the tip deflection is closest to the deflection target and the buckling performance of the globally blended design reaches its maximum. The buckling load achieved by the 1x17 regions concept is approximately 68% greater than the baseline performance, at the cost of a 4.8% increase in tip deflection. For the other two blade sections, a greater reduction in deflection performance is reached when introducing blending constraints. Until a certain region layout refinement, increasing the number of design regions is suggested to be beneficial in reducing the performance losses due to the enforcement of blending constraints.

Overall, the methodology presented in this research highlights the potential improvements achieved with straight-fibre variable stiffness laminates when applied to a blade section under flapwise bending. Specifically, when refining the number of regions present on the trailing-edge panels, improvements in buckling performance are achieved without jeopardising the tip deflection of the blade.

14

Recommendations

Although the potential for straight-fibre variable stiffness design in large-scale structures such as wind turbine blades has been highlighted, further work is required to improve the fidelity of the design tool. The following potential improvements are proposed to further detail the design framework:

- **Local stiffness optimisation objective** | A contribution made in the present research was the definition of an optimisation scheme to define a lamination parameters design matching a deflection target while maximising its buckling performance. Besides buckling and deflection, one could consider achieving aeroelastic tailoring through material adaptive design as an objective for the optimisation of a lamination parameters design, as discussed in Chapter 4.

- **Hybrid material blending** | Currently, the framework is limited to the use of a single-ply material. This limitation namely originates from the retrieval process of lamination parameters to a stacking sequence. The opportunity to retrieve a hybrid material stacking sequence from a given lamination parameter set would allow the consideration of sandwich materials in a given design. Answering the question of how to retrieve a discrete sandwich stacking sequence from a set of lamination parameters would then expand the possible application of straight-fibre variable stiffness.

- **Multi-cell beam modelling** | The parametric model extended in the present research only considers the definition of prismatic single-cell beams. As such, shear webs that are commonly used in blade structural design to resist shear loads were not considered, knocking down the baseline performance that can be achieved. Hence, extending the formulation of a parametric finite element model to multi-cell beam geometries would allow a more reasonable comparison of structures featuring such complex geometries.

- **Spanwise variable stiffness** | In the present analysis, blade sections with constant laminate regions in the spanwise direction were defined. Evaluating the effect of introducing multiple design regions in the axial direction would be of interest. In fact, having multiple design regions over the span of a blade section, for instance, could be beneficial to introduce spanwise load redistribution. Spanwise variable stiffness could especially provide structural improvements for bending load cases.

Besides the extension of the straight-fibre variable stiffness design tool, further work is recommended to incorporate it within an aero-structural design framework. Even though the iteration scheme for the design of a full blade with laminate blending was described in this report, the analysis was limited to a blade section. Hence, extending the framework to consider a full blade design would be a next step such that load redistribution enabled through laminate blending is accommodated.

Bibliography

Abdalla, M., Gandhi, F., van Bussel, G., & Dillinger, J. (2017). Aeroelastic optimization of composite wind turbine blades using variable stiffness laminates. *AHS International 73rd Annual Forum & Technology Display*.

Ashwill, T. D. (2010a). Passive load control for large wind turbines. *51st AIAA/ASME/ASCE/AHS/ASC Structures, Structural Dynamics, and Materials Conference*. https://doi.org/10.2514/6.2010-2577

Ashwill, T. D. (2010b). *Sweep-twist adaptive rotor blade : Final project report.* (SAND2009-8037). Sandia National Laboratories (SNL), Albuquerque, NM, and Livermore, CA (United States). https://doi.org/10.2172/973353

Bak, C. (2013). 3 - aerodynamic design of wind turbine rotors. In P. Brøndsted & R. P. L. Nijssen (Eds.), *Advances in wind turbine blade design and materials* (pp. 59–108). Woodhead Publishing. https://doi.org/10.1533/9780857097286.1.59

Bak, C., Zahle, F., Bitsche, R., Taesong, K., Yde, A., Henriksen, L. C., Natarajan, A., & Hansen, M. H. (2013, July). *Description of the DTU 10 MW reference wind turbine* (DTU Wind Energy Report-I-0092). DTU Wind Energy.

Barnes, R. H., Morozov, E. V., & Shankar, K. (2015). Improved methodology for design of low wind speed specific wind turbine blades. *Composite Structures*, *119*, 677–684. https://doi.org/10.1016/j.compstruct.2014.09.034

Barr, S. M., & Jaworski, J. W. (2019). Optimization of tow-steered composite wind turbine blades for static aeroelastic performance. *Renewable Energy*, *139*, 859–872. https://doi.org/10.1016/j.renene.2019.02.125

Berggreen, C., Branner, K., Jensen, J., & Schultz, J. (2007). Application and analysis of sandwich elements in the primary structure of large wind turbine blades. *Journal of Sandwich Structures & Materials*, *9*(6), 525–552. https://doi.org/10.1177/1099636207069071

Blasques, J. P. A. A. (2012). *User's manual for BECAS: A cross section analysis tool for anisotropic and inhomogeneous beam sections of arbitrary geometry* (Report Risoe-R No. 1785(EN)). Risø DTU – National Laboratory for Sustainable Energy.

Bortolotti, P., Bay, C., Barter, G., Gaertner, E., Dykes, K., McWilliam, M., Friis-Moller, M., Molgaard Pedersen, M., & Zahle, F. (2022). *System modeling frameworks for wind turbines and plants: Review and requirements specifications* (NREL/TP-5000-82621). https://doi.org/10.2172/1868328

Bottasso, C., Campagnolo, F., Croce, A., & Tibaldi, C. (2013). Optimization-based study of bend–twist coupled rotor blades for passive and integrated passive/active load alleviation. *Wind Energy*, *16*(8), 1149–1166. https://doi.org/10.1002/we.1543

Buckney, N., Green, S., Pirrera, A., & Weaver, P. M. (2013). On the structural topology of wind turbine blades. *Wind Energy*, *16*(4), 545–560. https://doi.org/10.1002/we.1504

Buckney, N., Pirrera, A., Green, S. D., & Weaver, P. M. (2013). Structural efficiency of a wind turbine blade. *Thin-Walled Structures*, *67*, 144–154. https://doi.org/10.1016/j.tws.2013.02.010

Capellaro, M. (2012). Design limits of bend twist coupled wind turbine blades. *53rd AIAA/ ASME/ ASCE/ AHS/ ASC Structures, Structural Dynamics and Materials Conference*. https://doi.org/10.2514/6.2012-1501

Capuzzi, M., Pirrera, A., & Weaver, P. M. (2014a). A novel adaptive blade concept for large-scale wind turbines. part i: Aeroelastic behaviour. *Energy*, *73*, 15–24. https://doi.org/10.1016/j.energy.2014.06.044

Capuzzi, M., Pirrera, A., & Weaver, P. M. (2014b). A novel adaptive blade concept for large-scale wind turbines. part II: Structural design and power performance. *Energy*, *73*, 25–32. https://doi.org/10.1016/j.energy.2014.04.073

Capuzzi, M., Pirrera, A., & Weaver, P. M. (2015). Structural design of a novel aeroelastically tailored wind turbine blade. *Thin-Walled Structures*, *95*, 7–15. https://doi.org/10.1016/j.tws.2015.06.006

Chetan, M., Sakib, M. S., Griffith, D. T., & Yao, S. (2019). Aero-structural design study of extreme-scale segmented ultralight morphing rotor blades. *AIAA Aviation 2019 Forum*. https://doi.org/10.2514/6.2019-3347

Fedorov, V. (2012). *Bend-twist coupling effects in wind turbine blades* (Doctoral dissertation). Technical University of Denmark (DTU).

Fedorov, V., Dimitrov, N. K., Berggreen, C., Krenk, S., Branner, K., & Berring, P. (2010). Investigation of structural behavior due to bend-twist couplings in wind turbine blades. *NAFEMS NORDIC Seminar: Simulating Composite Materials and Structures*.

Ghiasi, H., Fayazbakhsh, K., Pasini, D., & Lessard, L. (2010). Optimum stacking sequence design of composite materials part II: Variable stiffness design. *Composite Structures*, *93*(1), 1–13. https://doi.org/10.1016/j.compstruct.2010.06.001

Gomaa, M. (2019). *Laminate blending demonstrator: A buckling experimental campaign of a physical laminate blending demonstrator* (MSc Thesis). Delft University of Technology (TU Delft). Delft, The Netherlands.

Gray, J. S., Hwang, J. T., Martins, J. R. R. A., Moore, K. T., & Naylor, B. A. (2019). OpenMDAO: An open-source framework for multidisciplinary design, analysis, and optimization. *Structural and Multidisciplinary Optimization*, *59*(4), 1075–1104. https://doi.org/10.1007/s00158-019-02211-z

Griffin, D. A. (2002). *Evaluation of design concepts for adaptive wind turbine blades* (SAND2002-2424). Sandia National Lab. (SNL-NM), Albuquerque, NM (United States); Sandia National Lab. (SNL-CA), Livermore, CA (United States). https://doi.org/10.2172/801399

Griffin, D. A. (2004). *Blade system design studies volume II : Preliminary blade designs and recommended test matrix.* (SAND2004-0073). Sandia National Laboratories (SNL), Albuquerque, NM, and Livermore, CA (United States). https://doi.org/10.2172/918295

Griffin, D. A., & Ashwill, T. D. (2003). Alternative composite materials for megawatt-scale wind turbine blades: Design considerations and recommended testing. *Journal of Solar Energy Engineering*, *125*(4), 515–521. https://doi.org/10.1115/1.1629750

Gürdal, Z., IJsselmuiden, S., & van Campen, J. (2010). Composite laminate optimization with discrete variables. In *Encyclopedia of aerospace engineering*. John Wiley & Sons, Ltd. https://doi.org/10.1002/9780470686652.eae499

Haftka, R. T., & Gürdal, Z. (1992). *Elements of structural optimization* (Vol. 11). Springer Netherlands. https://doi.org/10.1007/978-94-011-2550-5

Hansen, M. O. L. (2015). *Aerodynamics of wind turbines: Third edition*. https://doi.org/10.4324/9781315769981

Hansen, M. H., Henriksen, L. C., Tibaldi, C., Bergami, L., Verelst, D., Pirrung, G., & Riva, R. (2018). *HAWCStab2 user manual*. Department of Wind Energy. Technical University of Denmark (DTU).

Hvejsel, C. F. (2011). *Multi-material design optimization of composite structures* (Doctoral dissertation). Institut for Mekanik og Produktion, Aalborg Universitet. Aalborg.

IJsselmuiden, S. T., Abdalla, M. M., & Gurdal, Z. (2010). Optimization of variable-stiffness panels for maximum buckling load using lamination parameters. *AIAA Journal*, *48*(1), 134–143. https://doi.org/10.2514/1.42490

Joosse, P. A., van Delft, D. R. V., Kensche, C., Soendergaard, D., van den Berg, R. M., & Hagg, F. (2002). Cost effective large blade components by using carbon fibers. *Journal of Solar Energy Engineering*, *124*(4), 412–418. https://doi.org/10.1115/1.1510526

Jureczko, M., & Mrówka, M. (2022). Multiobjective optimization of composite wind turbine blade. *Materials*, *15*(13), 4649. https://doi.org/10.3390/ma15134649

Kassapoglou, C. (2013). *Design and analysis of composite structures: With applications to aerospace structures*. John Wiley & Sons, Incorporated. https://doi.org/10.1002/9781118536933

Lambe, A. B., & Martins, J. R. R. A. (2012). Extensions to the design structure matrix for the description of multidisciplinary design, analysis, and optimization processes. *Structural and Multidisciplinary Optimization*, *46*(2), 273–284. https://doi.org/10.1007/s00158-012-0763-y

Larsen, T. J., & Hansen, A. M. (2007). *How 2 HAWC2, the user's manual*. Risø DTU - National Laboratory for Sustainable Energy.

Lobitz, D. W., Veers, P. S., Eisler, G. R., Laino, D. J., Migliore, P. G., & Bir, G. (2001). *The use of twist-coupled blades to enhance the performance of horizontal axis wind turbines* (SAND2001-1303). Sandia National Lab. (SNL-NM), Albuquerque, NM (United States); Sandia National Lab. (SNL-CA), Livermore, CA (United States). https://doi.org/10.2172/783086

Lund, E., & Stegmann, J. (2005). On structural optimization of composite shell structures using a discrete constitutive parametrization. *Wind Energy*, *8*(1), 109–124. https://doi.org/10.1002/we.132

Mandell, J. F., Samborsky, D. D., Miller, D. A., Agastra, P., & Sears, A. T. (2016). *Analysis of SNL/MSU/DOE fatigue database trends for wind turbine blade materials 2010-2015* (SAND2016-1441). Sandia National Laboratories.

McMahon, M. T., Watson, L. T., Soremekun, G. A., Gürdal, Z., & Haftka, R. T. (1998). A FORTRAN 90 genetic algorithm module for composite laminate structure design. *Engineering with Computers*, *14*(3), 260–273. https://doi.org/10.1007/BF01215979

McWilliam, M. K., Zahle, F., Dicholkar, A., Verelst, D., & Kim, T. (2018). Optimal aero-elastic design of a rotor with bend-twist coupling. *Journal of Physics: Conference Series*, *1037*, 042009. https://doi.org/10.1088/1742-6596/1037/4/042009

Mishnaevsky, L., Branner, K., Petersen, H., Beauson, J., McGugan, M., & Sørensen, B. (2017). Materials for wind turbine blades: An overview. *Materials*, *10*(11), 1285. https://doi.org/10.3390/ma10111285

Mølholt Jensen, F., & Branner, K. (2013). 1 - introduction to wind turbine blade design. In P. Brøndsted & R. P. L. Nijssen (Eds.), *Advances in wind turbine blade design and materials* (pp. 3–28). Woodhead Publishing. https://doi.org/10.1533/9780857097286.1.3

Nijssen, R. P. L., & Brøndsted, P. (2013). 6 - fatigue as a design driver for composite wind turbine blades. In P. Brøndsted & R. P. L. Nijssen (Eds.), *Advances in wind turbine blade design and materials* (pp. 175–209). Woodhead Publishing. https://doi.org/10.1533/9780857097286.2.175

Pirrera, A., Capuzzi, M., Buckney, N., & Weaver, P. (2012). Optimization of wind turbine blade spars. *53rd AIAA/ASME/ASCE/AHS/ASC Structures, Structural Dynamics and Materials Conference*. https://doi.org/10.2514/6.2012-1500

Roepman, T. (2021). *Patching a fuselage: Application of straight fiber variable stiffness laminates in large aerospace structures* (MSc Thesis). Delft University of Technology (TU Delft). Delft, The Netherlands.

Rosemeier, M., & Bätge, M. (2014). A concept study of a carbon spar cap design for a 80m wind turbine blade. *Journal of Physics: Conference Series*, *524*(1), 012039. https://doi.org/10.1088/1742-6596/524/1/012039

Rouhi, M., Ghayoor, H., Hoa, S. V., & Hojjati, M. (2017). Computational efficiency and accuracy of multi-step design optimization method for variable stiffness composite structures. *Thin-Walled Structures*, *113*, 136–143. https://doi.org/10.1016/j.tws.2017.01.019

Scott, S., Capuzzi, M., Langston, D., Bossanyi, E., McCann, G., Weaver, P. M., & Pirrera, A. (2017). Effects of aeroelastic tailoring on performance characteristics of wind turbine systems. *Renewable Energy*, *114*, 887–903. https://doi.org/10.1016/j.renene.2017.06.048

Söker, H. (2013). 2 - loads on wind turbine blades. In P. Brøndsted & R. P. L. Nijssen (Eds.), *Advances in wind turbine blade design and materials* (pp. 29–58). Woodhead Publishing. https://doi.org/10.1533/9780857097286.1.29

Sørensen, B. F., Jørgensen, E., Debel, C., Jensen, F. M., Jensen, H., Jacobsen, T., & Halling, K. (2004). *Improved design of large wind turbine blade of fibre composites based on studies of scale effects (phase 1). summary report* (Report No. 87-550-3176-5). Risø National Laboratory. Roskilde.

Sørensen, S. N., Sørensen, R., & Lund, E. (2014). DMTO – a method for discrete material and thickness optimization of laminated composite structures. *Structural and Multidisciplinary Optimization*, *50*(1), 25–47. https://doi.org/10.1007/s00158-014-1047-5

Stanford, B. K., Jutte, C. V., & Chauncey Wu, K. (2014). Aeroelastic benefits of tow steering for composite plates. *Composite Structures*, *118*, 416–422. https://doi.org/10.1016/j.compstruct.2014.08.007

Thomsen, O. T. (2009). Sandwich materials for wind turbine blades — present and future. *Journal of Sandwich Structures & Materials*, *11*(1), 7–26. https://doi.org/10.1177/1099636208099710

van den Oord, E. (2018). *Overcoming the curse of dimensionality in composite laminate blending: A CA-based algorithm for blending laminated composite plates with a large amount of sections* (MSc Thesis). Delft University of Technology (TU Delft). Delft, The Netherlands.

van den Oord, E., & van Campen, J. (2020). Straight fibre variable stiffness laminates: Using laminate blending instead of fibre steering. *ICCS23 - 23rd International Conference on Composite Structures; MECHCOMP6 - 6th International Conference on Mechanics of Composites*.

van Campen, J. (2011). *Optimum lay-up design of variable stiffness composite structures* (Doctoral dissertation). Delft University of Technology (TU Delft). Delft, The Netherlands.

van Campen, J., & Gürdal, Z. (2009). Retrieving variable stiffness laminates from lamination parameters distribution. *50th AIAA/ASME/ASCE/AHS/ASC Structures, Structural Dynamics, and Materials Conference*. https://doi.org/10.2514/6.2009-2183

van Campen, J., Seresta, O., Abdalla, M., & Gürdal, Z. (2008). General blending definitions for stacking sequence design of composite laminate structures. *49th AIAA/ASME/ASCE/AHS/ASC Structures, Structural Dynamics, and Materials Conference, 16th AIAA/ASME/AHS Adaptive Structures Conference,10th AIAA Non-Deterministic Approaches Conference, 9th AIAA Gossamer Spacecraft Forum, 4th AIAA Multidisciplinary Design Optimization Specialists Conference*. https://doi.org/10.2514/6.2008-1798

Veers, P., Lobitz, D., & Bir, G. (1998). *Aeroelastic tailoring in wind-turbine blade applications* (SAND-98-1208C; CONF-980437-). Sandia National Lab. (SNL-NM), Albuquerque, NM (United States). Retrieved December 22, 2022, from https://www.osti.gov/biblio/672151

Zabinsky, Z. (1994). Global optimization for composite structural design. In *35th structures, structural dynamics, and materials conference*. American Institute of Aeronautics; Astronautics. https://doi.org/10.2514/6.1994-1494

Zahle, F., Tibaldi, C., Pavese, C., McWilliam, M. K., Blasques, J. P. A. A., & Hansen, M. H. (2016). Design of an aeroelastically tailored 10 MW wind turbine rotor. *Journal of Physics: Conference Series*, *753*(6). https://doi.org/10.1088/1742-6596/753/6/062008

Zahle, F., Tibaldi, C., Verelst, D. R., Bak, C., Bitsche, R., & Blasques, J. P. A. A. (2015). Aero-elastic optimization of a 10 MW wind turbine. *33rd AIAA/ASME Wind Energy Symposium*, *1*, 201–223.

Zuteck, M. (2002). *Adaptive blade concept assessment: Curved platform induced twist investigation* (SAND2002-2996). Sandia National Lab. (SNL-NM), Albuquerque, NM (United States); Sandia National Lab. (SNL-CA), Livermore, CA (United States). https://doi.org/10.2172/803289

A

Results from the Straight-Fibre Variable Stiffness Laminate Design of a Blade Section

The present chapter is a collection of additional results of the blade section patching optimisation that were not included in the main text. Those results are presented for the three blade section concept considered, where continuity between trailing-edge and leading-edge panels is enforced. The following plots are mainly aimed at providing a complete overview of the results at each stage of the optimisation for the designs considered.
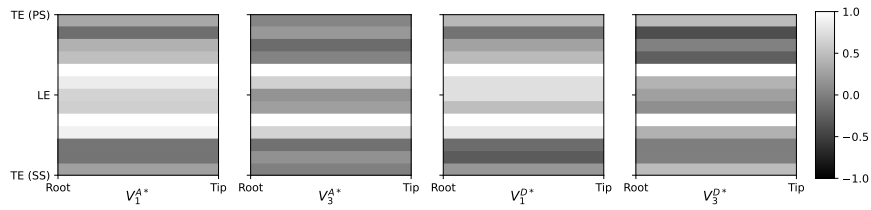
(a) Blade section 1x13.
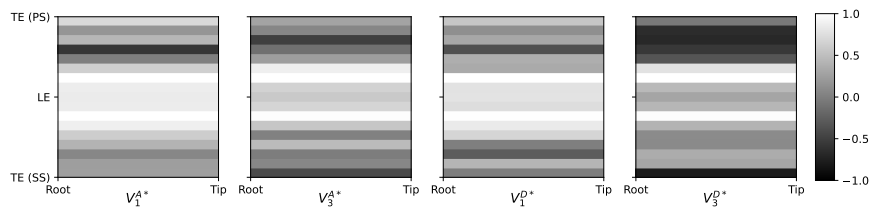
(b) Blade section 1x17.
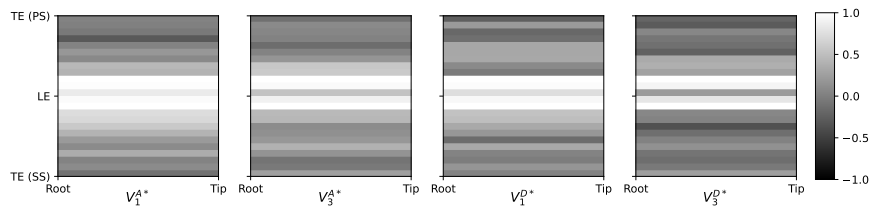
(c) Blade section 1x24.

Figure A.1: Optimal lamination parameters distributions.

(a) Blade section 1x13.

(b) Blade section 1x17.

(c) Blade section 1x24.
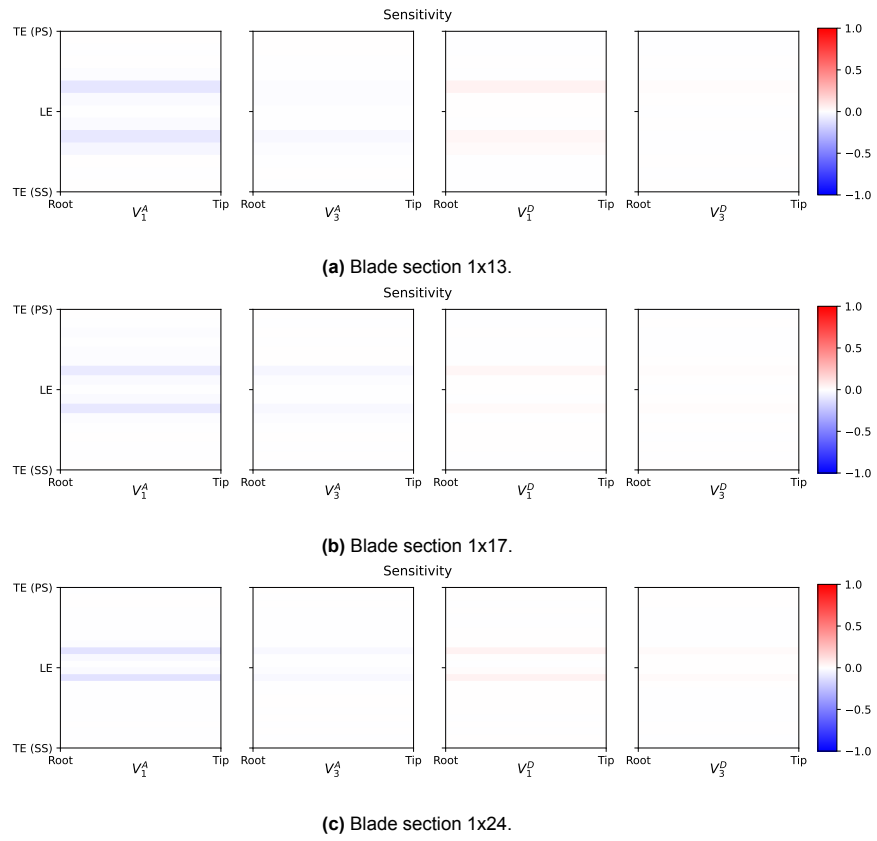
Figure A.2: Sensitivities of the optimal lamination parameters conversion to stacking sequence designs.
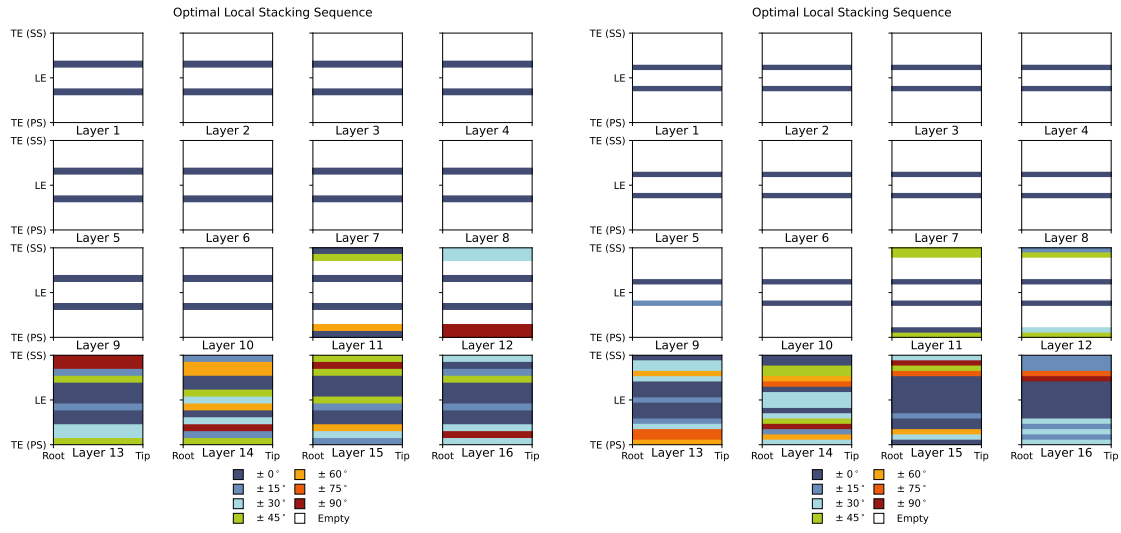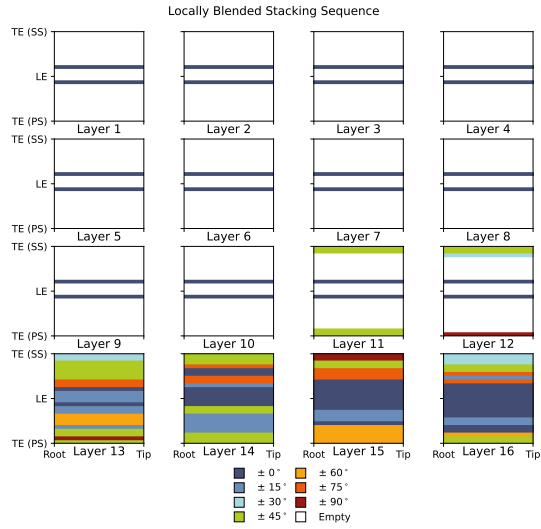
(a) Blade section 1x13.

(b) Blade section 1x17.
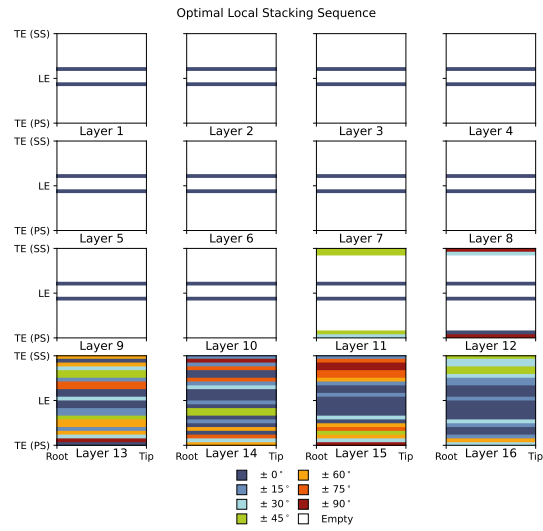
(c) Blade section 1x24.
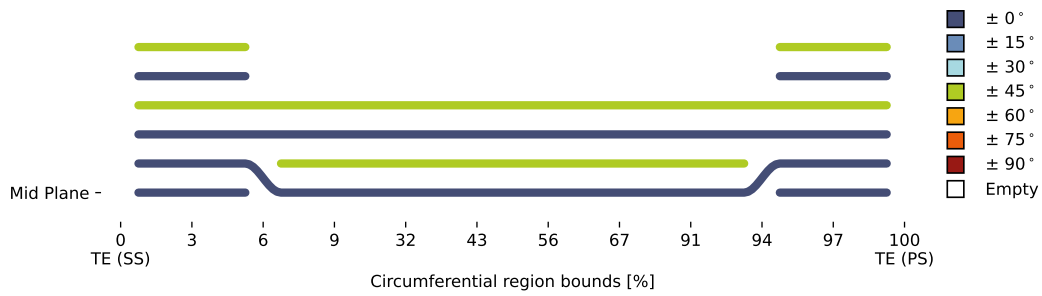
Figure A.3: Locally optimal stacking sequences.
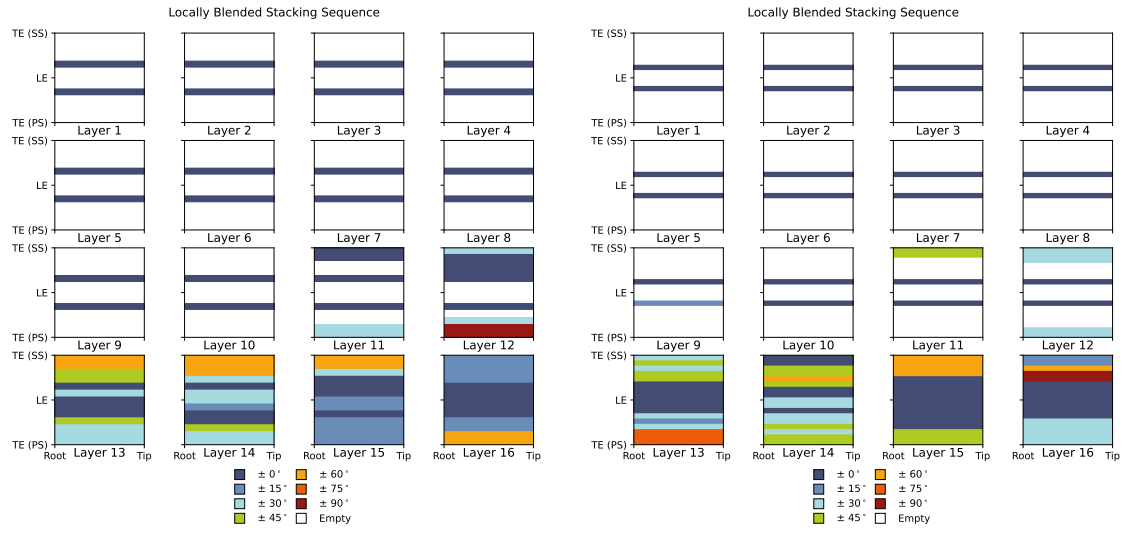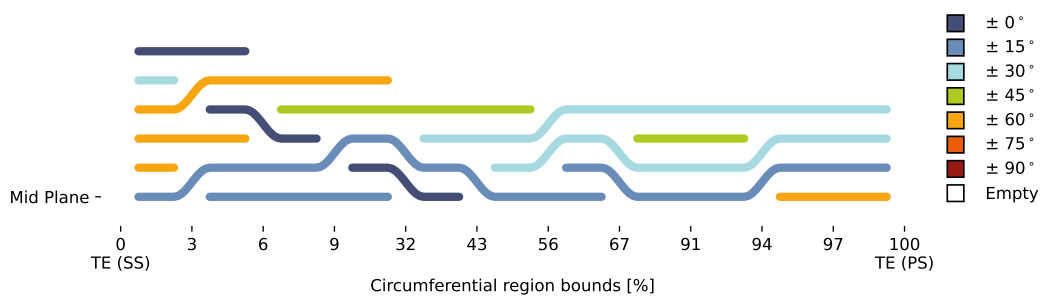
(a) Blade section 1x13.

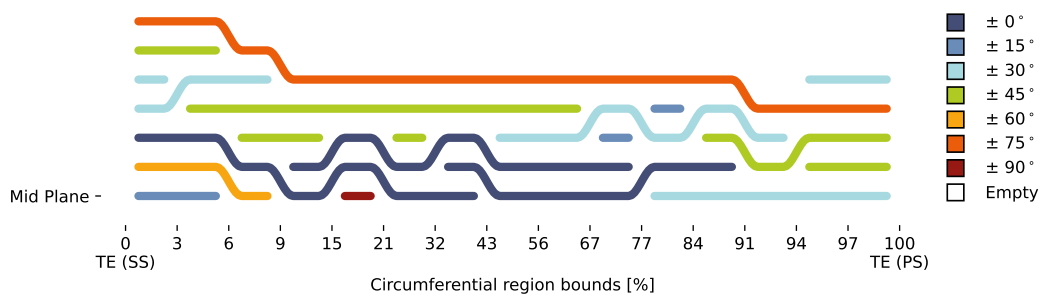**(b)** Blade section 1x17.

(c) Blade section 1x24.

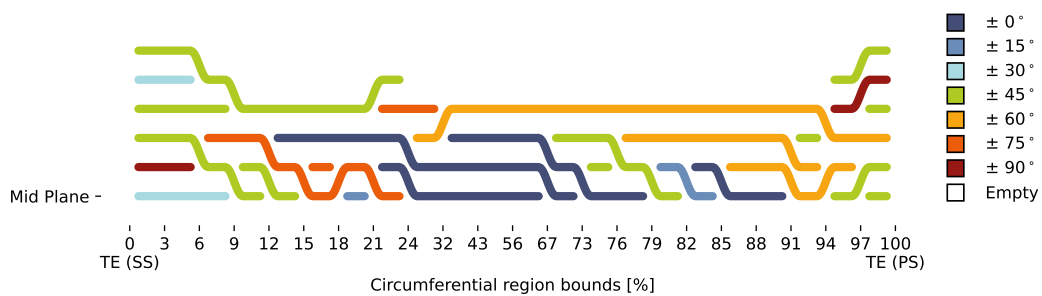**Figure A.4:** Locally blended stacking sequences.

(a) Baseline blade section 1x13 (i.e. material distribution of the DTU 10MW blade).

(b) Blade section 1x13.

(c) Blade section 1x17.

(d) Blade section 1x24.

Figure A.5: Globally blended stacking sequences shown as an unwrapped cross-section.